

A User's Guide to the Mapping Class Group: Once Punctured Surfaces

LEE MOSHER

September, 1994

An automatic structure for the mapping class group of a surface of finite type was described in [M]. This document is intended as a practical guide to computations using a variant of this automatic structure, in the special case of a once-punctured, oriented surface S . As such, we shall try to be more descriptive and less theoretical than in [M], leaving the reader to consult [M] for detailed proofs. Our primary goal is that the reader may learn, as quickly as possible, how to compute in the mapping class group of a once-punctured surface: we describe a quadratic time algorithm for the word problem, henceforth called *the algorithm*, which can be implemented with pencil and paper. A *Mathematica* version of the algorithm is (or will soon be) available; check the software library at the Mathematical Sciences Research Institute (e-mail address: msri.org), or the Geometry Center (geom.umn.edu).

As with any computational method, it is necessary to learn some of the theory in order to learn the algorithm. We spend some time developing various combinatorial tools, with enough justification supplied to aid understanding and lessen the steepness of the learning curve. There is a trade-off involved here: time invested understanding theory may be time wasted gaining proficiency; I do not know if I have found the right balance. Also, despite my stated purpose, in a few places I have put in perhaps too much detail about items of combinatorica that interest me, but which are not really to the point, so the reader is forewarned.

The algorithm described herein can be adapted to arbitrary punctured surfaces, with or without boundary and orientation. The data structures needed do not lend themselves quite so nicely to pencil and paper calculation, so we do not pursue the issue here; details can be found in [M]. And while an automatic structure for the mapping class group of a closed surface is described in [M], in this case the results are *not* suited for practical calculation, because of the non-constructive nature of the proof; hopefully a practical automatic structure will emerge from a deeper understanding of closed surfaces.

For the rest of the paper, let S be an oriented, once-punctured surface which is not the 2-sphere. We regard S as a closed surface with a distinguished point p , the *puncture*. The mapping class group is $\mathcal{MCG}(S) = \text{Homeo}(S)/\text{Homeo}_0(S)$, where $\text{Homeo}(S)$ is the group of all orientation preserving homeomorphisms of S fixing p , and $\text{Homeo}_0(S)$ is the normal subgroup of all homeomorphisms isotopic to the identity leaving p stationary throughout the isotopy.

We shall describe an explicit 2-complex $X = X(S)$ whose fundamental group is the mapping class group $\mathcal{MCG}(S)$. The set of homotopy classes of edge paths in any complex form a groupoid under the operation of concatenation, called the *edge path groupoid* of that complex; a more descriptive but longer name would be “edge path homotopy groupoid”, but we stick with the shorter name. In the particular case of $X(S)$, the edge path groupoid will be called the *mapping class groupoid*, denoted $\mathcal{MCGD}(S)$.

The author was partially supported by NSF grant # DMS-9204331
Research at MSRI partially supported by NSF grant # DMS-9022140

Recall that a *combing* (with uniqueness) for the edge path groupoid of X consists of a base vertex in X , and a choice of a unique representative called the *normal form* for each homotopy class of edge paths in X starting at the base vertex. When these normal forms satisfy certain computational properties we say that the set of normal forms is an *automatic structure*. First, there is a finite automaton which checks whether a given path is a normal form, so the set of normal forms is a regular language. Second, for each edge in X there is a finite automaton called a *multiplier automaton*, which checks whether two normal forms differ by that edge, up to homotopy. The second condition can be replaced by the equivalent *fellow traveller property*: if two normal forms v, w differ up to homotopy by a generator, then (letting $v(t)$ be the prefix of length t of v , or $v(t) = v$ if t is greater than the length of v) we have that $v(t)^{-1}w(t)$ is homotopic to a path whose length is bounded, by a constant independent of v, w, t . Another important notion is that of an *asynchronous automatic structure*, where the fellow traveller property is replaced by the weaker *asynchronous fellow traveller property*: if two normal forms v, w differ up to homotopy by a generator, then there are sequences $0 = s_0 < s_1 < \dots < s_M$ and $0 = t_0 < t_1 < \dots < t_M$ with bounded differences $s_{i+1} - s_i, t_{i+1} - t_i$, such that $v(s_i)^{-1}w(t_i)$ is homotopic to a path of bounded length. By contrast, an ordinary automatic structure is sometimes called a *synchronous automatic structure*. The reader is referred to [ECHLPT] for formal definitions.

In [M], asynchronous and synchronous automatic structures on the groupoid $\mathcal{MCGD}(S)$ are described. Associated to the edge path groupoid on a complex is the group of homotopy classes of closed edge paths, the fundamental group. By a general result of [ECHLPT], given an automatic structure on a groupoid one may obtain an automatic structure on the associated group. By another general result, given an automatic structure on a group (or groupoid) one may obtain a quadratic time algorithm for computing normal forms. Combining these results, we obtain a quadratic time algorithm for the word problem in $\mathcal{MCGD}(S)$ or $\mathcal{MCG}(S)$.

Instead of appealing to these general results, we directly construct a quadratic time algorithm for computing normal forms in the groupoid \mathcal{MCGD} , and by restricting the input to closed edge paths one obtains an algorithm for the group \mathcal{MCG} . Our normal forms will come from the *asynchronous automatic structure* described in [M]. The algorithm we describe for computing these normal forms will run in quadratic time; this will be proved by comparing the asynchronous automatic structure to another, synchronous automatic structure. Our proof will use a special property of the normal forms for \mathcal{MCGD} , the “suffix uniqueness property”, discussed in section IV. Because of the suffix uniqueness property, our quadratic time algorithm is more efficient than the one described in [ECHLPT].

The automatic structure we describe is very large. As a function of the genus g , the number of states in the word acceptor grows at least as fast as g^g ; see figure 19. As such, our algorithm does *not* require explicitly computing and storing the word acceptor and multiplier automata. In a sense, our algorithm constructs local portions of the automata as they are needed for calculation.

Thus, despite the size of the automatic structures the computations are quite efficient. With practice, the algorithm can be implemented quite efficiently with pencil and paper by drawing lots of funny pictures called “chord diagrams”; we give profuse illustrations of such calculations. The author is able to compute the normal forms for a once-punctured surface of genus 2, starting from an edge path of length n , in at most $25n^2$ minutes, given a sufficient quantity of paper, pencils, and coffee. In actual practice, the computations are much faster (although errors, and the correction thereof using an eraser, may slow down computation time).

Another issue arises from the fact that the complex X is so large, so one would not want to write down a presentation for \mathcal{MCG} using X . This raises the question of what form the algorithm uses for input. The direct form of input is an edge path in X . However, there are well-known “small” presentations for $\mathcal{MCG}(S)$ described in the literature whose size grows linearly with the genus. The *Mathematica* implementation of the algorithm allows the user to input a word in standard generators. This word is converted into an edge path in X in linear time, and then the algorithm works on the edge path. We shall not describe this conversion process here.

I. THE COMPLEX X

In this section we construct a finite complex X whose fundamental group is \mathcal{MCG} . First we construct a contractible complex Y on which \mathcal{MCG} acts with finite cell stabilizers and finitely many orbits; the complex Y was first described by Harer [Har]. We are only interested in the 2-skeleton $Y^{(2)}$. Then we resolve finite cell stabilizers of $Y^{(2)}$ to obtain a 2-complex \tilde{X} on which \mathcal{MCG} acts freely with finitely many cell orbits. The quotient of \tilde{X} by \mathcal{MCG} yields X .

Ideal arc systems and the complex Y .

Let I be the closed unit interval. An *ideal arc* is the image h of a map

$$(I, \partial I, \text{int } I) \mapsto (S, p, S - p)$$

which is injective in $\text{int } I$, such that h does not bound a disc; this map is called a *characteristic map* of h . The image of $\text{int } I$ is called the *interior* of h , denoted $\text{int}(h)$. Two ideal arcs h, h' are *isotopic* if there exists $\phi \in \text{Homeo}_0(S)$ such that $\phi(h) = h'$. In general, for any set of objects on which $\text{Homeo}(S)$ acts, two objects are *isotopic* if they differ by an element of $\text{Homeo}_0(S)$.

Given two ideal arcs h_1, h_2 , it is easy to decide whether they are isotopic. In the first case where the interior are disjoint, then h_1, h_2 are isotopic if and only if they bound a disc. In the second case where the interiors intersect, perturb h_1, h_2 so that the interiors have a finite number of transverse intersection points, and then successively isotop them to remove any complementary components which are discs, decreasing the number of intersection points. If this process stops with a positive number of intersection points then h_1, h_2 are not isotopic; otherwise we have reduced to the first case.

An *ideal arc system* γ is a collection of non-isotopic ideal arcs with disjoint interiors, such that each component of $S - \gamma$ is a disc. Figure 1 gives several examples of ideal arc systems. Figure 1(a) is the standard method for cutting a surface of genus 2 into an octagon. By adding arcs to this octagon we obtain figure 1(b), which cuts the surface into six triangles. Figure 1(c) shows another such ‘‘ideal triangulation’’. Note that (b) and (c) are not isotopic, because (b) has a separating ideal arc while (c) has none.

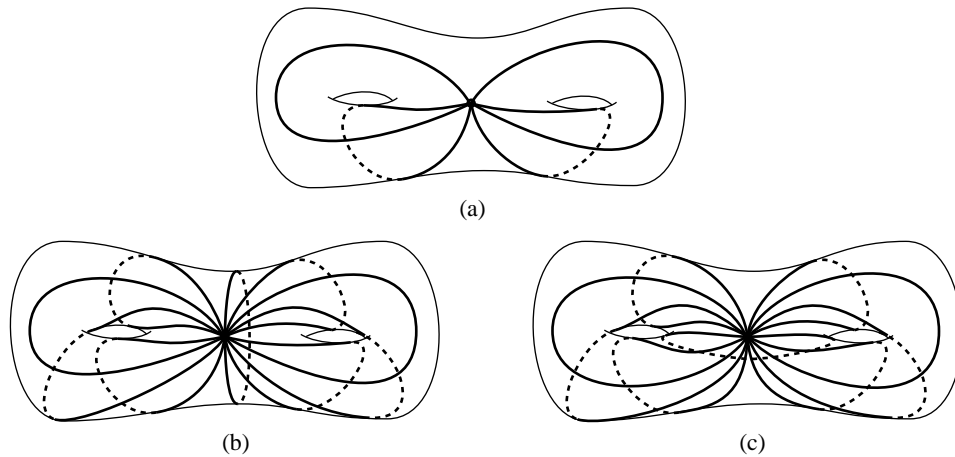


FIGURE 1. Some ideal arc systems

The group $\text{Homeo}(S)$ acts on the set of ideal arc systems. Given an ideal arc system γ and $\phi \in \text{Homeo}_0(S)$, if $\phi(\gamma) = \gamma$ then ϕ fixes each arc of γ setwise (because distinct arcs are pairwise non-isotopic), and preserves the orientation (because $\pi_1(S)$ has no torsion). Thus, ϕ preserves the ends of arcs in γ . We refer to this fact as *Rigidity of Ends*.

A complementary component C of an ideal arc system γ is called a *polygon* of γ . There is a characteristic map $D \mapsto S$ for C , where D is a convex Euclidean polygon, so that each vertex of D goes to p , each side of D gives a characteristic map of some ideal arc of γ , and $\text{int}(D)$ goes to C . The number of sides of C is defined to be the number of sides of D . Polygons are referred to as *triangles*, *quadrilaterals*, *pentagons* etc. depending on the number of sides; in general an n -sided polygon is called an n -gon. Note that there are no 1-gons or 2-gons.

Examples: The polygons of γ are all triangles if and only if $|\gamma| = 6g - 3$. At the other extreme, γ has a single polygon if and only if $|\gamma| = 2g$, in which case the polygon is a $4g$ -gon. These facts are easily verified using the Euler characteristic.

Given a polygon, there is a certain well-defined number of ideal arcs that can be added to triangulate the polygon: for a quadrilateral, add 1 arc; for a pentagon add 2 arcs; for an n -gon add $n - 3$ arcs (while there are many different ways to add these arcs, the number of arcs added is always $n - 3$; the number of distinct ways to add the arcs, up to isotopy, is given by the Catalan number $\frac{1}{m+1} \binom{2m}{m}$ where $m = n - 2$ [STT]). It follows that for an ideal arc system γ , by adding over all polygons one obtains a certain well-defined number of ideal arcs that can be added to triangulate γ ; this number is called the *defect* of γ . Since a triangulation always has $6g - 3$ arcs, the defect is equal to $6g - 3 - |\gamma|$.

If one ideal arc system γ' is obtained by adding arcs to another ideal arc system γ , then we say that γ' is a *refinement* of γ . For example, every γ can be refined to become an ideal triangulation.

Now we construct Y . In general Y has one k -cell for each isotopy class of ideal arc systems of defect k . For example, the 0-cells of Y are in 1-1 correspondence with isotopy classes of ideal triangulations. To describe the attaching maps of cells, suppose the $(k - 1)$ -skeleton $Y^{(k-1)}$ has been constructed, and let γ be an ideal arc system of defect k . The isotopy classes of all possible refinements of γ form a subcomplex of $Y^{(k-1)}$. Now check that this subcomplex is a topological $(k - 1)$ -sphere, and attach a k -cell to this sphere corresponding to γ . We will explicitly study the attaching maps for 1 and 2-cells below.

The complex Y was first described in [Har], where Y is proved to be contractible using Strebel differentials. See [Hat] for an elementary proof of contractibility.

Since the number of arcs in an ideal arc system is always at least $2g$, it follows that the defect is always at most $6g - 3 - 2g = 4g - 3$, so the dimension of Y is $4g - 3$. Harer proves [Har] that this is the minimum possible, by showing that the virtual cohomological dimension of \mathcal{MCG} is $4g - 3$.

0-cells of Y : ideal triangulations.

The 0-cells of Y are in 1-1 correspondence with isotopy classes of ideal triangulations of S . Figures 1(b,c) show two non-isotopic ideal triangulations. In general there are infinitely many isotopy classes of ideal triangulations, because \mathcal{MCG} is infinite, and for each ideal triangulation δ there are only finitely many $\Phi \in \mathcal{MCG}$ such that $\Phi[\delta] = [\delta]$ (this follows from *Rigidity of Ends*). In fact, we will see that the stabilizer of $[\delta]$ is a finite cyclic subgroup of \mathcal{MCG} whose order can take only finitely many values depending on the genus.

This begs the question: how many orbits of ideal triangulations are there under \mathcal{MCG} ? This question is particularly easy to answer on a once-punctured torus. We shall take this up later.

1-cells of Y : elementary moves.

The 1-cells of Y are in 1-1 correspondence with isotopy classes of ideal arc systems γ of defect 1. The polygons of γ consist of one quadrilateral Q and the rest triangles. An example is given in figure 2, with Q shaded. A quadrilateral can be triangulated by inserting an ideal arc, and there are two ways to do this insertion, as shown schematically in figure 3 (a schematic picture like this can be thought of as the domain of a characteristic map for the quadrilateral, so all vertices will be identified to the puncture, and there may be certain pairwise side identifications as well). This gives two ideal triangulations, forming two 0-cells of Y , to which a 1-cell is attached corresponding to γ (see figure 3). Using the γ given in figure 2, the two ideal triangulations refining γ are shown in figures 1(b,c), producing a particular 1-cell in Y .

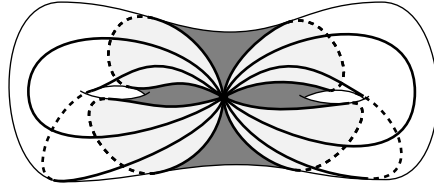


FIGURE 2. An ideal arc system of defect 1. The quadrilateral, part of which wraps around back, is shaded.

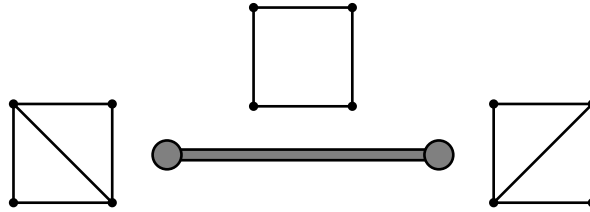


FIGURE 3. The two triangulations of a quadrilateral, giving two 0-cells at the ends of a 1-cell in Y .

Here is a way to think about an *oriented* 1-cell of Y . Start with an ideal triangulation δ and an arc h of δ . Notice that h cannot lie on two sides of a single triangle of δ , for when two sides of a triangle are identified then there must be two or more punctures; see figure 4. Therefore, when h is removed from δ the two adjacent triangles form a quadrilateral Q in a defect 1 ideal arc system γ . The arc h forms one diagonal of Q ; let h' be the opposite diagonal. Inserting h into γ yields a new ideal triangulation δ' . We shall indicate this operation by saying that $\delta \rightarrow \delta'$ is an *elementary move*, and that the elementary move is *performed on h* , with *opposite diagonal h'* . To emphasize the role of h we also write $\delta \xrightarrow{h} \delta'$, and in pictures such as figure 5 we thicken h . Also, we say that the quadrilateral Q is the *support* of the elementary move $\delta \rightarrow \delta'$. To summarize, there is a natural 1-1 correspondence between: oriented 1-cells of Y , isotopy classes of pairs (δ, h) , and pairs of the form $([\delta], [\delta'])$ where $\delta \rightarrow \delta'$ is an elementary move; the corresponding 1-cell in Y is denoted $[\delta \rightarrow \delta']$.

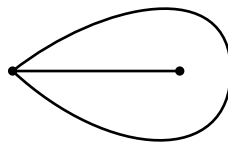


FIGURE 4. In an ideal triangulation δ on an oriented surface, if a triangle has two sides identified then that surface must have at least two punctures.

Note that elementary moves are symmetric: if $\delta \rightarrow \delta'$ is an elementary move then so is $\delta' \rightarrow \delta$. Note also that for each ideal triangulation δ , there are $6g - 3$ outgoing elementary moves, one performed on each ideal arc of δ ; by reversing the directions we also see that there are $6g - 3$ incoming elementary moves.

Returning to our only example so far, from figures 1(b,c) we obtain the elementary move $\delta \xrightarrow{h_1} \delta_1$ shown in figure 5(a), with intervening defect 1 ideal arc system γ_1 . Figure 5(b) shows another elementary move $\delta \xrightarrow{h_2} \delta_2$ starting from the same δ , with intervening arc system γ_2 . Note that γ_2 has a quadrilateral with one pair of opposite sides identified. Also, note that δ and δ_2 differ by a mapping class, namely the Dehn twist around the core curve of the handle on the right side of the surface. Therefore, the 0-cells of Y corresponding to $[\delta]$ and $[\delta_2]$ are in the same orbit under the action of \mathcal{MCG} .

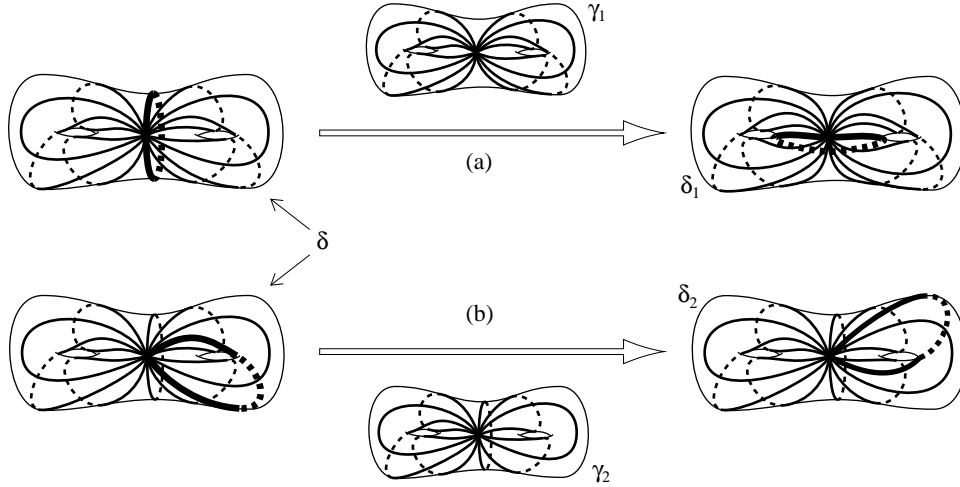


FIGURE 5. Some elementary moves

2-cells of Y : commutator and pentagon relators.

The 2-cells of Y are in 1-1 correspondence with ideal arc systems γ of defect 2. This can happen in two ways: the polygons of γ can consist of two quadrilaterals and the rest triangles; or one pentagon and the rest triangles.

If γ has two quadrilaterals, each quadrilateral can be independently triangulated in one of two ways, yielding four distinct triangulations which refine γ . The four corresponding 0-cells in Y are connected up by four 1-cells as shown in figure 6, forming a closed edge path in Y of length four. Attached to this edge path is a 2-cell of Y corresponding to γ . If δ is one of the four triangulations, and if h_1, h_2 are the two diagonals inserted into γ to form δ , then the two adjacent sides of the 2-cell are given by elementary moves $\delta \xrightarrow{h_1} \delta_1$ and $\delta \xrightarrow{h_2} \delta_2$. There are also elementary moves $\delta_1 \xrightarrow{h_2} \delta'$ and $\delta_2 \xrightarrow{h_1} \delta'$, as shown in figure 6. For this reason, we can say that the elementary moves performed on h_1 and on h_2 commute with each other, and thus we say that this attached 2-cell is a *commutator relator*.

Now suppose γ has one pentagon. This pentagon can be triangulated in one of five ways as shown in figure 7, forming a closed edge path in Y of length five, to which a 2-cell is attached. This 2-cell is called a *pentagon relator*. Note that if δ is one of the five ideal triangulations, if h_1, h_2 are the arcs inserted into γ to form δ , and if $\delta \xrightarrow{h_1} \delta_1$ and $\delta \xrightarrow{h_2} \delta_2$ are the two sides of the relator incident to δ , then the next two sides are $\delta_1 \xrightarrow{h_2} \delta'_1$ and $\delta_2 \xrightarrow{h_1} \delta'_2$, and there is a fifth side $\delta'_1 \rightarrow \delta'_2$.

One computation which arises over and over is the following. Given an ideal triangulation δ and ideal arcs $h_1 \neq h_2 \in \delta$, consider the two elementary moves $\delta \xrightarrow{h_1} \delta_1$ and $\delta \xrightarrow{h_2} \delta_2$. Do these two elementary moves lie on a unique relator? If so, is it a commutator relator or a pentagon relator?

These questions can be answered by examining the adjacencies of ends of h_1, h_2 . Each ideal arc has two ends. Given an end of h_1 and an end of h_2 , these ends are *adjacent* in δ if they are incident to some corner of some polygon of δ . It cannot happen that h_1 has two ends adjacent to a single end of h_2 , for then we

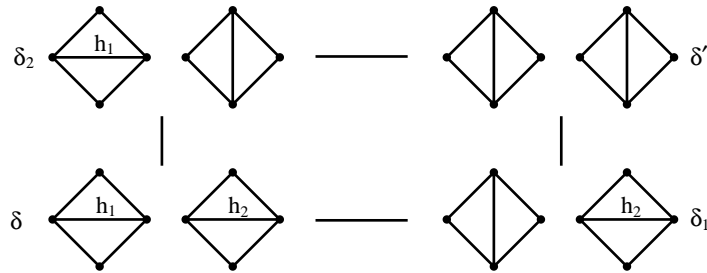


FIGURE 6. A commutator relator

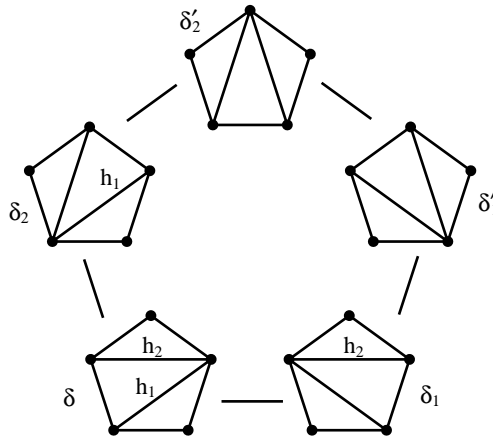


FIGURE 7. A pentagon relator

obtain a folded triangle as in figure 4. Thus, h_1 and h_2 can have zero, one, or two pairs of adjacent ends, and if two then the pairs are disjoint.

If h_1, h_2 have no pairs of adjacent ends, then removal of h_1, h_2 yields an ideal arc system with two quadrilaterals, and we obtain a commutator relator. If h_1, h_2 have one pair of adjacent ends, their removal produces an ideal arc system with a pentagon, and we get a pentagon relator. If h_1, h_2 have two pairs of adjacent ends, then removal of h_1, h_2 creates a collection of ideal arcs with an annulus complementary component (see figure 8 for an example). This violates the definition of ideal arc system, so there is no 2-cell in Y corresponding to this collection of ideal arcs.

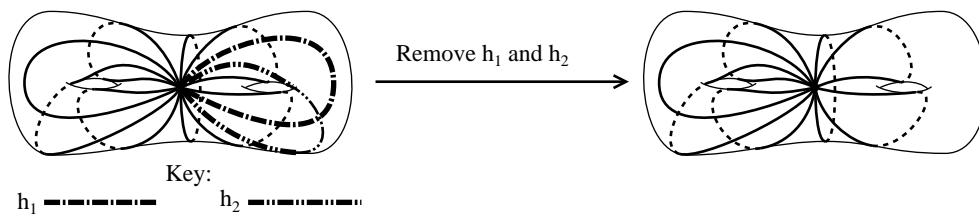


FIGURE 8. If each end of h_1 is adjacent to an end of h_2 , removal of h_1 and h_2 creates an annulus, and no relator is obtained.

The action of \mathcal{MCG} on Y .

In general, whenever there is a set of objects on which $\text{Homeo}(S)$ acts, then \mathcal{MCG} acts on the isotopy classes. Now $\text{Homeo}(S)$ acts in the obvious way on the set of ideal arc systems, so \mathcal{MCG} acts on their isotopy classes. Also, the action of \mathcal{MCG} preserves the relation of refinement, hence $\mathcal{MCG}(S)$ acts on the complex Y by cellular homeomorphisms.

We need some notation for this action. In general, given an ideal arc system γ the isotopy class of γ is denoted $[\gamma]$. Thus, given $\Phi \in \mathcal{MCG}$ represented by $\phi \in \text{Homeo}(S)$, then $\Phi[\gamma] = [\phi(\gamma)]$.

Combinatorial equivalence and chord diagrams.

The main goal of this section is to present a calculus which allows us to understand cell stabilizers and cell orbits of the action of \mathcal{MCG} on Y . This calculus will enable us to understand why cell stabilizers are finite, why the number of cell orbits is finite, and it will guide us in “resolving” finite order cell stabilizers, leading up to the definition of the complex X .

Two ideal arc systems γ, γ' are said to be *combinatorially equivalent*, or to have the same *combinatorial type*, if they are in the same orbit under the action of $\text{Homeo}(S)$, i.e. $\phi(\gamma) = \gamma'$ for some $\phi \in \text{Homeo}(S)$. Equivalently, their isotopy classes $[\gamma], [\gamma']$ are in the same orbit under the action of \mathcal{MCG} . The combinatorial equivalence class of γ is denoted $\{\gamma\}$. We now associate to each γ a finitistic object called its *combinatorial diagram*, which will encode the combinatorial type of γ . Then we show how to represent the combinatorial diagram pictorially with the *chord diagram*.

Let γ be an ideal arc system. Let $\mathcal{E}(\gamma)$ be the set of ends of ideal arcs of γ . If h is an ideal arc, then an end of h is just an end, in the usual sense, of the topological space $h - p$, so each ideal arc has two ends. An end of h can be represented by a *half-arc* of h , which is the closure of a component of $h - \{p, x\}$ for some $x \in \text{int}(h)$. Now we put some extra structure on $\mathcal{E}(\gamma)$.

Recall that a *circular ordering* on a finite set is just a permutation with one cycle. There is a natural way to use the orientation on S to put a circular ordering on $\mathcal{E}(\gamma)$. Choose a disc D containing p so that $D \cap \gamma$ is a union of radii of D . These radii form half-arcs of γ , and they are in 1-1 correspondence with $\mathcal{E}(\gamma)$. The orientation on S determines a boundary orientation on ∂D , which determines in turn the circular ordering on $\mathcal{E}(\gamma)$. Denote this circular ordering by $\mathcal{E}(\gamma) \xrightarrow{\text{Succ}} \mathcal{E}(\gamma)$, the *successor* map. The inverse permutation is called the *predecessor* map, denoted $\mathcal{E}(\gamma) \xrightarrow{\text{Pred}} \mathcal{E}(\gamma)$. Next recall that a *transposition* on a finite set is a permutation where every cycle has length 2. The correspondence between opposite ends of the same arc determines a transposition on $\mathcal{E}(\gamma)$ denoted $\mathcal{E}(\gamma) \xrightarrow{\text{Opp}} \mathcal{E}(\gamma)$, the *opposite end* map. The *combinatorial diagram* of γ is defined to be the ordered triple $(\mathcal{E}(\gamma), \text{Opp}, \text{Succ})$.

Given ordered triples $(\mathcal{E}_i, o_i, \sigma_i)$, $i = 1, 2$, where \mathcal{E}_i is a finite set and o_i, σ_i are permutations of \mathcal{E}_i , we say these triples are *isomorphic* if there is a bijection $\mathcal{E}_1 \xrightarrow{\phi} \mathcal{E}_2$ such that $\phi \circ \sigma_1 = \sigma_2 \circ \phi$ and $\phi \circ o_1 = o_2 \circ \phi$.

The fact we need is that two ideal arc systems are combinatorially equivalent if and only if their combinatorial diagrams are isomorphic. For if γ_1, γ_2 are combinatorially equivalent then the homeomorphism between them induces an isomorphism of their combinatorial diagrams. Conversely, if their combinatorial diagrams are isomorphic then one can construct the desired homeomorphism up through the skeleta by induction: since the opposite end maps correspond the homeomorphism can be extended over the 1-skeleta, and since the successor maps correspond it can be extended over the polygons preserving orientation.

We can immediately see why there are finitely many combinatorial equivalence classes of ideal arc systems on S : the size of $\mathcal{E}(\gamma)$ is bounded by $12g - 6$, and for a set \mathcal{E} of bounded size there are only finitely many equivalence classes of triples (\mathcal{E}, o, σ) . Also, using *Rigidity of Ends* we can see why cell stabilizers are finite, because the subgroup of \mathcal{MCG} stabilizing $[\gamma]$ is isomorphic to the set of automorphisms of the combinatorial diagram of γ , which is cyclic of order bounded by $12g - 6$, because an automorphism must commute with the successor map. The optimal order bound is somewhat smaller than $12g - 6$, because an automorphism also commutes with the opposite end map; on a surface of genus 2 the optimal order bound is 3.

The combinatorial diagram of γ can be represented pictorially by the *chord diagram*. Draw a circle on a piece of paper, oriented counterclockwise, and draw $12g - 6$ points on the circle corresponding to $\mathcal{E}(\gamma)$, so

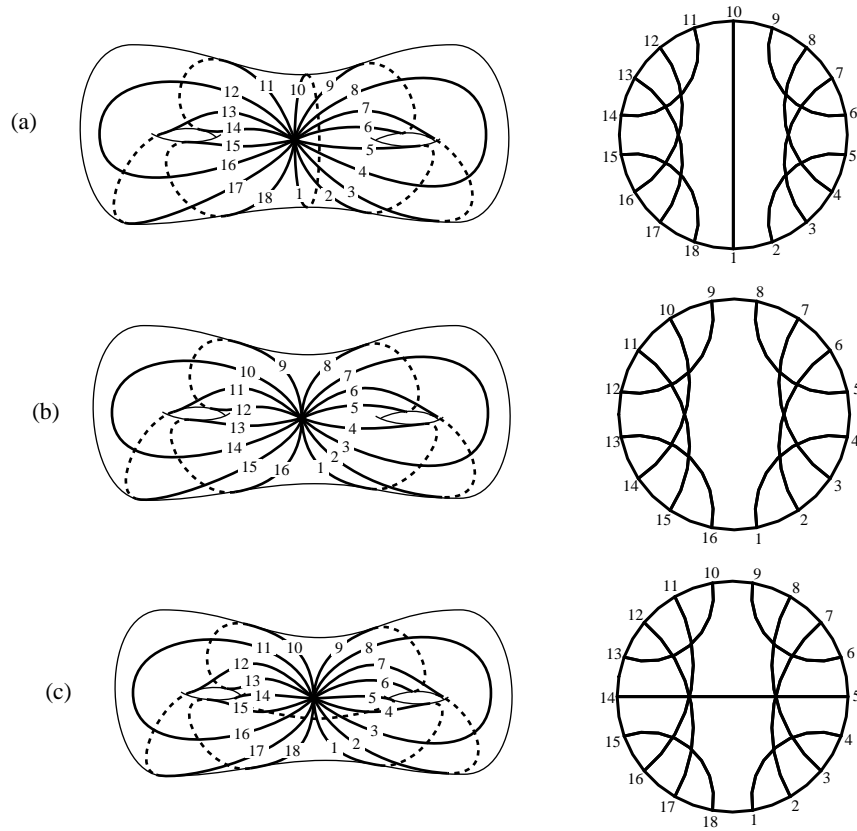


FIGURE 9. Chord diagrams of some ideal arc systems

that the counterclockwise ordering corresponds to Succ. Now draw chords connecting up the points in pairs, using the transposition Opp; in diagrams we use chords which are hyperbolic geodesics in the Poincaré disc model, i.e. arcs of circles orthogonal to the boundary. Figure 9 shows three examples, two ideal triangulations and a defect 1 ideal arc system, taken from the first elementary move pictured in figure 5. In order for the reader to get used to the chord diagrams, in these figures we have indexed the arc ends with integers, but we will not use any indexing in future chord diagrams.

In the second elementary move $\delta \rightarrow \delta_2$ of figure 5, one can check that δ and δ_2 have the same chord diagram, verifying the earlier statement that they are combinatorially equivalent.

It is easy to distinguish combinatorial types by viewing the chord diagram. If the points representing ends are spaced regularly around the circle, and if the chords are drawn with hyperbolic geodesics, then the chord diagram itself is a complete invariant of the combinatorial type, regarding two chord diagrams as being isomorphic if they differ by a Euclidean similarity. It is also easy to recognize the automorphism group of a chord diagram, by just looking for circular symmetries of the diagram. These tasks are easily accomplished even with slightly sloppy hand drawings of chord diagrams.

Since the combinatorial diagram or the chord diagram completely determines the combinatorial type, one can derive from either of them any combinatorial properties of ideal arc systems. In general, for any set of objects on which $\text{Homeo}(S)$ acts, a *combinatorial property* defined on those objects is a property invariant under the action of $\text{Homeo}(S)$. For example, the *polygon type* of an ideal arc system γ is a combinatorial property: this is the sequence (i_3, i_4, \dots) where i_n is the number of n -gons in γ . To determine

the polygon type from the combinatorial diagram $(\mathcal{E}(\gamma), \text{Opp}, \text{Succ})$, define a permutation $\mathcal{E}(\gamma) \xrightarrow{\text{Next}} \mathcal{E}(\gamma)$ as $\text{Next} = \text{Succ} \circ \text{Opp}$). Then the n -cycles of Next are in $1-1$ correspondence with the n -gons of γ , for each $n \geq 3$. For example, in the defect 1 chord diagram of figure 10, the permutation Next has cycle structure $\{(1, 5, 9, 13), (2, 7, 4), (3, 8, 6), (10, 15, 12), (11, 16, 14)\}$, showing one 4-gon and four 3-gons. Tracing out the boundary of the 4-gon starting with end 1, and then successively applying Opp and Succ , we obtain:

$$1 \xrightarrow{\text{Opp}} 4 \xrightarrow{\text{Succ}} 5 \xrightarrow{\text{Opp}} 8 \xrightarrow{\text{Succ}} 9 \xrightarrow{\text{Opp}} 12 \xrightarrow{\text{Succ}} 13 \xrightarrow{\text{Opp}} 16 \xrightarrow{\text{Succ}} 1$$

as shown in figure 10(a).

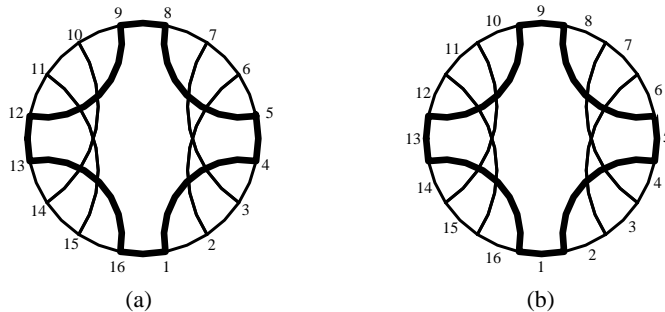


FIGURE 10. A 4-gon in a defect 1 chord diagram

An important concept which plays a central role later on is that of a *prong* of an ideal arc system γ . Informally, a prong of γ is a corner of a polygon of γ . Formally, a prong is an ordered pair (e, e') in $\mathcal{E}(\gamma)$ such that $e' = \text{Succ}(e)$. In a chord diagram, a prong is represented as the circular arc between adjacent ends; we shall call this an *end gap*. Thus, when we represent a polygon in a chord diagram as in figure 10, what is actually drawn are the chords representing the sides of the polygon and the end gaps representing the prongs of the polygon. If we index each prong (e, e') using the index of the second end e' in the pair, then each cycle of Next lists the prong indices of the corresponding polygon. Figure 10(b) shows prong indices, making clear the correspondence between the 4-gon and the cycle $(1, 5, 9, 13)$.

Here is an exercise: prove that given a set \mathcal{E} of size $12g - 6$, if Succ is a cyclic permutation and Opp is a transposition, then the triple $(\mathcal{E}, \text{Opp}, \text{Succ})$ is isomorphic to the combinatorial type of an ideal triangulation on a surface of genus g if and only if the permutation $\text{Next} = \text{Succ} \circ \text{Opp}$ has a cycle structure consisting solely of 3-cycles. This idea is used in appendix 2 of [P] to obtain an asymptotic formula, given in the next section, for the number of combinatorial types of ideal triangulations on a surface of genus g .

Chord diagrams of ideal triangulations.

In this section we shall make several observations about chord diagrams of ideal triangulations. These observations serve two purposes: they help in learning to recognize features of chord diagrams; and they can be used to enumerate the chord diagrams on a surface of genus 2. This enumeration was first obtained by [Jorgensen, Martineen]. We shall also report on enumerations for higher genus, and an asymptotic formula.

Suppose δ is an ideal triangulation. Let T be a triangle of δ , and let (e_1, e_2, e_3) be the corresponding 3-cycle of Next . Every distinct ordered triple in $\mathcal{E}(\delta)$ is either *positive* or *negative*. We say that (e_1, e_2, e_3) is positive if there is a circular enumeration $\mathcal{E}(\delta) = \{f_1, \dots, f_K\}$, i.e. an enumeration with $\text{Succ}(f_k) = f_{k+1}$ for $k \in \mathbf{Z}/K$, so that if $e_i = f_{k_i}$ then $k_1 < k_2 < k_3$.

Figure 11 shows how the two types of triangles appear in a chord diagram: a positive 3-cycle of Next yields an *untwisted* triangle, and a negative 3-cycle yields a *twisted* triangle. Note that T is untwisted if and

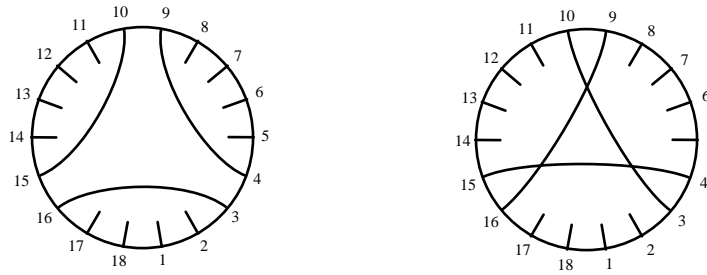


FIGURE 11. The untwisted triangle corresponds to the positive or “increasing” 3-cycle (4, 10, 16), while the twisted triangle corresponds to the negative or “decreasing” 3-cycle (16, 10, 4)

only if its regular neighborhood is homeomorphic to a three holed sphere, and T is twisted if and only if the regular neighborhood is homeomorphic to a one holed torus.

Fact. *If S is a once-punctured surface of genus g , then in any ideal triangulation δ the number of twisted triangles is $2g$ and the number of untwisted triangles is $2g - 2$.*

Proof #1. Construct a single “base” example of an ideal triangulation with $2g$ twisted and $2g - 2$ untwisted triangles, observe that the count of twisted and untwisted triangles is unchanged when doing an elementary move, and then apply connectivity of the complex Y . \diamond

This proof has the disadvantage that it is not intrinsic to δ : one must find a path of elementary moves from δ to the base example. Here is an intrinsic proof:

Proof #2. Let d be a disc neighborhood of p chosen so that $\delta \cap d$ is a union of radii of d . Let $\hat{S} = S - \text{int}(d)$. We shall use δ to put a piecewise Euclidean metric on \hat{S} . This metric will have concentrated negative curvature corresponding to the twisted triangles. By applying the Gauss-Bonnet theorem we obtain a count of the number of twisted triangles. To set up the metric requires some alterations on δ .

Let δ_1 be obtained from δ by replacing each ideal arc h of δ with two copies of h bounding a bigon, still intersecting d in radii. Now consider a triangle T of δ_1 . If T is twisted, then alter T near each prong by taking two half-arcs incident to that prong extending slightly beyond d , and pinching their ends together, as shown in figure A1; make sure that the half-arcs are left unchanged in d , still intersecting d in radii. The triangle T is divided into four regions: a pinched triangle, and three pinched prongs. Making this alteration for each twisted triangle of δ_1 , the resulting collection of ideal arcs is denoted δ_2 . Now let $\hat{\delta}$ be obtained by intersecting δ_2 with \hat{S} . This has the effect of truncating each untwisted triangle, each bigon, and each pinched prong; pinched triangles are left intact.

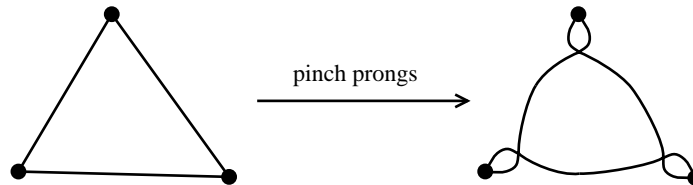


FIGURE A1. Pinch the prongs of each twisted triangle

Consider the chord diagram D of δ . Let \hat{D} be obtained from D by doubling each chord, replacing it with two parallel chords, then straightening all chords to become Euclidean segments instead of hyperbolic lines

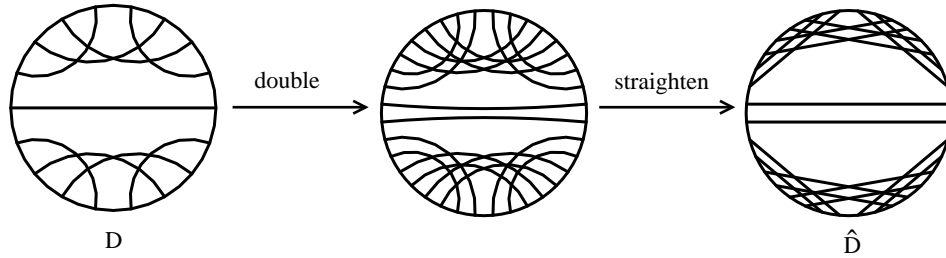


FIGURE A2. To obtain \hat{D} , double each chord of D then straighten

(see figure A2).

We regard \hat{D} as lying in the Euclidean plane \mathbf{E}^2 , and we construct a map $f: \hat{S} \rightarrow \mathbf{E}^2$ whose picture is given by \hat{D} , as follows. The boundary of \hat{S} goes to the boundary circle of \hat{D} . Each truncated arc of $\hat{\delta}$ goes to the corresponding chord of \hat{D} . Each component of $\hat{S} - \hat{\delta}$ is either a truncated untwisted triangle, truncated bigon, truncated pinched prong, or pinched triangle; for each of these regions the boundary is already mapped to a simple closed curve in \mathbf{E}^2 , and there is an extension of f to an embedding of the region, as shown in figure A3.

Notice that for each pinch point x , the map f creates a “pleat” at x ; see figure A4. Another way to say this is that each twisted triangle is “twisted” by the map f , at each pinch point of the triangle.

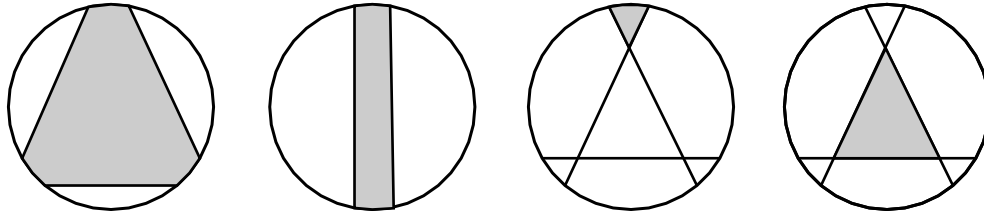


FIGURE A3. Embedding a truncated untwisted triangle, truncated bigon, truncated pinched prong, and pinched triangle into \hat{D} ■

By pulling back the Euclidean metric from \mathbf{E}^2 to \hat{D} , we obtain a piecewise Euclidean metric on S . The boundary has total geodesic curvature 2π . Consider a pinch point x . We must compute the Euclidean cone angle θ_x . The pinched triangle incident to x has a certain interior angle α_x , and as figure A4 shows we have $\theta_x = 2\pi + 2\alpha_x$. Therefore at x there is an angle defect of $2\pi - \theta_x = -2\alpha_x$.

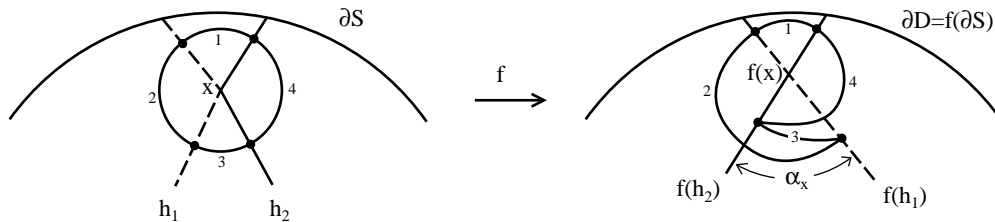


FIGURE A4. At a pinch point x , if the pinched triangle has an interior angle α_x , then the cone angle at x is $2\pi + 2\alpha_x$.

A pinched triangle with vertices x, y, z therefore contributes an angle defect of $-2(\alpha_x + \alpha_y + \alpha_z)$. But this equals -4π , since $\alpha_x, \alpha_y, \alpha_z$ are the interior angles of a Euclidean triangle. Therefore, if K is the number of twisted triangles, then by the Gauss-Bonnet theorem we have

$$2\pi - 4\pi K = 2\pi\chi(\hat{S}) = 2\pi(1 - 2g)$$

so $K = 2g$. ◇

The twisted and untwisted triangles in an ideal triangulation arrange themselves into several larger structures, whose visualization helps in recognizing a chord diagram.

If two untwisted triangles share a side, then they cannot share any other side, and their union forms an “untwisted 4-gon”; the chord diagrams of ideal triangulations in figures 9(a,c) each have an untwisted 4-gon. Continuing inductively, if an untwisted n -gon shares a side with an untwisted triangle, then they cannot share another side, and their union forms an untwisted $n + 1$ -gon. Maximal untwisted polygons are called *untwisted islands*. Figure 12(a) shows a genus 2 chord diagram whose two untwisted islands are both triangles. As an exercise, check that this chord diagram is obtained from figure 9(c) by an elementary move on the arc with ends labelled 1 and 4 (hint: see figure 24(a)). Figure 12(b) shows a genus 3 chord diagram with one untwisted island, a hexagon.

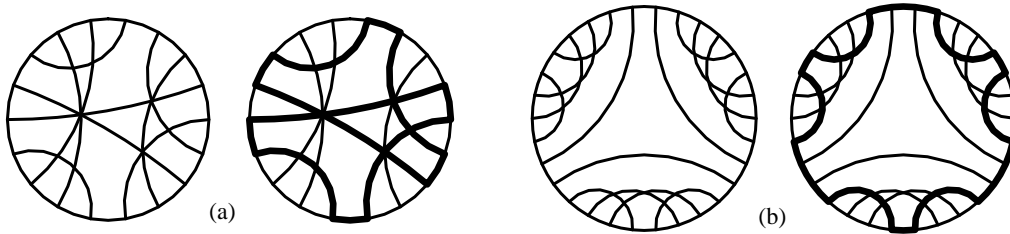


FIGURE 12. Untwisted polygons

On the other hand, two twisted triangles can share either one, two, or all three sides. If they share all three sides, then they close up to form a torus, with the chord diagram shown in figure 13. Thus, on a higher genus surface a pair of twisted triangles can share at most two sides. If two twisted triangles share two sides, then they form a *1-handle piece*. The triangulations in figures 9(a) and (c) each have two 1-handle pieces, figure 12(a) has one, and figure 12(b) has three.

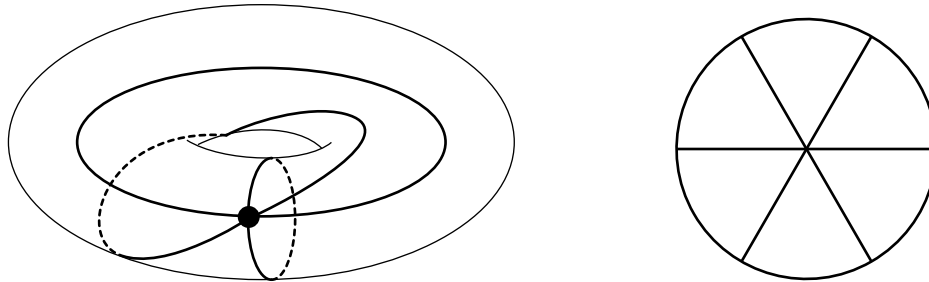


FIGURE 13. Two twisted triangles sharing three sides form a torus.

If two twisted triangles share only one side, then they form a twisted 4-gon, see, for example, figure 14(a) which shows the same triangulation as 12(a). Continuing inductively, if $n \geq 4$ and a twisted n -gon shares a side with a twisted triangle, then they cannot share another side, and their union forms a twisted $(n+1)$ -gon. A maximal twisted polygon is called a *twisted island*. Figure 14(b) shows a genus 2 chord diagram with a twisted hexagon; this triangulation comes from figure 9(c) by doing two elementary moves one after another, first on the arc with ends 1, 4 and then on the arc with ends 10, 13.

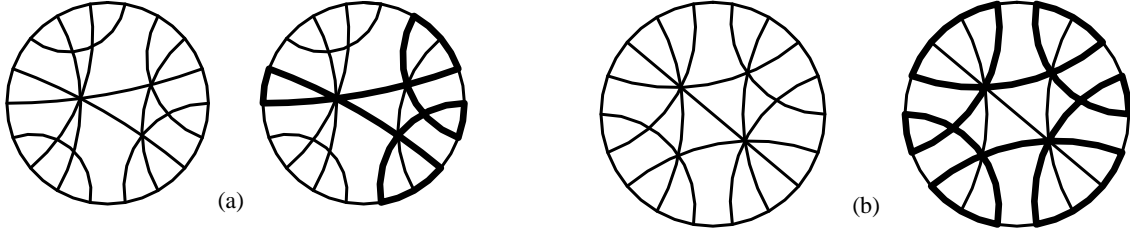


FIGURE 14. Twisted polygons

Thus, any ideal triangulation can be decomposed into untwisted islands, twisted islands, and 1-handle pieces. We may therefore enumerate chord diagrams by the “island” method, as follows. First choose a partition of the $2g - 2$ untwisted triangles into islands. Then choose how the prongs of these islands interleave in the circular ordering. This choice determines the twisted islands and the number of 1-handle pieces. Now choose triangulations of the twisted and untwisted islands, using the enumeration by Catalan numbers.

Now we use the island method to enumerate chord diagrams for low genus surfaces. A “connectivity” proof is given later, using connectivity of Y .

Suppose first that S has genus 1. Then there are no untwisted triangles and two twisted triangles T_1, T_2 . The sides of T_1 and T_2 must be glued in 1-1 correspondence, and the prongs must interleave on the chord diagram. Thus, the chord diagram is forced to be the one shown in figure 13. This shows that all ideal triangulations of a once-punctured torus are combinatorially equivalent, and the automorphism group of each one is cyclic of order 6.

Now suppose S has genus 2. An ideal triangulation has two untwisted and four twisted triangles. The untwisted triangles can form either a 4-gon island or two triangle islands.

Suppose first that there is a 4-gon island, which contains a diagonal arc separating it into two triangles. The four sides of this island must bound two 1-handle pieces, which can arrange themselves in one of three ways as shown in figure 15. The 1-handle pieces may be parallel to the diagonal arc as in T_1 ; they may cross the diagonal arc but not cross each other as in T_2 ; or they may cross the diagonal arc *and* each other as in T_3 . The orders of the automorphism groups are also shown in figure 15. Note that the unoriented automorphism groups are dihedral groups of twice the size.

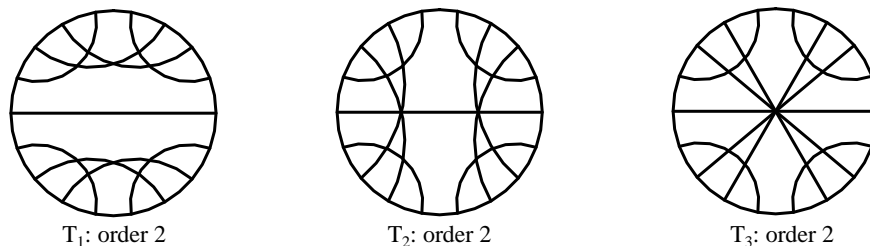


FIGURE 15. Genus 2 chord diagrams with two 1-handle pieces

Now suppose there are two triangle islands. The prongs of these islands may interleave in one of two ways, as shown in figure 16.



FIGURE 16. Untwisted triangle islands in genus 2

In figure 16(a), there must be one 1-handle piece and one twisted 4-gon island. There are two ways to insert a diagonal in the twisted 4-gon, yielding the two chord diagrams T_4 and T_5 shown in figure 17; these are the only chord diagrams in genus 2 with one 1-handle piece. Their automorphism groups have order 1; their unoriented automorphism groups have order 2.

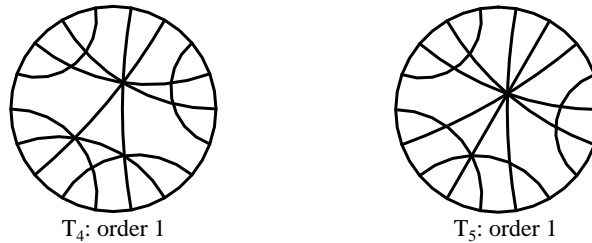


FIGURE 17. Two genus 2 chord diagrams with one 1-handle piece

In figure 16(b), there is a single twisted island, a hexagon. Up to rotation there are four ways to triangulate this hexagon, yielding the four chord diagrams in figure 18, the only chord diagrams in genus 2 with no 1-handle pieces. Both T_6 and T_7 , which are orientation reversals of each other, have oriented and unoriented automorphism groups cyclic of order 2. The diagram T_8 has trivial automorphism group, and the unoriented automorphism group is dihedral of order two. The diagram T_9 has automorphism group cyclic of order 3, and unoriented automorphism group dihedral of order 6.

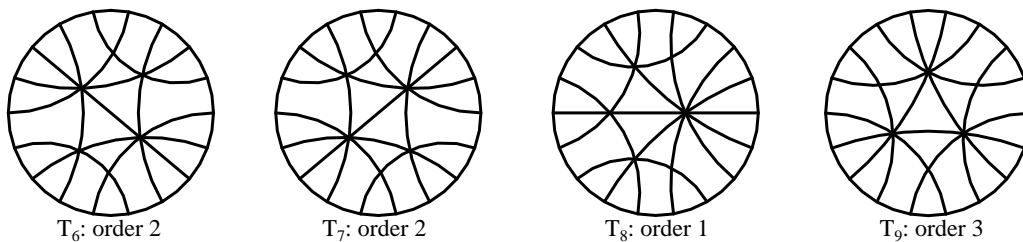


FIGURE 18. Four genus 2 chord diagrams with no 1-handle pieces

To summarize, figures 15,17 and 18 show the nine combinatorial types of ideal triangulations on a once-punctured surface of genus 2.

The island method used to obtain this enumeration is rather inefficient, although it is good for learning to recognize chord diagrams. Despite this inefficiency, when I was young and energetic I used the island method to enumerate the chord diagrams on a once-punctured surface of genus 3. I then wrote a computer program implementing the connectivity method (explained later), obtaining 1726 combinatorial types. This did not accord exactly with the island method, so I went through and found some errors, correcting the result of the island method, still not obtaining the same answer. After iterating this process a few time, I obtained a count of 1726 chord diagrams, and quit.

An asymptotic formula for n_g , the number of distinct chord diagrams in genus g , is given in appendix B of [P]:

$$n_g \sim \frac{(2g)!}{6g-3} \left(\frac{e}{g}\right)^{-2g}$$

where $x(g) \sim y(g)$ means that $x(g)/y(g) - 1 = O(1/g)$.

Figure 19 summarizes what I know about the numbers of combinatorial types of ideal triangulations, compared to the above asymptotic formula. The purpose of this table is to drive home the point that one would not want to enumerate chord diagrams, or any objects derived from them such as the states of the automatic structure, and store them all in one place, if it were not absolutely necessary for computation. On the other hand, methods for generating the objects as needed are very useful; this is how our algorithm for the word problem works.

FIGURE 19. A table of chord diagrams

Genus	n_g	$\frac{(2g)!}{6g-3} \left(\frac{g}{e}\right)^{2g}$
1	1	3
2	9	63
3	1726	5551
4	?	1,081,820

Labelling ideal triangulations: the zero skeleton of X .

In this section we introduce the machinery needed to define the zero-skeleton of \tilde{X} and of X itself. The point is this: we already have an action of \mathcal{MCG} on the zero-skeleton of Y , but that action has some non-trivial point stabilizers. In order to obtain the zero-skeleton of \tilde{X} we need an action of \mathcal{MCG} with trivial point stabilizers. Thus, we must somehow break the symmetries of an ideal triangulation, by labelling it with extra data.

A *labelled ideal triangulation* consists formally of an ordered pair (δ, e) where δ is an ideal triangulation and e is an arc end of δ . The mapping class group acts on isotopy classes of labelled ideal triangulations, with trivial stabilizers. In later sections, we will often suppress the labelling e , and speak of “a labelled ideal triangulation δ ”. For now, we stick with the formal notation (δ, e) .

We now define the zero skeleton of \tilde{X} to be the set of isotopy classes of labelled ideal triangulations on S . The zero skeleton of X is therefore the set of combinatorial types of labelled ideal triangulations. The combinatorial type of a labelled ideal triangulation (δ, e) is described by a *labelled chord diagram*, obtained from the chord diagram for δ by drawing a solid dot at the chord end corresponding to e . An example is shown in figure 20, where the labelled end is represented by a shaded half-arc.

Now we enumerate the 0-cells of X in low dimensions, using the fact that a chord diagram, with $12g - 6$ ends and automorphism group cyclic of order k , yields $(12g - 6)/k$ labelled chord diagrams.

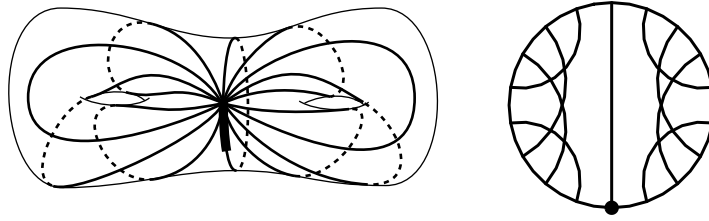


FIGURE 20. A labelled ideal triangulation and the corresponding labelled chord diagram

If S has genus 1, the unique chord diagram has six chord ends and the automorphism group permutes them transitively, so there is a unique chord diagram of a labelled ideal triangulation. Therefore, X has one 0-cell.

If S has genus 2, each chord diagram has 18 chord ends, so using the orders of the automorphism groups given in figures 15,17,18 the number of labelled chord diagrams is

$$3 \cdot 18 + 5 \cdot \frac{18}{2} + 1 \cdot \frac{18}{3} = 105$$

so there are 105 0-cells in X .

If S has genus 3, since $12g - 6 = 30$ then an upper bound on the number of 0-cells is $30 \cdot 1726 = 51780$, but this number will be strictly smaller after taking automorphism groups into account. A computer calculation has yielded 50050 0-cells in X .

The construction of \tilde{X} , X , and the mapping class groupoid.

It is now possible to give a purely abstract definition of the mapping class groupoid \mathcal{MCGD} , as was done in [M]. Recall that an abstract groupoid is a category with invertible morphisms. Let \tilde{D} be the set of isotopy classes of labelled ideal triangulations on S . Then \mathcal{MCG} acts freely on \tilde{D} , and the diagonal action on $\tilde{D} \times \tilde{D}$ is also free. The objects of \mathcal{MCGD} are the orbits of the action of \mathcal{MCG} on \tilde{D} , i.e. the combinatorial types of labelled ideal triangulations. The morphisms of \mathcal{MCGD} are the orbits of the diagonal action of \mathcal{MCG} on $\tilde{D} \times \tilde{D}$. If δ, δ' are labelled ideal triangulations (suppressing the labellings), then the orbit of the pair $([\delta], [\delta'])$, denoted $\{\delta, \delta'\}$, has as its initial object $\{\delta\}$ and as its terminal object $\{\delta'\}$. The composition rule is as follows. Given morphisms $m_1 = \{\delta_1, \delta'_1\}$ and $m_2 = \{\delta_2, \delta'_2\}$ such that the terminal object $\{\delta'_1\}$ of m_1 equals the initial object $\{\delta_2\}$ of m_2 , then δ'_1 and δ_2 are combinatorially equivalent. Therefore there exists $\Phi \in \mathcal{MCG}$ such that $\Phi[\delta'_1] = [\delta_2]$. Note that $m_2 = \{\Phi(\delta_2), \Phi(\delta'_2)\}$, abusing notation. Then $m_1 \circ m_2$ is defined to be $\{\delta_1, \Phi(\delta'_2)\}$.

One easily checks that if \tilde{D} is the 0-skeleton of a simply connected complex \tilde{X} on which \mathcal{MCG} acts freely, then the abstract groupoid constructed above is naturally isomorphic to the edge path groupoid of the quotient complex $X = \tilde{X} / \mathcal{MCG}$. We now proceed to the construction of \tilde{X} .

We have already constructed $\tilde{X}^{(0)} = \tilde{D}$, the set of isotopy classes of labelled ideal triangulations. Now we construct \tilde{X} , together with a cellular map $q: \tilde{X} \rightarrow Y$ which is useful in proving simple connectivity of X . The construction is by “abstract nonsense”. Each k -cell will come equipped with a “boundary certificate”, which is a total ordering of the cells of all dimensions on its boundary, and the boundary certificate determines the k -cell. This convention will allow us to define the action of \mathcal{MCG} up through the skeleta of \tilde{X} by induction; we will similarly prove that the action has trivial cell stabilizers.

Any unordered pair of 0-cells in $\tilde{X}^{(0)}$ to which an edge is attached will be called a *boundary 0-cycle*. Given any boundary 0-cycle, each of the two possible ordering will be the boundary certificate of some 1-cell. With this convention, to specify the 1-cells of X we need only specify which vertex pairs are boundary 0-cycles.

Similarly, any edge cycle γ in $\tilde{X}^{(1)}$ to which a 2-cell is attached will be called a *boundary 1-cycle*. Given any boundary 1-cycle γ , if you choose a vertex and an orientation, then you obtain a boundary certificate by starting with that vertex and reading off the cells encountered by going around in that order. If γ has k vertices then there are $2k$ possible choices, each of which is the boundary certificate of some 2-cell, and these are the only 2-cells attached to γ . Again, with this convention we need only specify what the boundary 1-cycles are, in order to specify the 2-cells of X .

Consider a vertex $[\delta]$ of Y ; we begin by constructing the part of \tilde{X} lying over $[\delta]$, also known as $q^{-1}[\delta]$. We already know that the 0-cells lying over $[\delta]$ are the isotopy classes $[\delta, e]$ of labellings of δ .

Every unordered pair of vertices in $q^{-1}[\delta]$ will be a boundary 0-cycle. Thus, for every ordered pair of ends e_1, e_2 of δ there is a 1-cell with boundary certificate $([\delta, e_1], [\delta, e_2])$. We denote this 1-cell as $[\delta, e_1, e_2]$. The image of this cell downstairs in X is called a *relabelling generator* of X .

Every edge cycle of length 2 or 3 in the 1-skeleton of $q^{-1}[\delta]$ will be a boundary 1-cycle. To determine a boundary 1-cycle γ of length 2, choose a set of two labels $\{e_1, e_2\}$, so the edges of γ are $[\delta, e_1, e_2]$ and $[\delta, e_2, e_1]$. To determine a boundary 1-cycle γ of length 3, choose a set of three labels $\{e_1, e_2, e_3\}$, and choose an ordering for each of the sets $\{e_1, e_2\}$, $\{e_2, e_3\}$, $\{e_3, e_1\}$ to obtain the edges of γ . The images downstairs in X of these 2-cells will be called *relabelling relators*.

Now consider an elementary move $\delta \rightarrow \delta'$, yielding a 1-cell $[\delta \rightarrow \delta']$ of Y . We already know that the 0-skeleton of $q^{-1}[\delta \rightarrow \delta']$ is $q^{-1}[\delta] \cup q^{-1}[\delta']$. Each pair of a vertex in $q^{-1}[\delta]$ and a vertex in $q^{-1}[\delta']$ is a boundary 0-cell. The images downstairs in X of the attached 1-cells will be called *elementary move generators*.

To determine the 2-cells in $q^{-1}[\delta \rightarrow \delta']$, note that in the 1-skeleton of $q^{-1}[\delta \rightarrow \delta']$, each edge cycle contains an even number of edges mapping to $[\delta \rightarrow \delta']$ under q ; between two such edges the cycle may wander around for a while in $q^{-1}[\delta]$ or $q^{-1}[\delta']$. The boundary 1-cycles in $q^{-1}[\delta \rightarrow \delta']$ are the ones which have exactly two edges mapping to $[\delta \rightarrow \delta']$, and which contain at most one edge each in $q^{-1}[\delta]$ and $q^{-1}[\delta']$. The images downstairs in X of the attached 2-cells will be called *elementary move relabellings*.

This finishes the description of $q^{-1}(Y^{(1)})$.

Finally, given a 2-cell c of Y , each edge cycle in $\tilde{X}^{(1)}$ projecting homeomorphically to ∂c is a boundary 1-cycle, and the attached 2-cell maps homeomorphically to c . Depending on the nature of the 2-cell c , the images of these 2-cells in X will be called *labelled commutator relators* or *labelled pentagon relators*.

This completes the description of X .

The action of \mathcal{MCG} on $\tilde{X}^{(0)}$ is already defined, and each 0-cell has trivial stabilizer. A 1-cell is determined by its boundary certificate, which is an ordered pair of 0-cells, and clearly the set of such ordered pairs is invariant under the action of \mathcal{MCG} , so the action of \mathcal{MCG} extends over $\tilde{X}^{(1)}$ with trivial 1-cell stabilizers. Again, a 2-cell is determined by its boundary certificate, which is a sequence of 0-cells and 1-cells, and the set of such sequences is invariant under the action of \mathcal{MCG} , so the action of \mathcal{MCG} extends over 2-cells with trivial cell stabilizers.

The quotient complex $X = \tilde{X}/\mathcal{MCG}$ is now defined. It is evident that the map $q: \tilde{X} \rightarrow Y$ has the path lifting property as well as the homotopy lifting property for paths, so \tilde{X} is simply connected. It follows that $\pi_1(X) \approx \mathcal{MCG}$. Also, for any cell of Y the inverse image in \tilde{X} is a finite cell complex, and since Y has finitely many cell orbits it follows that X is a finite complex. We can now define the mapping class groupoid \mathcal{MCGD} as the edge path groupoid of X . Given an edge path w in X , the corresponding homotopy class is denoted $\bar{w} \in \mathcal{MCGD}$.

We now have a finite presentation for \mathcal{MCGD} , with the edges of X as generators and the 2-cells of X as relators. There are two types of edges: relabelling generators and elementary move generators. There are several types of relators: relabelling relators, elementary move relabellings, and labelled commutator and pentagon relators.

In the next two sections we whittle down the elementary move generators to a smaller subset called the “labelled elementary move generators”, which together with the relabelling generators will still generate \mathcal{MCGD} (this is the generating set used in [M]). In order to understand labelled elementary move generators,

we first initiate a study of chord diagrams of elementary moves.

Chord diagrams of elementary moves.

Consider an elementary move $\delta \rightarrow \delta'$ performed on the ideal arc h of δ , with opposite diagonal h' in δ' , and with support Q . Let D be the chord diagram of δ ; by abuse of notation we use h to stand for the chord representing the ideal arc h , and this chord will be shaded in the diagrams. Now we show how, using D and h as input, we may compute the chord diagram D' of δ' .

Look at the two triangles adjacent to h . There are several possibilities for these two triangles: both untwisted; one untwisted and one twisted, also known as *mixed*; or both twisted, with either one, two, or three side pair identifications. For each of these five cases, figure 21 shows how the elementary move appears “locally” in a chord diagram, i.e. the figure shows the support of the elementary move, with missing chord ends indicated by a twiddle “ \sim ”. The five cases can also be enumerated according to the chord diagram of the quadrilateral Q . We now go through the cases one by one.

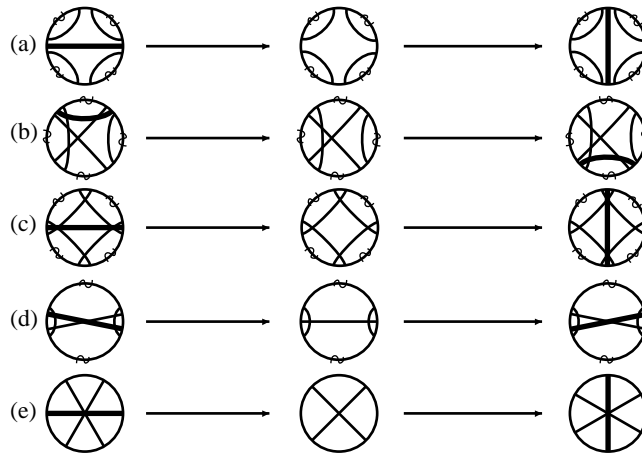


FIGURE 21. Chord diagrams of the support of an elementary move. Missing chord ends are indicated with a \sim .

First we dispose of the case where both triangles are twisted and there are three side pair identifications. This occurs only on the punctured torus, and is given in figure 21(e). The quadrilateral Q has two side pair identifications. Any elementary move on the punctured torus has this chord diagram. Thus, in genus 1 there is only one orbit of edges of Y under the action of \mathcal{MCG} .

With both triangles untwisted, then Q is an untwisted 4-gon, and we have an *untwisted-untwisted* elementary move (figure 21(a)). With both triangles twisted and one side pair identification, then Q is a twisted 4-gon, and we have a *twisted-twisted* elementary move (figure 21(c)). These two cases are the easiest to visualize. An untwisted-untwisted example is shown in figure 22(a); this is the chord diagram of the elementary move from figure 5(a). A twisted-twisted example is given in figure 22(b). In these chord diagrams the intervening defect 1 chord diagram is shown; after this section we will not usually show this. One general feature to note is that when one chord is removed and another inserted in a chord diagram, the chord endpoints should be repositioned so that they are evenly spaced; space will have to be contracted near the removed chord ends, and it will be expanded near the inserted chord ends.

With both triangles twisted and two side pair identifications, the triangles form a 1-handle piece and h is one of the two interior arcs of the 1-handle piece. The support quadrilateral Q has one side identification (figure 21(d)). An example is given in figure 23, which is the chord diagram of the elementary move from

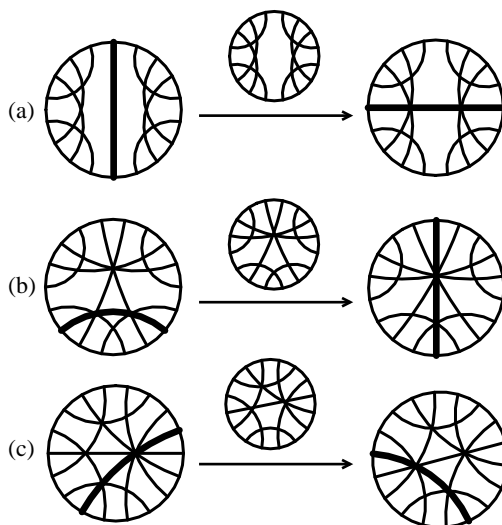


FIGURE 22. An untwisted-untwisted and two twisted-twisted elementary moves

figure 5(b). Notice that after the elementary move, a 1-handle piece forms again, and outside the 1-handle piece the chord diagram is unchanged, so δ and δ' have the same chord diagram. This means that there is a mapping class $\Phi \in \mathcal{MCG}$ such that $\Phi[\delta] = [\delta']$. This mapping class may always be taken to be a Dehn twist about the core of the 1-handle, as noted earlier for figure 5(b), and we call this a *Dehn twist elementary move* (if the chord diagram has symmetries, as in figure 23, we can also post-multiply the Dehn twist Φ by any mapping class which stabilizes $[\delta']$). The phenomenon of Dehn twist elementary moves is the tip of a big iceberg; in section V we make a general study of sequences of elementary moves representing Dehn twists, and this is used to obtain an automatic structure and prove quadratic computation time of our algorithm for the word problem in \mathcal{MCG} .

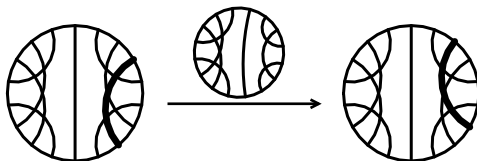


FIGURE 23. A Dehn twist elementary move

In the mixed case, Q is neither a twisted nor untwisted 4-gon and we say that Q is a *mixed* 4-gon (figure 21(b)). A *mixed* elementary move is usually the most difficult to visualize. Several examples of mixed elementary moves are shown in figure 24 and 25. Figure 24 shows examples where h lies on the boundary of a 1-handle piece, and figure 25 shows examples where h lies on the boundary of a twisted island; the opposite diagonal may be of one or the other type.

Exercise: Figures 24(c) and 25(b) are interesting because they return to the same chord diagram, hence δ and δ' differ by a mapping class. What are these mapping classes? To be more precise, how do they fit into Thurston's classification scheme of finite order, reducible, or pseudo-Anosov?

Exercise: Notice that among figures 22–25, we have managed to produce paths of elementary moves from

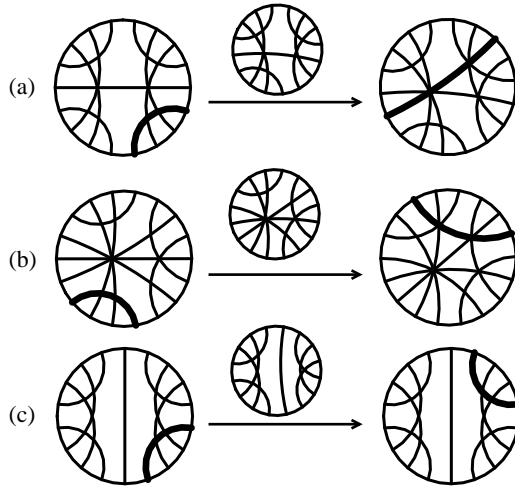


FIGURE 24. Mixed elementary moves where h bounds an untwisted island and a 1-handle piece

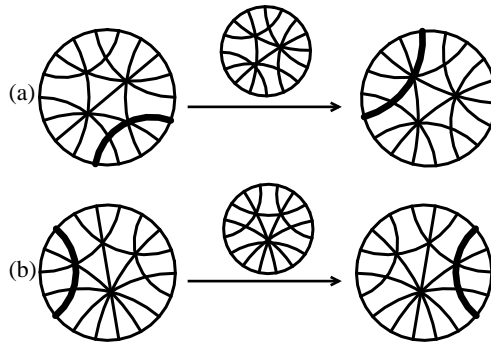


FIGURE 25. Mixed elementary moves where h bounds an untwisted island and a twisted island

T_1 to T_2, T_3, T_4, T_7, T_8 and T_9 . For example, follow the path

$$T_1 \xrightarrow{22(a)} T_2 \xrightarrow{24(a)} T_3 \xrightarrow{22(b)} T_4 \xrightarrow{24(b)} T_8 \xrightarrow{22(c)} T_7 \xrightarrow{25(a)} T_9$$

Construct enough chord diagrams of elementary moves to obtain the remaining chord diagrams T_5, T_6 . Getting T_5 is slightly tricky, because there is only one other chord diagram that T_5 may be accessed from by a single elementary move.

Exercise: How long is the shortest path from T_1 to T_7 ?

Having described in some detail how elementary moves are represented with chord diagrams, we remark that the computer representation of elementary moves using combinatorial diagrams is easily implemented. There is a simple algorithm which takes as input the combinatorial diagram $(\mathcal{E}, \text{Opp}, \text{Succ})$ of δ , together with the cycle of Opp representing h , and outputs the combinatorial diagram of δ' where $\delta \xrightarrow{h} \delta'$.

Once we know how to generate elementary moves on combinatorial diagrams, there is a simple algorithm for enumerating combinatorial types of ideal triangulations. The quotient of Y under the action of \mathcal{MCG} can be regarded as a finite, connected 1-complex, with a 0-cell for every combinatorial type of ideal triangulation,

and with a 1-cell for every combinatorial type of defect 1 arc system (more properly, the quotient complex should be thought of as an “orbi-complex” in the sense of Haefliger; for instance, if an edge in Y has an orientation reversing stabilizing element then its image in the quotient should be regarded as a half-edge with a “mirrored endpoint”). It is then easy to write an algorithm for constructing this 1-complex, say using a breadth first search: construct an initial chord diagram; initialize a queue with one entry for each chord of the initial chord diagram; now process the queue inductively, taking the first entry of the queue and performing the indicated elementary move; check if the new chord diagram has already been found, and if not add an entry to the end of the queue for each chord of the new chord diagram.

The result of this algorithm for a surface of genus 2 is shown in figure 26. This is what we call the “Connectivity Proof” for the enumeration of the nine chord diagrams in genus 2. Each chord is labelled, with chords in a diagram having the same label when there is an automorphism carrying one chord to the other. Elementary moves are also given labels; for instance, the elementary move between T_2 and T_3 labelled 1-5 means that chord 1 is removed from T_2 and chord 5 is inserted in T_3 (or vice versa). There is also a single mirrored 1-cell, which is drawn unmirrored as the edge labelled 7-7 going from T_5 to itself; note that this edge corresponds to a defect 1 chord diagram with an order 4 symmetry group that rotates the quadrilateral by $1/4$.

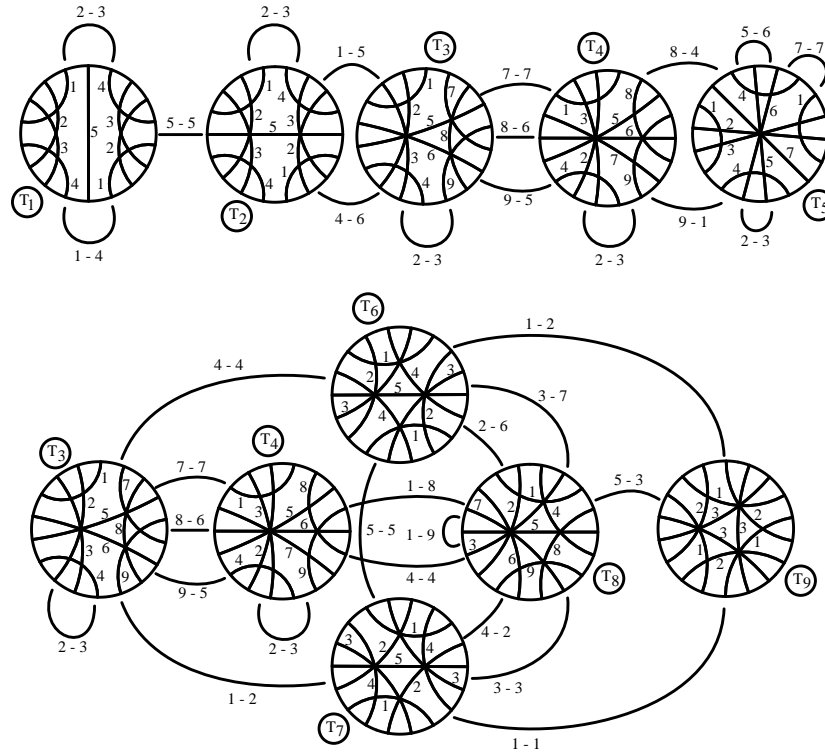


FIGURE 26. The chord diagrams of ideal triangulations and elementary moves on a once-punctured surface of genus 2. The top part of the diagram overlaps with the bottom part in triangulations T_3 and T_4 .

The end map of an elementary move.

For any elementary move $\delta \xrightarrow{h} \delta'$ where h' is the opposite diagonal of h , the ideal arc systems $\delta - h$ and $\delta' - h'$ are isotopic, hence by the lemma *Rigidity of ends* we have a well-defined bijection $\mathcal{E}(\delta - h) \rightarrow \mathcal{E}(\delta' - h')$

called the *end map*. This map may be implemented in chord diagrams as follows. Suppose that D is the chord diagram for δ , and let the chord corresponding to h also be denoted h . Index the chord ends of D except for h , starting at an arbitrary end with 1 and increasing in counter-clockwise order, skipping over the ends of h . Now when the chord h is erased and the opposite chord h' is inserted, resulting in the chord diagram D' , we have an indexing of the chord ends of D except for h . This indexing gives the end map, a bijection between chord ends of D except for h and chord ends of D' except for h' . Examples are shown in figures 27 and 28. The end map plays an important role in what follows.

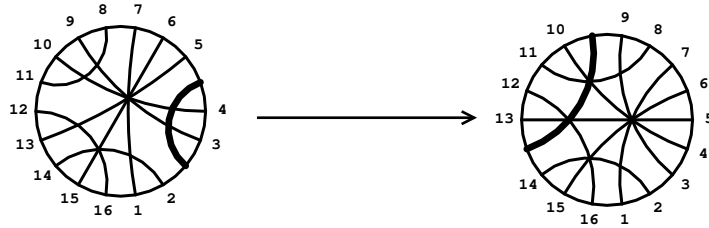


FIGURE 27. Chord ends with the same index correspond under the end map

Labelling elementary moves. Consider a labelled ideal triangulation (δ, e) , so that e is an end of an arc g of δ . Consider also an elementary move $\delta \rightarrow \delta'$ performed on an arc h of δ . We adopt the following convention for determining a labelling e' of δ' . If $g \neq h$ then set $e' = e$; whereas if $g = h$, let e' be the predecessor of e in $\mathcal{E}(\delta)$. In either case, e' lies on an arc of δ which is also an arc of δ' , hence the labelled ideal triangulation (δ', e') is defined. The complex \tilde{X} has a 1-cell with boundary certificate $([\delta, e], [\delta', e'])$. The image of this 1-cell downstairs in X is denoted $\{\delta, e\} \xrightarrow{h} \{\delta', e'\}$, and is called a *labelled elementary move*; in this notation, h should be regarded as a chord in the chord diagram for $\{\delta, e\}$.

In order to understand chord diagrams of labelled elementary moves, suppose that $D \rightarrow D'$ is the chord diagram of the labelled elementary move $\delta \rightarrow \delta'$. Let h be the removed chord of D , and let h' be the inserted chord of D' . Suppose that e is the labelled chord end in D . If e is not an end of h , then the labelled chord end e' of D' is just the image of e under the end map. On the other hand, if e is an end of h , then e' is the image under the end map of the predecessor of e , obtained by rotating e one notch clockwise. Examples are given in figure 27.

Relabelling moves.

We have already defined relabelling generators: given an ideal triangulation δ and two distinct arc ends e_1, e_2 of δ , there is an edge $[\delta, e_1, e_2]$ in X with boundary certificate $[\delta, e_1], [\delta, e_2]$. The image of this edge downstairs in X is denoted $\{\delta, e_1, e_2\}$ and is called a *relabelling generator*; it points from the vertex $\{\delta, e_1\}$ to $\{\delta, e_2\}$. Since the chord diagram D for δ has $12g - 6$ chord ends arrayed in circular order, then we can write $e_2 = \text{Succ}^r(e_1)$ for a unique $r \in \mathbf{Z}/12g - 6$. Then we say that e_2 is obtained from e_1 by *rotating r notches*, and we denote the relabelling generator as

$$\{\delta, e_1\} \xrightarrow{\text{Rotate}(r)} \{\delta, e_2\}$$

Figure 29 gives an example of a relabelling generator.

Proposition. *The groupoid \mathcal{MCGD} is generated by labelled elementary moves and relabelling generators. In fact, every groupoid element may be represented by a string of labelled elementary moves followed by a single relabelling generator.*

Proof. A few observations about relators make this obvious. First, by using relabelling relators, any consecutive sequence of relabelling generators may be replaced by a single relabelling generator. Second, by

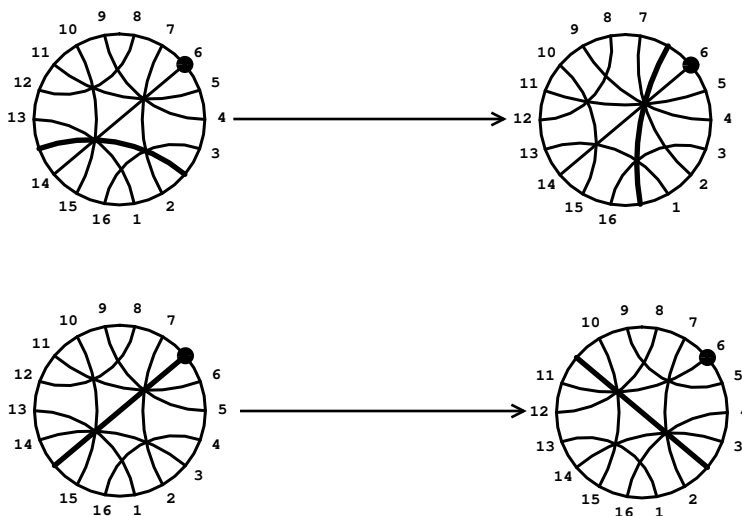


FIGURE 28. Some labelled elementary moves

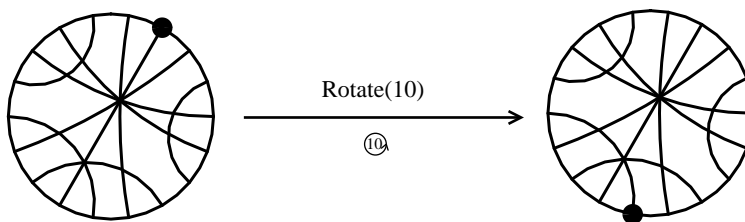


FIGURE 29. A relabelling generator (both notations will be used)

using elementary move relabellings, any relabelling generator followed by an elementary move generator may be replaced by an elementary move generator, followed by at most one relabelling generator. Third, also by using elementary move relabellings, any elementary move generator g_1 , may be replaced by a labelled elementary move g_2 followed by a relabelling generator. Given an arbitrary word, conglomerate all initial relabelling generators into one and push it past the first elementary move generator, then replace that by a labelled elementary move if necessary; now repeat the procedure starting with the next block of relabelling generators. \diamond

II. ASYNCHRONOUS NORMAL FORMS

In this section we describe normal forms for elements of \mathcal{MCGD} . The normal forms will be defined over the alphabet \mathcal{A}_0 consisting of all labelled elementary moves and relabelling generators. We shall construct a finite automaton \mathcal{M}_0 defined over \mathcal{A}_0 , and the normal forms will be the language \mathcal{L}_0 accepted by this automaton. First a quick review of finite automata over groupoid generators.

The automaton \mathcal{M}_0 will be a directed graph, whose vertices are called *states* and whose directed edges are called *arrows*. Each arrow will be named with an element of \mathcal{A}_0 . There will be a cellular map $p: \mathcal{M}_0 \rightarrow X$; each state s goes to a vertex $ps = D$, and each arrow going out of s is named by a generator going out of D which is identified with the image of that arrow under p . One state of \mathcal{M}_0 is specified as the *start state*, and it will map to the base vertex of X . Some subset of states are specified as the *accept states*. An *accept path* is a directed path from the start state to an accept state, and by reading off the names of edges along

that path we obtain a word in \mathcal{A}_0 , called an *accepted word*. The language \mathcal{L}_0 will be the set of all accepted words. Note that each accepted word represents an edge path in X starting at the base vertex.

The proof that \mathcal{L}_0 represents each element uniquely is given in section II.5 of [M], culminating in the proposition *Normal forms are regular* (the language \mathcal{L}_0 is defined differently in [M], but from the proof of *Normal forms are regular* the two definitions clearly give the same language). Section III describes an algorithm for computing the normal form representing a given word in the generators \mathcal{A}_0 ; from this description it is straightforward to show that \mathcal{L}_0 satisfies the asynchronous fellow traveller property, hence is an asynchronous automatic structure for \mathcal{MCGD} .

Remark 1: The words in \mathcal{L}_0 will each have at most one relabelling generator, and it is always the last letter. This is different from the convention adopted in the original version of [M], where the relabelling generator comes first. This change makes no difference in proving the asynchronous fellow traveller property, but it does simplify the description of an algorithm for computing normal forms.

Remark 2: From now on, we usually suppress the label in our notation for a labelled ideal triangulation, writing δ instead of the more formal (δ, e) .

The states of \mathcal{M}_0 .

Recall that normal forms for an asynchronous automatic structure on a groupoid must all start at some chosen base vertex. Once and for all, pick some labelled ideal triangulation δ_B as a base vertex of \tilde{X} , and the combinatorial type $\{\delta_B\}$ will be the base vertex of X . This choice is quite arbitrary, but for the figures to come we choose the base vertex given in figure 30. This pattern may be generalized to any genus g : take a chord diagram with g 1-handle pieces, none crossing any other, and then take the “fan triangulation” of the resulting untwisted $2g$ -gon, putting the labelled end just clockwise of the base of the fan.

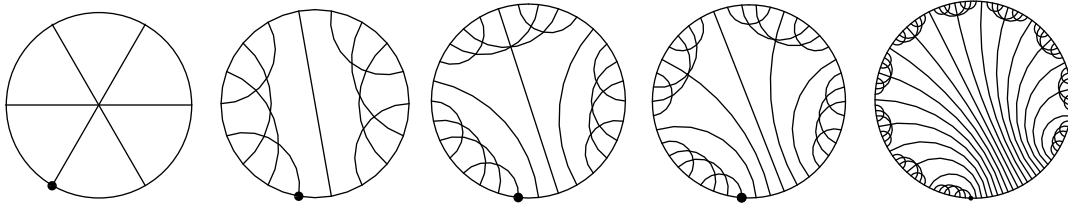


FIGURE 30. Our choice for a base vertex, in genus 1,2,3,4 and 10

A finite deterministic automaton can be thought of as a machine with a fixed, finite number of states and a memory of a fixed finite size. Usually the memory is incorporated into the state set, but thinking of the machine in this way allows us to focus on the question: what information does the machine need to remember? Answering this question tells us how to define the states.

The machine \mathcal{M}_0 that we construct will read edge paths in X starting at the base vertex. To motivate our description of \mathcal{M}_0 , we start with an informal description of the information that \mathcal{M}_0 has to remember as it reads along an edge path. Consider an edge path in X starting at $\{\delta_B\}$:

$$\{\delta_B\} \xrightarrow{e_1} \{\delta_1\} \xrightarrow{e_2} \dots \xrightarrow{e_I} \{\delta_I\}$$

This may be lifted uniquely to an edge path in \tilde{X} starting at δ_B :

$$\delta_B \rightarrow \delta_1 \rightarrow \dots \rightarrow \delta_I$$

As \mathcal{M}_0 reads the edge path in X , it will keep track of several pieces of information. It keeps track of the combinatorial type of δ_i , a finite amount of information. It also remembers some information about how δ_B is related to δ_i . In some cases certain arcs of δ_k will be isotopic to arcs of δ_B , and the automaton will

remember these arcs, again a finite amount of information. After a while, one would expect that there are none of these arcs left. But the automaton will still keep track of a tiny bit of information: where the end of an arc of δ_B is situated with respect to δ_i , again only a finite amount of information. This is formalized as follow.

In order to define the states of the automaton, pick once and for all an enumeration of the arcs of δ_B , $\{g_1, \dots, g_\kappa\}$ where $\kappa = \kappa(g) = 12g - 6$, and pick an orientation of each g_k , so we may speak of the *tail end* and *head end* of each g_k . (Note: we shall *not* need to list and orient the arcs of any other ideal triangulation; this choice is made only for δ_B .)

Consider an arbitrary ideal triangulation δ . As described in the *Tightness proposition* of [M], we may pull δ_B and δ tight with respect to one another, so that the following conditions are satisfied:

- (1) If some arc g_k of δ_B is isotopic to an arc of δ , then g_k is the same as some arc of δ . In this case we say that δ is *combed* along g_k .
- (2) If δ is uncombed along g_k then g_k is transverse to δ , and for each arc h of δ , there are no bigons of g_k and h . A *bigon* is a segment $\alpha \subset g_k$ and $\beta \subset h$, neither α nor β having p in its interior, such that $\alpha \cup \beta$ is a simple closed curve bounding a disc.

Furthermore, once δ is pulled tight with respect to δ_B , then δ is uniquely determined up to an isotopy preserving each arc of δ_B .

Having pulled δ tight with respect to δ_B , we may ask: Along which arcs of δ_B is δ combed? Furthermore, if δ is not combed along g_k , then the tail end of g_k must emerge from some prong of δ as shown in figure 31. From which prong of δ does $\text{Tail}(g_k)$ emerge?

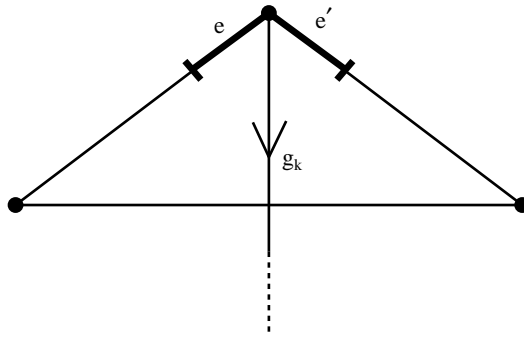


FIGURE 31. $\text{Tail}(g_k)$ emerges from $\pi = (e, e')$

The automaton \mathcal{M}_0 will keep track of the answers to these questions, but only up to the first uncombed arc in the list $\{g_1, \dots, g_\kappa\}$. That is, if g_k is the first uncombed arc, then the automaton marks the initial ends of g_1, \dots, g_{k-1} in δ , and it marks the prong of δ from which $\text{Tail}(g_k)$ emerges. Now we formalize the concept of a “marking” of δ .

Let δ be a labelled ideal triangulation. Let $\mathcal{E}(\delta)$ be the set of ends of δ , and let $\mathcal{P}(\delta)$ be the set of prongs. A *marking* of δ is an injective map μ , whose domain is an initial segment $\{1, \dots, k\}$ of $\{1, \dots, \kappa = 12g - 6\}$, and whose range is $\mathcal{E}(\delta) \cup \mathcal{P}(\delta)$. Additional conditions will be imposed on a marking below, but first we motivate these conditions by considering the marking that δ_B induces on δ .

Every ideal triangulation δ will have a *base marking*, which is induced by δ_B as follows. First of all, if $\delta = \delta_B$, then the initial end of each g_k is marked with a k , and no prong is marked. Next, assuming that $\delta \neq \delta_B$, then some arc of δ_B will be uncombed with respect to δ ; let g_k be the first uncombed arc. Then δ is combed along g_i for $1 \leq i < k$ and the initial end of g_i is marked with an i in δ . Furthermore, the prong from which g_k emerges will be marked with a k . This defines the base marking of an ideal triangulation.

Note that the base marking of δ is *not* a combinatorial invariant of δ . Nonetheless, base markings enjoy certain combinatorial properties, which we impose as defining conditions on a general marking. For a general marking μ of δ , we require:

- (1) For each arc h of δ , at most one end of h is marked by μ .
- (2) At most one prong is marked by μ .
- (3) If there is no marked prong, then every arc of δ has a marked end.
- (4) If there is a marked prong, it must be the last item marked.
- (5) If there is a marked prong, the arc opposite the marked prong must not have a marked end.

It may be that there is no marked end at all; in some sense this will be the generic case.

To see why property (5) is satisfied by the base marking, note in figure 31 that the arc opposite $\pi = (e, e')$ cannot have a marked end, because otherwise that arc would then be some g_i , and its interior would intersect the interior of g_k , contradicting the fact that $g_i, g_k \in \delta_B$ have disjoint interiors.

A *marked ideal triangulation* is a pair (δ, μ) where δ is a labelled ideal triangulation, and μ is a marking of δ . Note that properties (1–4) are combinatorial properties, hence $\text{Homeo}(S)$ acts on marked ideal triangulations, and we may speak about the combinatorial type of a marked ideal triangulation. The combinatorial type of (δ, μ) is denoted $\{\delta, \mu\}$.

The combinatorial type of a marked ideal triangulation (δ, μ) may be represented by a marked chord diagram. Let D be the chord diagram of δ . If $\mu(i)$ is a marked end of δ , we write the numeral i adjacent to the corresponding chord end of D . If $\mu(k)$ is a marked prong, we write a star $*$ next to the corresponding end gap of D ; it is unnecessary to actually write the k , because the value of k can be recovered as the least natural number which is not an end marking. Figure 32 gives an example of a marked ideal triangulation and its chord diagram; the end marked 1 is also the labelled end in this example.

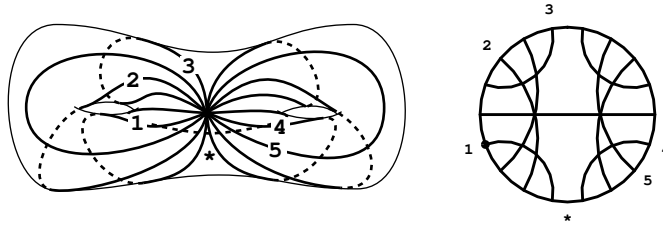


FIGURE 32. A marked ideal triangulation and its chord diagram

The states of \mathcal{M}_0 may now be defined. There will be one state for each combinatorial type of marked ideal triangulation, all of which are accept states. Furthermore there is one failure state F_v for each vertex v of X . The start state of \mathcal{M} is the combinatorial type of the base marking on δ_B itself.

We use the following convention for choosing the start state. We have already chosen a labelled end for δ_B . Mark that end with $k = 1$, and go around the ends in the clockwise direction; as an end of a new arc is encountered, mark that end with the next value of k . The end marked k is $\text{Tail}(g_k)$. Figure 33 shows start states for genus 1, 2, and 3, with markings chosen by this convention.

Arrows of \mathcal{M}_0 .

Before discussing arrows of \mathcal{M}_0 , we need some observations and notation concerning states. First observe how the mapping $p: \mathcal{M}_0 \rightarrow X$ is defined on a state s : identifying s with a marked chord diagram, erasing the marking leaves a labelled chord diagram which is identified with the image vertex $D = ps$. As mentioned earlier, for any arrow $s \xrightarrow{w} s'$ where $w \in \mathcal{A}_0$, the image of this arrow under p will be the edge in X identified with w . The arrows can be denoted in shorthand, using the fact that each element of \mathcal{A}_0 is either a relabelling generator or a labelled elementary move generator. If w is a $\xrightarrow{\text{Rotate}(k)}$ relabelling generator then the arrow

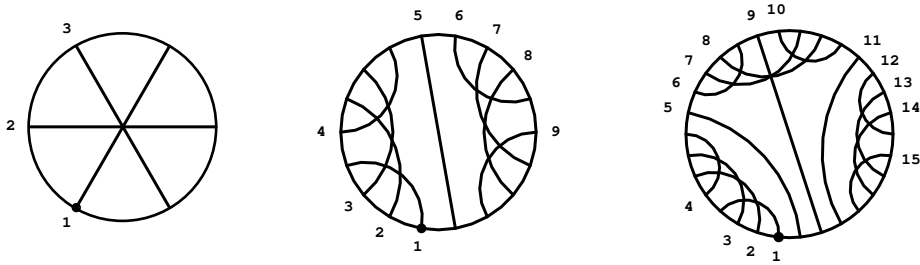


FIGURE 33. The start states for genus 1, 2, and 3

is denoted $s \xrightarrow{\text{Rotate}(k)} s'$, and if w is a labelled elementary move generator performed on a chord h then the arrow is denoted $s \xrightarrow{h} s'$. In the next several paragraphs we will describe further shorthand for determining the chord h .

Consider a marked ideal triangulation (δ, μ) . If there is a marked prong, the triangle having that prong as a corner is called the *marked triangle*, and the marked prong is indicated with a $*$. We usually orient the marked triangle so that the marked prong forms a downward pointing angle, bisected by the $-y$ direction, as in figure 34. The ends to the Left and Right of the marked prong are denoted e^L, e^R as in figure 34; formally the marked prong is equal to the ordered pair (e^L, e^R) . The arcs with these ends are denoted h^L, h^R . The third side of the marked triangle, the “arc opposite the $*$ ”, is denoted h^{Opp} . In a marked chord diagram, we usually place the “ $*$ ” at the bottom of the diagram, so that the chord ends e^L, e^R and the chords h^L, h^R, h^{Opp} are as shown in figure 34, depending on whether the marked triangle is twisted or untwisted.

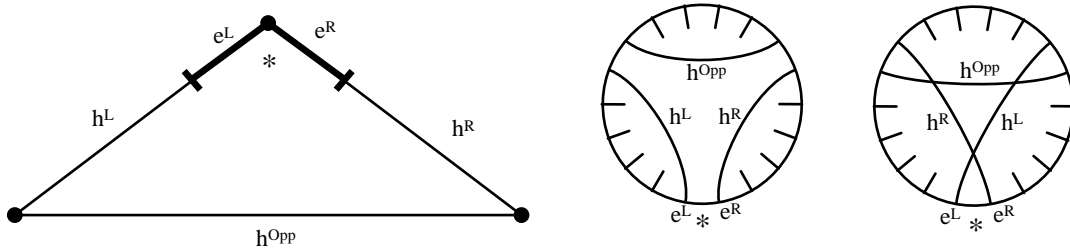


FIGURE 34. Items associated with the marked triangle

Given a marked ideal triangulation (δ, μ) , we define the combinatorial property of *consistency*:

- (1) If there is a marked end, then the end $\mu(1)$ is the labelled end.
- (2) If there is no marked end, then the end e^L is the labelled end.

In a marked chord diagram, consistency means that if there is a marked chord end then the labelling dot is located at the same chord end as the numeral 1; and if there is no marked chord end then the labelling dot is just to the left of the $*$. Thus, in a consistent marked chord diagram the marking determines the labelling; for this reason, we shall often leave the labelling dot out of our chord diagrams, so any unlabelled but marked chord diagram is assumed by default to be consistent. As we shall see, as long as an accept word consists of labelled elementary moves, it stays among the consistent states; as soon as the word has a relabelling generator it moves to an inconsistent state; and if any further letters occur it moves to the failure states.

Note that the start state is consistent, by our convention for marking δ_B .

Now we describe arrows of \mathcal{M}_0 , first the arrows leading out of failure states. For each generator $\alpha \in \mathcal{A}_0$ leading from a vertex v to a vertex w of X , there is an arrow $F_v \xrightarrow{\alpha} F_w$. Thus, the set of failure states forms a dead end set: all arrows leading out of this set lead back into it (from which it follows that the language \mathcal{L}_0 of accepted words is prefix closed).

Next we describe relabelling arrows. Consider a relabelling generator $v \xrightarrow{\text{Rotate}(r)} w$ and an accept state s lying over v . If s is inconsistent, there is a failure arrow $s \xrightarrow{\text{Rotate}(r)} F_w$. If s is consistent, then rotate the labelling dot r notches counterclockwise, leaving the marking unsullied, to obtain an inconsistent state s' lying over w , and define an arrow $s \xrightarrow{\text{Rotate}(r)} s'$. See figure 35 for an example.

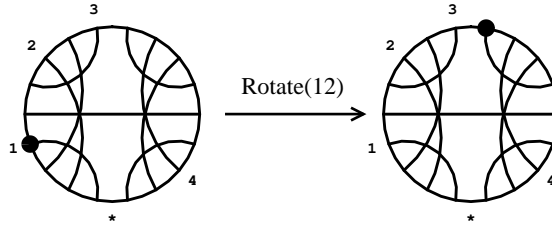


FIGURE 35. A relabelling arrow

To describe labelled elementary move arrows, consider a consistent marked ideal triangulation (δ, μ) , and a labelled elementary move $\delta \xrightarrow{h} \delta'$. There will be an arrow $\{\delta, \mu\} \xrightarrow{h} s$, whose tip s is some state lying over the vertex $\{\delta'\}$, either the failure state $F_{\{\delta'\}}$ or the accept state $\{\delta', \mu'\}$ for some marking μ' of δ' . The rule for specifying s is given in three cases:

- (1) h has a marked end.
- (2) h has no marked end but one of e^L or e^R is an end of h .
- (3) None of the above.

Note that these cases are combinatorial properties of the triple (δ, μ, h) .

Case (3) can be dispensed with immediately: the tip of the arrow is the failure state $s = F_{\{\delta'\}}$.

In each of cases (1) and (2), we must specify a marking μ' of δ' , and the tip of the arrow will be the state $\{\delta', \mu'\}$. Despite the fact that case (3) has been dispensed with, in certain subcases of case (3) we will also specify a marking μ' ; this will be useful in describing the algorithm for computing normal forms.

The rule for specifying μ' must be combinatorially invariant, that is, the chord diagram for $\{\delta, \mu\}$, together with the chord for h , must determine the chord diagram for $\{\delta', \mu'\}$. Also, assuming that μ is the base marking of δ , then μ' must be the base marking of δ' . We shall keep these considerations in mind in defining the rule for μ' .

Case 1: h has a marked end. Suppose that an end of h is marked with j . Assuming for the moment that μ is the base marking of δ , we may derive the base marking μ' of δ' as follows. Since h has an end marked j , then $h = g_j$. Also, δ is combed along the arcs g_1, \dots, g_{j-1} ; since h is distinct from these arcs, then δ' is also combed along these arcs, so μ' places the marks $1, \dots, j-1$ on the same arc ends that μ placed them. Finally, g_j is the first arc along which δ' is uncombed, and figure 36 shows the prong of δ' from which g_j emerges, which is therefore the marked prong of δ' .

These properties of μ' may be stated as a combinatorial property in the following manner.

- (1) The domain of μ' is $1 \leq i \leq j$.
- (2) If $1 \leq i < j$, then $\mu(i)$ is an end of δ' as well as of δ , and we define $\mu'(i) = \mu(i)$.
- (3) In $\mathcal{E}(\delta)$, let $e' = \text{Pred}(\mu(j))$ and let $e'' = \text{Succ}(\mu(j))$. Then the prong (e', e'') is an element of $\mathcal{P}(\delta')$, and we define $\mu'(j) = (e', e'')$.

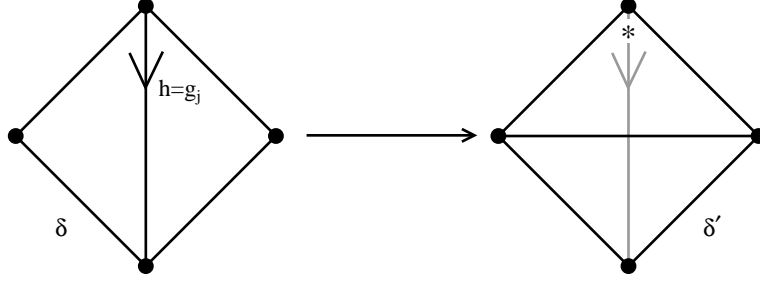


FIGURE 36. An elementary move $\delta \xrightarrow{h} \delta'$ where $h = g_j$ has an end marked j

We may now define an arrow $\{\delta, \mu\} \xrightarrow{h} \{\delta', \mu'\}$ in \mathcal{M}_0 . This arrow is called a j -marked elementary move or a j -marked arrow, and is denoted in shorthand as $\{\delta, \mu\} \xrightarrow{j} \{\delta', \mu'\}$.

Observe that the marked ideal triangulation (δ', μ') is still consistent. To see why, if $j > 1$ then by consistency of (δ, μ) , the labelled end of δ is $\mu(1)$; since this is also an arc end of δ' then it is the labelled end of δ' by definition of a labelled elementary move; but this end is also $\mu'(1)$ by definition of μ' , proving consistency. And if $j = 1$ then the rule for a labelled elementary move says that the labelling is moved to e' , the predecessor of $\mu(1)$, which is then the labelled end of δ' ; but this equals e^L in δ' , and since δ' has no marked ends then consistency is proved.

To implement a j -marked arrow on chord diagrams, suppose s is the marked chord diagram for $\{\delta, \mu\}$, and the elementary move is performed on the chord h with an end marked j . Now erase all end markings greater than j , erase the chord h , place a $*$ in the gap vacated by the end marked j , then draw in the new chord to obtain the marked chord diagram s' for $\{\delta', \mu'\}$. Some examples are given in figure 37.

Case 2: h has no marked end, but one of e^L or e^R is an end of h . We define a *parity* to be an element of the set $\{L, R\}$, and we often use the variable d to represent a parity. Let $* = \mu(j)$ be the marked prong, so $* = (e^L, e^R)$. Fix $d \in \{L, R\}$ so that e^d is an end of h .

Assuming for the moment that μ is the base marking of δ , then the base marking μ' of δ' may be derived as follows. For $1 \leq i < j$ then δ is combed along g_i and $h \neq g_i$, therefore δ' is combed along g_i , so μ' places the marks $1, \dots, j-1$ on the same arc ends that μ placed them. Figure 38 shows the two situations where e^L and e^R are ends of h : the prong $*$ is the one from which g_j emerges in δ , and when the elementary move is performed then $*$ coalesces with another prong of δ to form a prong of δ' , from which g_j emerges in δ' , hence this prong is $\mu'(j)$, marked $*$ in δ' . This determines the marking μ' , as shown in figure 38.

The rule for μ' may be stated in a combinatorially invariant way as follows.

- (1) The domain of μ' is equal to the domain of μ , namely $\{1, \dots, j\}$.
- (2) If $1 \leq i < j$ then $\mu(i)$ is an end of δ' as well as of δ , and we define $\mu'(i) = \mu(i)$.
- (3) If e^d is an end of h for some parity $d \in \{L, R\}$, in $\mathcal{E}(\delta)$ let $e' = \text{Pred}(e^d)$ and let $e'' = \text{Succ}(e^d)$. Then the prong (e', e'') is an element of $\mathcal{P}(\delta')$ and we set $\mu'(j) = (e', e'')$.

We now define an arrow $\{\delta, \mu\} \xrightarrow{h} \{\delta', \mu'\}$. This arrow is called a d -marked elementary move or just a d -arrow, and is denoted $\{\delta, \mu\} \xrightarrow{d} \{\delta', \mu'\}$. We also say that this is a *parity* arrow, and a j -marked arrow is a *non-parity* arrow.

Observe again that the marked ideal triangulation (δ', μ') is consistent. If $j > 1$ then by consistency of (δ, μ) the labelled end of δ is $\mu(1)$; and since this is not an end of h then this is also the labelled end of δ' , and it is equal to $\mu'(1)$, proving consistency. Whereas if $j = 1$, then e^L is the labelled end in δ by consistency; then if $d = R$, then e^L is still an end of δ' so it is the labelled end of δ' , but it is also e^L in δ' proving consistency; whereas if $d = L$ then the label is first moved to the predecessor e' of e^L , which is then the labelled end of δ' , but this is also e^L in δ' , proving consistency.

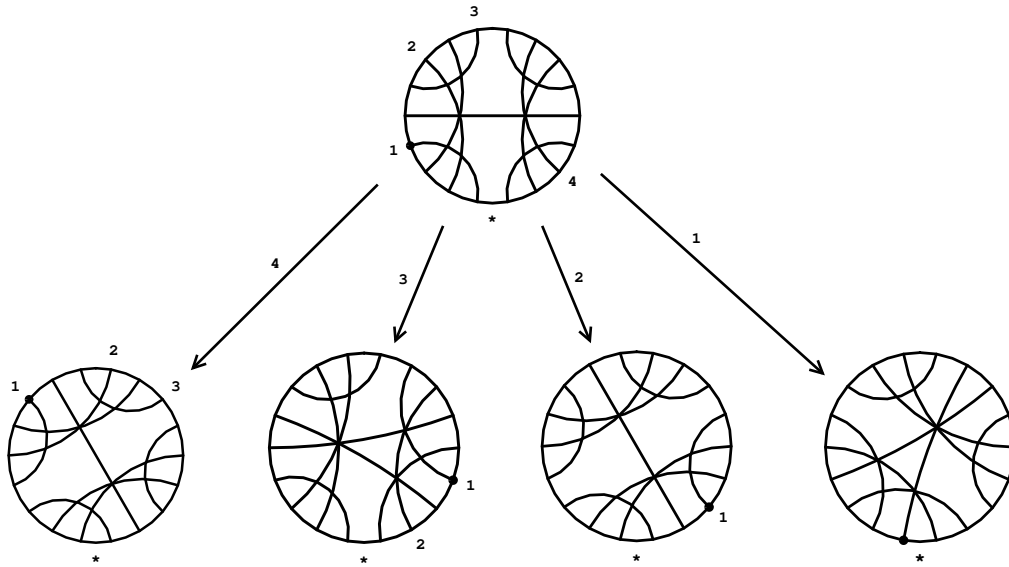


FIGURE 37. Leaving from the same state as the arrow in figure 35, there are j -marked arrows for each $j = 1, 2, 3, 4$. After doing the elementary move, putting the $*$ in the gap vacated by j , and erasing end marks greater than j , then the chord diagram is rotated so that the $*$ appears at the bottom.

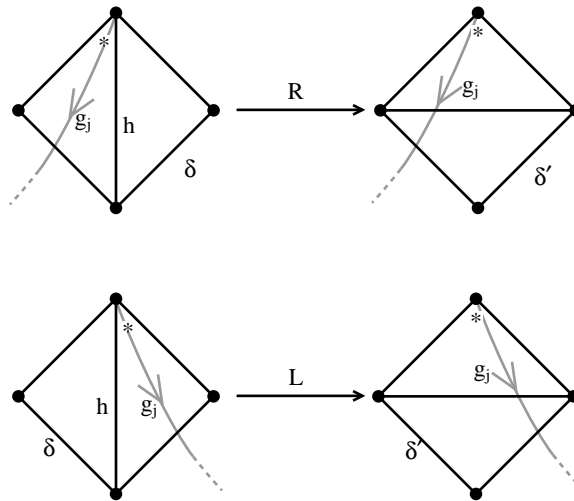


FIGURE 38. An elementary move $\delta \xrightarrow{h} \delta'$ where h has no marked end, but h has either e^L or e^R as an end

To implement a parity d elementary move on the chord diagram s for $\{\delta, \mu\}$, first locate the chord end e^d adjacent to the $*$, then erase that chord, coalescing $*$ and another gap of s into a larger gap, leave the

marking $*$ in the larger gap, leave all end markings where they are, then insert the opposite chord to form the chord diagram s' for $\{\delta', \mu'\}$. Some examples are shown in figure 39.

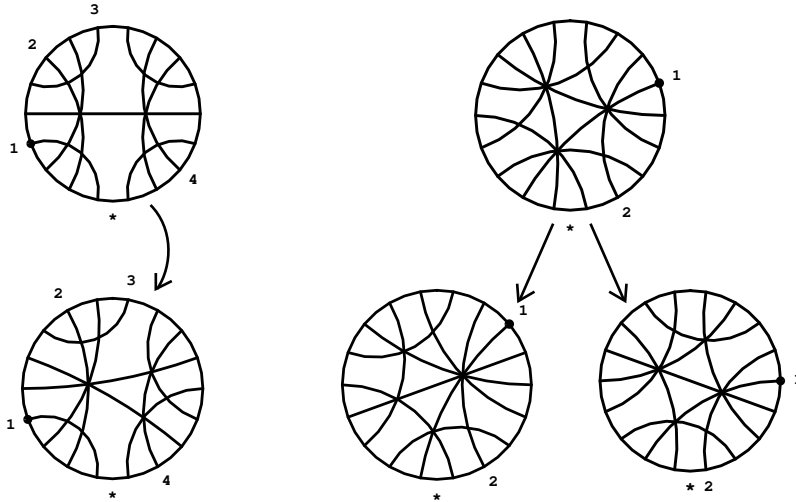


FIGURE 39. Some parity arrows. Parity is indicated by which side of the $*$ the tail of the arrow is closest to. The first example uses, once again, the same initial state as figure 35; there is only a Right parity arrow with this initial state, because only h^R has no marked ends. The second example has both Left and Right parity arrows.

In each of cases 1 and 2, we have constructed an accept arrow of \mathcal{M}_0 . Collectively, these arrows, the parity and non-parity arrows, will be called *good elementary moves*. Here are a few random comments about good elementary moves.

Comment 1: Observe that the start state is consistent, and a good elementary move always leads from a consistent state to a consistent state. Therefore:

Consistency lemma. *Every path of good elementary moves in \mathcal{M}_0 , beginning at the start state, stays among consistent states.* \diamond

This observation is what prompted us to change the normal forms from the early version of [M], where the relabelling arrow was located at the beginning. When the relabelling arrow is located at the end, then the consistency lemma makes it easy to keep track of the labelled end, and there are some simplifications in the algorithm for computing normal forms.

Comment 2: In figures, we depict good elementary moves vertically, drawing D above D' . Bad elementary moves, defined below in case 3, are depicted as nonvertical arrows.

Comment 3: If $D \rightarrow D'$ is a good elementary move, then the chord diagram D' always has a marked prong $*$, and the inserted chord in D' is always the chord opposite the $*$.

Comment 4: As shown by example in figure 39, given a consistent state D of \mathcal{M}_0 , there may be both Right and Left arrows leading from D , or just one, or neither, depending on which of the chords h^L, h^R have marked ends. For example, the start state never has parity arrows, since every chord has a marked end.

Case 3: h has no marked end, and neither e^L nor e^R is an end of h . We have already constructed a failure arrow $\{\delta, \mu\} \xrightarrow{h} F_{\{\delta'\}}$. Nonetheless, in one subcase of case 3 we shall specify a marking μ' of δ' , and we shall say that $\{\delta, \mu\} \xrightarrow{h} \{\delta', \mu'\}$ is a *bad elementary move*. This will *not* be an arrow in the automaton \mathcal{M}_0 ,

but it will be a useful relation among states of \mathcal{M}_0 . In another subcase, we shall also see how *inverse good elementary moves* arise. Bad and inverse good elementary moves will be useful in describing the algorithm for computing normal forms.

Recall the notation h^{OPP} for the arc of δ opposite the marked prong $*$. We consider two subcases of case 3, distinguished by whether or not $h = h^{\text{OPP}}$. Note that “ $h = h^{\text{OPP}}$ ” is a combinatorial property of the triple (δ, μ, h) .

Case 3.1: $h \neq h^{\text{OPP}}$. Assuming μ is the base marking of δ , the base marking μ' for δ' is determined as follows. Let $* = \mu(j)$ be the marked prong of δ . Then δ is combed along the arcs g_1, \dots, g_{j-1} . Not being in case 1, then h has no marked end, so δ' is also combed along the arcs g_1, \dots, g_{j-1} , and μ' places the marks $1, \dots, j-1$ on the same arcs that μ placed them. Not being in case 2, then $h \neq h^L, h^R$, and being in case 3.1 then $h \neq h^{\text{OPP}}$, hence the prong $*$, from which g_j emerges in δ , is still a prong of δ' and g_j still emerges from it, so μ' places the mark j on $*$.

This rule may be stated in a combinatorially invariant manner as follows:

- (1) The domain of μ' is the same as μ , namely $\{1, \dots, j\}$.
- (2) $\mu(i) = \mu'(i)$ for $1 \leq i \leq j$.

It is evident that (δ', μ') is consistent. We shall say that $\{\delta, \mu\} \rightarrow \{\delta', \mu'\}$ is a *bad elementary move*. We emphasize: this does *not* define an arrow in \mathcal{M}_0 , merely a relation among states in \mathcal{M}_0 .

The chord diagram for a bad elementary move is easily implemented: starting with the chord diagram D for $\{\delta, \mu\}$, the removed chord h has no marked end, no end adjacent to the $*$, and is not opposite the $*$; hence the end markings and the $*$ may all be left in place as the chord is removed and the opposite chord is inserted, yielding the chord diagram D' for $\{\delta', \mu'\}$. In figures, bad elementary moves are depicted as nonvertical arrows, with D' usually to the right of D , and with the removed chord of D darkened. An example is shown in figure 40. In depicting bad elementary moves, there are no special conventions for specifying the chord on which the move is performed, so we adopt the convention of darkening that chord.

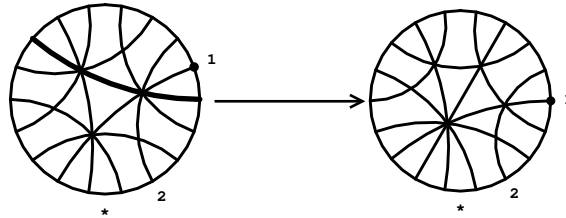


FIGURE 40. A bad elementary move

Case 3.2: $h = h^{\text{OPP}}$. In this case, assuming that μ is the base marking of δ , it is impossible to give a combinatorially invariant description of the base marking μ' of δ' . The reason is that the elementary move $\delta' \rightarrow \delta$, in which h^{OPP} is the inserted arc, gives rise to a good elementary move $\{\delta', \mu'\} \rightarrow \{\delta, \mu\}$, and this could be either a parity marked elementary move of either parity $d \in \{L, R\}$, or a nonparity elementary move marked by some value $j = 1, \dots, \kappa$; the combinatorial type $\{\delta', \mu'\}$ depends on the value of d or j , and on the placing of additional end markings in $\{\delta', \mu'\}$. Whatever case applies, we refer to $\{\delta, \mu\} \rightarrow \{\delta', \mu'\}$ as an *inverse good elementary move*.

Normal forms. We have finished the construction of \mathcal{M}_0 , and the language \mathcal{L}_0 accepted by \mathcal{M}_0 is our language of normal forms. In [M] it is proved that \mathcal{L}_0 contains a unique representative for each element of \mathcal{MCGD} whose initial vertex is the base vertex of X . Here is a quick summary of the proof.

Suppose that δ is an arbitrary unlabelled ideal triangulation on S . Our task is to define a path of elementary moves $\delta_B = \delta_N \rightarrow \dots \rightarrow \delta_0 = \delta$, so that when the ideal triangulation δ_i is equipped with its

base marking μ_i , then we obtain an accept edge in the automaton $\{\delta_N, \mu_N\} \rightarrow \cdots \rightarrow \{\delta_0, \mu_0\}$. The path is defined in reverse order, as follows. Assume by induction that $\delta_0, \dots, \delta_n$ have been defined. Recall the *Tightness proposition* of [M], which says that δ_n and δ_B may be pulled tight with respect to one another. Let g_i be the first arc of δ_B along which δ_n is uncombed. Then g_i must emerge from a certain prong of δ_n , as shown in figure 31 (this is the marked prong “*”, using the base marking). Now let h be the first arc of δ crossed by g_i (this is the arc h^{OPP} , using the base marking). Then δ_{n+1} is obtained by performing the elementary move $\delta_n \xrightarrow{h} \delta_{n+1}$. The main work of the proof is to show (1) this sequence eventually stops at δ_B ; and (2) $\{\delta_{n+1}, \mu_{n+1}\} \rightarrow \{\delta_n, \mu_n\}$ is an arrow in \mathcal{M}_0 .

The structure of the automaton \mathcal{M}_0 . Before proceeding with the description of the algorithm for computing normal forms, we discuss the automaton \mathcal{M}_0 and its language \mathcal{L}_0 . As mentioned earlier, the language \mathcal{L}_0 forms an asynchronous automatic structure for \mathcal{MCGD} , and we must understand certain of its properties in order to construct a synchronous automatic structure.

We have seen that the set of failure states is a dead end set. The accept states are partitioned into consistent and inconsistent states; each relabelling arrow from a consistent state goes to an inconsistent state, and each arrow from an inconsistent state goes to a failure state. All arrows leading between consistent states are labelled elementary move arrows. This forces each word in \mathcal{L}_0 to consist of a sequence of zero or more labelled elementary moves, followed by zero or one relabelling move.

The consistent accept states can be partitioned into subsets called *levels*, forming a sequence $\mathcal{M}_0^B, \mathcal{M}_0^\kappa, \dots, \mathcal{M}_0^1$ where $\kappa = 12g - 6$. First there is the *base level* \mathcal{M}_0^B , consisting of those consistent marked chord diagrams where every chord has a marked end and no prong is marked. The start state lies in \mathcal{M}_0^B . Going to deeper levels, each consistent accept state not in \mathcal{M}_0^B has a prong marked by some $k = 1, \dots, \kappa$, and this state lies in \mathcal{M}_0^k . Recall that our convention in diagrams is to mark the prong with a *, and k is characterized as the least integer ≥ 1 which is not an end marking. Thus, the deepest level \mathcal{M}_0^1 consists of states with no end markings.

If $1 \leq k < \kappa$, and if s is a state in some level above \mathcal{M}_0^k , then there is a k -arrow leading from s into the level \mathcal{M}_0^k ; just do an elementary move on the chord of s with end marked k . Notice that each elementary move arrow leading out of the start state (or any state in \mathcal{M}_0^B) leads to an accept state, because in the chord diagram for the start state each chord has a marked end. Given $1 \leq k \leq \kappa$ and a state D in \mathcal{M}_0^k , and given $d \in \{L, R\}$, if the chord h^d has no marked end then there is a d -elementary move arrow leading from D to another state in \mathcal{M}_0^k . Thus, each arrow either stays in the same level or leads to a lower level, the lowest level being \mathcal{M}_0^1 .

Note that there are many inaccessible states in \mathcal{M}_0 . In particular, every state in \mathcal{M}_0^B except the start state is inaccessible. However, note also that our choice of a base vertex in X and a start state in \mathcal{M}_0^B is somewhat arbitrary: we could choose any state in \mathcal{M}_0^B as the start state, thereby choosing the image vertex in X as the base vertex. These will all lead to different asynchronous automatic structures on \mathcal{MCGD} .

We may count states in each level of \mathcal{M}_0 as follows. Let m_g be the number of vertices in X , i.e. the number of labelled chord diagrams. We have seen earlier that $m_2 = 105$ and $m_3 = 50050$. The number of states in \mathcal{M}_0^1 is m_g , because there is a unique way to insert a marked prong in a labelled chord diagram to make a consistent marked chord diagram: insert the prong just counterclockwise of the labelled end. The number of states in \mathcal{M}_0^2 is $m_g(\kappa - 2)$, because the end marking 1 must be on the labelled end, and the marked prong may be chosen freely among all κ prongs except that it may not be one of the two prongs opposite the marked chord. The number of states in \mathcal{M}_0^3 is $m_g(\kappa - 2)(\kappa - 4)$, because the end marking 1 is determined, the end marking 2 may be chosen freely among the ends of the remaining unmarked chords, and the prong marking may be chosen freely among the prongs not opposite the two marked chords. In general, the number of states in \mathcal{M}_0^k is $m_g(\kappa - 2)(\kappa - 4) \dots (\kappa - 2k + 2)$. By far most of these states are inaccessible, especially in the base level and the highest levels. On the other hand, it is possible to show that \mathcal{M}_0^1 is a strongly connected graph, hence all of its states are accessible. If one wanted to efficiently construct all the accessible states, it would be best to use a breadth or depth first search algorithm beginning with the

start state.

From the structure of \mathcal{M}_0 just described, every word in \mathcal{L}_0 may be factored as follows. If w is an accepted word, then we may factor w into subwords as $w = w^k \circ \dots \circ w^1 \circ r$, where the subword w^j , if it is not empty, begins with a j -arrow and is followed by parity arrows in \mathcal{M}^j , and the subword r is either empty or is a single relabelling move. We call this the factorization of w into *uncombing blocks*; the idea is that as a new uncombing block is entered, a new ideal arc is being uncombed. Any non-empty uncombing block w^j may be written uniquely as a single j -elementary move, followed by maximal subwords of constant parity; the non-parity move is absorbed into the following subword of constant parity, and we obtain the factorization of w^j into *parity blocks*. This factorization is crucial to understanding synchronization.

III. AN ALGORITHM FOR COMPUTING NORMAL FORMS

To start the algorithm:

Input. A path of labelled elementary moves and relabelling moves, starting at the base vertex D_0 of X :

$$w := D_0 \xrightarrow{w_1} D_1 \xrightarrow{w_2} \dots \xrightarrow{w_N} D_N$$

This path can be described with pencil and paper as a sequence of labelled chord diagrams, with the initial diagram D_0 chosen, say, by the convention given in figure 30. An example is given in figure 41.

Throughout the description of the algorithm, we use the following notational conventions. Capital letters like D or V, W, U will be used to denote labelled but unmarked chord diagrams, and the lower case letter s will be used to denote marked chord diagrams, and on a consistent state we will often omit the labelling. Given a marked chord diagram denoted with subscripts or primes, such as s'_0 , the corresponding unmarked chord diagram ps'_0 will be denoted V'_0 . We will also use lower case letters like w, v for paths of marked or unmarked chord diagrams.

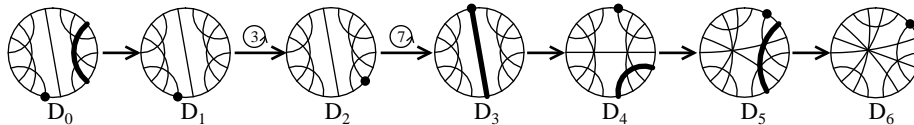


FIGURE 41. Example input for the algorithm

The algorithm will work by successively computing, for $t = 0, \dots, N$, the normal form v^t representing the groupoid element $\bar{w}(t)$ where $w(t)$ is the length t prefix of w :

$$w(t) := D_0 \xrightarrow{w_1} D_1 \xrightarrow{w_2} \dots \xrightarrow{w_t} D_t$$

Once v^{t-1} is computed, then v^t will be computed by homotoping the path $v^{t-1}w_t$ through a sequence of relators in X . In section V we shall estimate the number of relators used, and we will prove that the total number of relators needed to calculate v^N is bounded by $(12g - 6)N^2$; from the results of this section it will be clear that the task of deciding which relator to apply at any moment takes constant time.

The algorithm is initialized by computing v^0 and v^1 :

Initialization, step 1. Let s_0 be the start state of \mathcal{M}_0 . Set v^0 to be the empty path in \mathcal{M}_0 based at s_0 .

This step can be implemented by marking the chord ends of the base vertex D_0 , say by the convention chosen in figure 33, which in genus 2 is reproduced in figure 42.

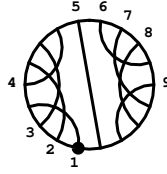


FIGURE 42. The normal form v^0 is the empty path based at the start state s_0 .

Initialization, step 2. Given the start state s_0 , the generator $w_1 := (ps_0 = D_0) \rightarrow D_1$ lifts to an arrow $s_0 \xrightarrow{w_1} s'_0$, which is the normal form v^1 .

To justify this step, note that any arrow $s_0 \xrightarrow{w_1} s'_0$ is an accept arrow when s_0 is the start state. If $w_1 := D_0 \xrightarrow{\text{Rotate}(r)} D_1$ is a relabelling arrow this follows because s_0 is consistent, and we get a relabelling generator $s_0 \xrightarrow{\text{Rotate}(r)} s'_0$. If $w_1 := D_0 \xrightarrow{h} D_1$ is a labelled elementary move, this follows because every chord in s_0 has a labelled end, so we get a j -marked arrow $s_0 \xrightarrow{j} s'_0$ where h has an end marked j .

Using $D_0 \rightarrow D_1$ as given in figure 41, we see that this yields a j -marked arrow with $j = 8$, as shown in figure 43. In figure 43 and later examples, we represent normal forms as vertical paths going downward; unmarked paths in X are represented as nonvertical paths going rightward.

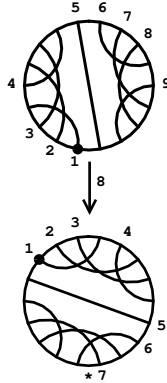


FIGURE 43. v^1 consists of a single arrow, the j -marked arrow with $j = 8$, coming out of the start state

Main loop. For each $n = 1, \dots, N$, let $v^{n-1} := s_K \rightarrow \dots \rightarrow s_0$ be the normal form representing $\overline{w}(n-1)$. Using the subroutine Do one move, compute the normal form v^n representing $\overline{w}(n)$.

The reason for backwards indexing of states in a normal form, such as $v^{n-1} := s_K \rightarrow \dots \rightarrow s_0$, is that our algorithm will process normal forms from back to front.

Subroutine: Do one move. Let $s_K \rightarrow \dots \rightarrow s_0$ be a normal form, and let $V = ps_0$. Let $V \xrightarrow{w} V'$ be a generator in \mathcal{A}_0 , and break into cases: for a relabelling generator, use the subroutine Do a relabelling generator; otherwise use Do an elementary move generator. The result is to compute the normal form representing the same groupoid element as $ps_K \rightarrow \dots \rightarrow (ps_0 = V) \xrightarrow{w} V'$.

Subroutine: Do a relabelling generator. Starting with a normal form $s_K \rightarrow \dots \rightarrow s_0$ and a relabelling generator $ps_0 = V \xrightarrow{\text{Rotate}(r)} V'$, break into cases depending on whether or not $s_1 \rightarrow s_0$ is a relabelling arrow.

Case 1. If $s_1 \rightarrow s_0$ is not a relabelling arrow, then the edge $V \xrightarrow{\text{Rotate}(r)} V'$ lifts to a relabelling arrow $s_0 \xrightarrow{\text{Rotate}(r)} s'$, and the required normal form is $s_K \rightarrow \cdots \rightarrow s_0 \xrightarrow{\text{Rotate}(r)} s'$.

An example of case 1 is shown in figure 44. We have already computed the normal form v^1 for $w(1)$ in figure 43. The next generator from figure 42 is a relabelling move $D_1 \xrightarrow{\text{Rotate}(3)} D_2$, and the last arrow of v^1 is not a relabelling arrow, so case 1 applies. The resulting normal form v^2 is shown in figure 44.

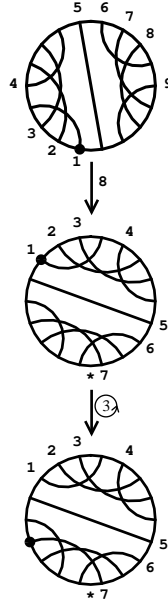


FIGURE 44. v^2 is obtained from v^1 by concatenating with a $\xrightarrow{\text{Rotate}(3)}$ relabelling arrow.

Case 2. If $s_1 \xrightarrow{\text{Rotate}(a)} s_0$ is a relabelling arrow, then we can apply a pure relabelling relator to replace $p(s_1) \xrightarrow{\text{Rotate}(a)} p(s_0) = V \xrightarrow{\text{Rotate}(r)} V'$ with $p(s_1) \xrightarrow{\text{Rotate}(n)} V'$, where $n \equiv r + a \pmod{\kappa}$. If $n \not\equiv 0 \pmod{\kappa}$ then this generator lifts to a relabelling arrow $s_1 \xrightarrow{\text{Rotate}(n)} s'$, and the required normal form is $s_K \rightarrow \cdots \rightarrow s_1 \xrightarrow{\text{Rotate}(n)} s'$. If $n \equiv 0 \pmod{\kappa}$ then the required normal form is $s_K \rightarrow \cdots \rightarrow s_1$.

An example of case 2 is shown in figure 45. Starting from v^2 as in figure 44, and using the next generator $D_2 \xrightarrow{\text{Rotate}(7)} D_3$ from figure 42, then the last letter of v^2 is a relabelling arrow, so case 2 applies and we get v^3 as in figure 45.

A word of explanation about figure 45. In paper and pencil computations, we shall sometimes redraw a certain state, connecting the two copies of that state via a \approx sign, as in figure 45. These computations will also explicitly show the relators that are applied, such as the relator in figure 45 which, despite the fourth side labelled \approx , is a three sided relabelling relator. In general, the computations carried out by the subroutine *Do one move* are represented by such diagrams, whose input is the left hand vertical side of the diagram followed by the bottom horizontal edge, and whose output is the right hand side. When I do computations by hand, I usually do as little extra copying as necessary by not copying the merged portion of the two normal forms, but for clarity's sake the figures here will always copy the entire merged portion.

This finishes the subroutine *Do one relabelling generator*. That was easy!

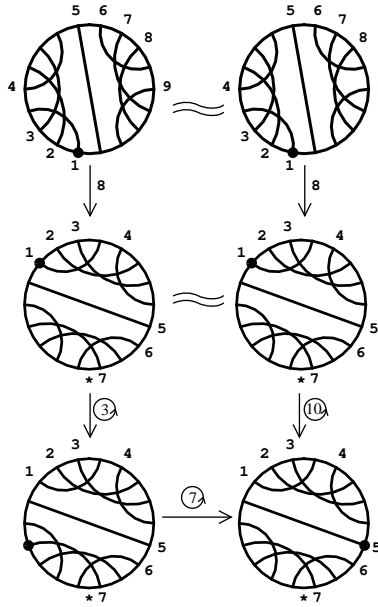


FIGURE 45. v^3 is obtained from v^2 by applying a relabelling relator, which replaces the final $\xrightarrow{\text{Rotate}(3)}$ arrow, followed by the generator $D_2 \xrightarrow{\text{Rotate}(7)}$ D_3 , with a $\xrightarrow{\text{Rotate}(10)}$ arrow.

Subroutine: Do an elementary move generator. Starting with a normal form $v := s_K \rightarrow \cdots \rightarrow s_0$ and a labelled elementary move generator $ps_0 = V \xrightarrow{h} V'$, do the following steps to compute the normal form $v' := s'_{K'} \rightarrow \cdots \rightarrow s'_0$ representing the same groupoid element as $ps_K \rightarrow \cdots \rightarrow ps_0 = V \xrightarrow{h} V'$.

Before giving a detailed explanation we give a brief overview, summarized schematically in figure 46. The normal form will be computed in the backwards direction. If the final arrow $s_1 \rightarrow s_0$ is a relabelling generator we process that by applying an elementary move–relabelling relator, replacing $ps_1 \xrightarrow{\text{Rotate}(n)} ps_0 = V \xrightarrow{h} V'$ with an elementary move $ps_1 \rightarrow V''$ followed by a relabelling move $V'' \rightarrow V'$. Then we analyze the move $ps_1 \rightarrow V''$ into three cases: good, bad, or inverse good elementary move. In the good and inverse good cases we quickly complete the computation of v' . To handle the bad case, we compute markings on V'' and V' to produce a bad elementary move $s_1 \rightarrow s'_1$ followed by a relabelling arrow $s'_1 \rightarrow s'_0$. Then we enter a loop. Typically the loop will take a sequence of good elementary moves $s_i \rightarrow \cdots \rightarrow s_j$ followed by a bad one $s_j \rightarrow s'_{j'}$, and, by applying either a commutator or pentagon relator, replace it with a bad elementary move $s_i \rightarrow s'_{i'}$ followed by a sequence of good ones $s'_{i'} \rightarrow \cdots \rightarrow s'_{j'}$; the differences $i - j$ and $i' - j'$ will always be either 1 or 2 (until the final relator, when 3 can also occur). This has the effect of “raising” the bad elementary move $s_j \rightarrow s'_{j'}$ to a higher one $s_i \rightarrow s'_{i'}$, closer to the end $s_K = s'_{K'}$. Eventually, one final relator will be used to produce not a bad elementary move but instead an equation $s_i = s'_{i'}$. A schematic diagram of the computation is given in figure 46.

Step 1: Process a final relabelling arrow. In this step, suppose that $s_1 \xrightarrow{\text{Rotate}(r)} s_0$ is a relabelling arrow. Apply an elementary move–relabelling relator, to replace the sequence $ps_1 \xrightarrow{\text{Rotate}(r)} ps_0 = V \xrightarrow{h} V'$ with a sequence $ps_1 \xrightarrow{h'} V'' \xrightarrow{\text{Rotate}(n)} V'$. To explain how this is done, under the relabelling move $s_1 \xrightarrow{\text{Rotate}(r)} s_0$ there is a 1-1 correspondence between chords of s_0 and of s_1 , and also between chord ends. In particular, the chord h of s_0 corresponds to a chord h' of s_1 , yielding the elementary move $ps_1 \xrightarrow{h'} V''$. To see how

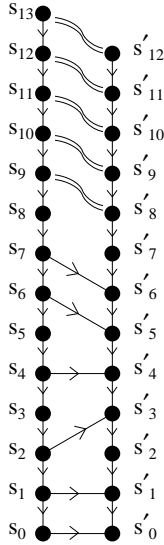


Figure 46 Starting from an input normal form $v := s_K \rightarrow \dots \rightarrow s_0$ and an elementary move generator $\alpha := ps_0 \rightarrow V'$, we typically produce an output normal form $v' := s'_{K'} \rightarrow \dots \rightarrow s'_0$ connected to v by a sequence of relators and bad elementary moves, so the words v and $v'\alpha$ represent the same groupoid elements. In these computations, good elementary move arrows and relabelling arrows will be drawn vertically, whereas bad elementary moves, like rungs of a deformed ladder, will always be nonvertical, possibly with a non-zero vertical component. The deformation is caused by the different rate at which the endpoints of the rungs are raised on the two sides of the ladder.

n is computed, let e_i be the labelled chord end in s_i . Enumerate the chord ends of ps_1 as $\eta_i = \text{Succ}^i(e_1)$, so the labelled end of s_1 is η_0 and the labelled end of s_0 is η_r . Consider the ends η_1, \dots, η_r , and let a be the number of them which are ends of the chord h . Enumerate the chord gaps as $\pi_i = (\eta_{i-1}, \eta_i)$, and among the gaps π_1, \dots, π_r let b be the number into which an end of the opposite diagonal to h will be inserted. Then $n = r - a + b$ modulo κ . It may happen that $n = 0$ modulo κ , in which case the sequence $ps_1 \xrightarrow{\text{Rotate}(r)} ps_0 = V \xrightarrow{h} V'$ is replaced just with $ps_1 \xrightarrow{h'} V'$.

Figure 47 gives several examples, showing how different configurations of the ends of h and its opposite diagonal can give rise to different values of a and b . In figure 48, we continue our main example, where $v^3 := s_2 \xrightarrow{8} s_1 \xrightarrow{\text{Rotate}(10)} s_0$ is followed by the elementary move $(ps_0 = D_3) \rightarrow D_4$. Applying step 1, we obtain an elementary move $ps_1 \rightarrow V'_1$ followed by a relabelling arrow $V'_1 \rightarrow (V'_0 = D_4)$.

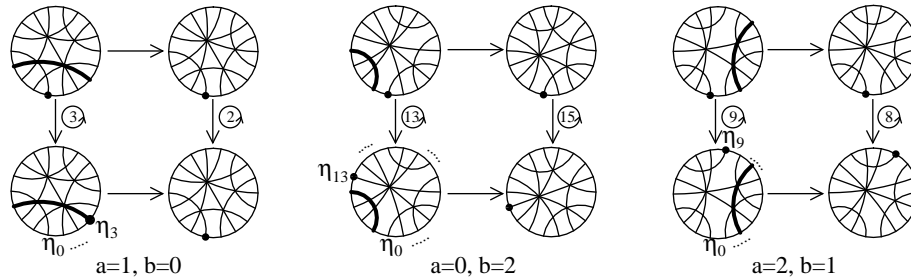


FIGURE 47. Processing a final relabelling move with an elementary move–relabelling relator

Having completed step 1, we now rename everything to obtain the following data: an accepted path $s_K \rightarrow \dots s_1$, followed by a labelled elementary move $(ps_1 = V_1) \xrightarrow{h} V'_1$, followed possibly by a relabelling move $V'_1 \xrightarrow{\text{Rotate}(r)} V'_0$.

Step 2: Classify the elementary move $(ps_1 = V_1) \xrightarrow{h} V'_1$. This move will be classified as either a good elementary move, an inverse good elementary move, or a bad elementary move. Locate h in the chord

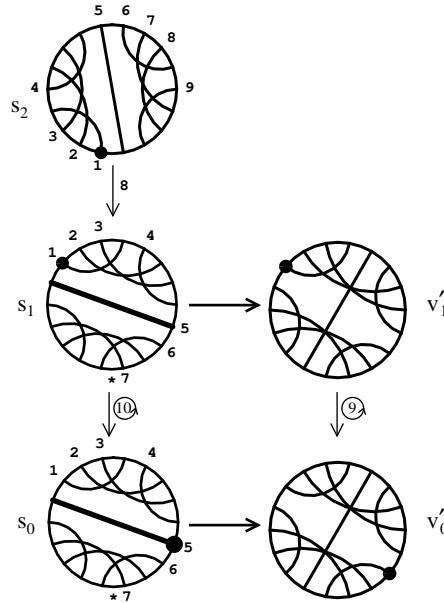


FIGURE 48. Applying step 1 to start the computation of v^4 . The normal form v^3 , read off from the right side of figure 45, is reproduced here as the left side.

diagram for s_1 . If h has an end marked j , or one of the ends e^L, e^R , then the move is good. If h is the chord opposite the marked prong, then the move is inverse good. Otherwise, the move is bad.

Step 3: Process the elementary move $(ps_1 = V_1) \xrightarrow{h} V'_1$, using whichever of the three subroutines applies: Do a good elementary move, Do an inverse good elementary move, or Do a bad elementary move.

Subroutine: Do a good elementary move. Consider the state s_1 and the chord h . If h has an end marked j , then compute the j -marked arrow $s_1 \rightarrow s'_1$; and if h has no marked end but e^d is an end of h for $d \in \{L, R\}$, compute the parity d arrow $s_1 \rightarrow s'_1$. If a relabelling move $V'_1 \xrightarrow{\text{Rotate}(m)} V'_0$ is appended, compute the relabelling arrow $s'_1 \xrightarrow{\text{Rotate}(m)} s'_0$. Then $s_K \rightarrow \dots \rightarrow s_1 \rightarrow s'_1$, with $s'_1 \xrightarrow{\text{Rotate}(m)} s'_0$ appended if necessary, is the normal form required to finish the subroutine Do one move.

For example, in figure 48 the elementary move $ps_1 \rightarrow V'_1$ is performed on the chord with end marked $j = 5$, so we can compute the marking on V'_1 by doing a j -marked elementary move on s_1 , as shown in figure 49. The marking on V'_0 is then obtained by computing the $\xrightarrow{\text{Rotate}(9)}$ arrow on V'_1 , also shown in figure 49. This completes the computation of $v^4 := s'_3 \xrightarrow{8} s'_2 \xrightarrow{5} s'_1 \xrightarrow{\text{Rotate}(9)} s'_0$.

The subroutine *Do an inverse good elementary move* is next. Roughly speaking, all we do is cancel the inverse good elementary move with the last good elementary move. However, there is one problem: the label might not return to its original position. More precisely, consider a labelled elementary move $\delta \xrightarrow{h} \delta'$ with inserted chord h' , and consider the labelled elementary move on δ' performed on h' . If the label of δ is not on an end of h , then the inverse move results in δ with the label in the same position, so there is a relator $\delta \xrightarrow{h} \delta' \xrightarrow{h'} \delta$; in our earlier terminology this is called an elementary move–relabelling relator, although there are no relabelling moves in this particular relator. On the other hand, if the label of δ is on an end of h then the inverse move $\delta' \xrightarrow{h'} \delta''$ results in a labelled ideal triangulation δ'' obtained from δ by rotating the label one notch clockwise, as shown in figure 50. To cancel the effect of this rotation, we must apply a

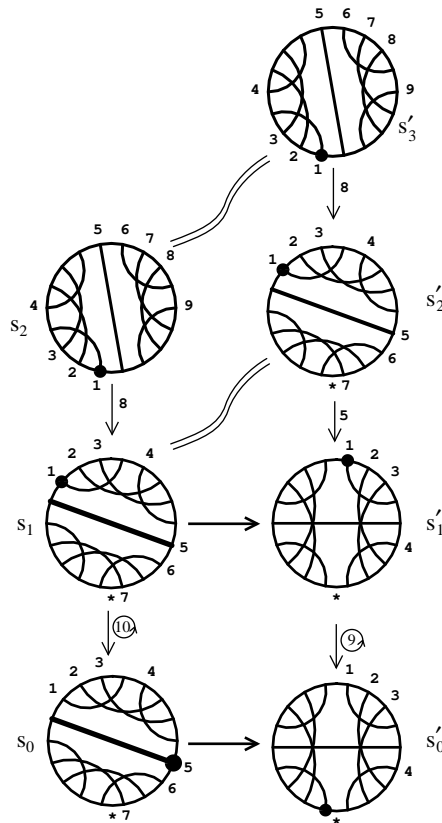


FIGURE 49. Finishing the computation of v^4

$\xrightarrow{\text{Rotate}(1)}$ relabelling move, producing an elementary move–relabelling relator $\delta \xrightarrow{h} \delta' \xrightarrow{h'} \delta'' \xrightarrow{\text{Rotate}(1)} \delta$. This relator can be applied to replace the sequence $\delta \xrightarrow{h} \delta' \xrightarrow{h'} \delta''$ by the sequence $\delta \xrightarrow{\text{Rotate}(-1)} \delta''$.

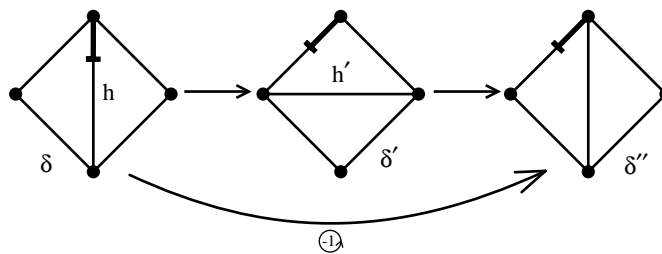


FIGURE 50. Cancelling inverse labelled elementary moves, when the first move is performed on the labelled arc

Applying these ideas to an inverse good elementary move, we obtain:

Subroutine: Do an inverse good elementary move, case 1. *If the arrow $s_2 \rightarrow s_1$ is a Right arrow or a j -marked arrow with $j \neq 1$, so the move is not performed on the labelled chord, then apply an elementary*

move–relabelling relator to replace the sequence $p(s_2) \rightarrow p(s_1) = V_1 \rightarrow V'_1$ with the constant sequence at $p(s_2) = V'_1$. Then if there is an appended relabelling move $V'_1 \xrightarrow{\text{Rotate}(r)} V'_0$, append the relabelling arrow $s_2 \xrightarrow{\text{Rotate}(r)} s''$ to obtain the required normal form $s_K \rightarrow \cdots \rightarrow s_2 \xrightarrow{\text{Rotate}(m)} s''$. Otherwise, if there is no appended relabelling move, then $s_K \rightarrow \cdots \rightarrow s_2$ is the required normal form.

Subroutine: Do an inverse good elementary move, case 2. If the arrow $s_2 \rightarrow s_1$ is a Left arrow or a 1-marked arrow, so the move is performed on the labelled chord, apply an elementary move–relabelling relator to replace the sequence $p(s_2) \rightarrow p(s_1) = V_1 \rightarrow V'_1$ with the relabelling move $p(s_2) \xrightarrow{\text{Rotate}(-1)} V'_1$. Then if there is an appended relabelling move $V'_1 \xrightarrow{\text{Rotate}(r)} V'_0$ with $r \not\equiv 1 \pmod{\kappa}$, apply another relabelling relator, replacing $p(s_2) \xrightarrow{\text{Rotate}(-1)} V'_1 \xrightarrow{\text{Rotate}(r)} V'_0$ with $p(s_2) \xrightarrow{\text{Rotate}(m)} V'_0$ where $m \equiv r - 1 \pmod{\kappa}$, and we obtain the required normal form $s_K \rightarrow \cdots \rightarrow s_2 \xrightarrow{\text{Rotate}(m)} s''$; whereas if $r \equiv 1 \pmod{\kappa}$ then the effect of the relabelling relator will be to cancel the two relabelling moves, resulting in the normal form $s_K \rightarrow \cdots \rightarrow s_2$. If there is no appended relabelling move, then $s_K \rightarrow \cdots \rightarrow s_2 \xrightarrow{\text{Rotate}(-1)} s''$ is the required normal form.

An example of case 2 is shown in figure 51. The example shows the last arrow of a normal form, a Left arrow, followed by a labelled elementary move. Applying step 2, the elementary move is classified as an inverse good, and then *Do an inverse good elementary move* is applied.

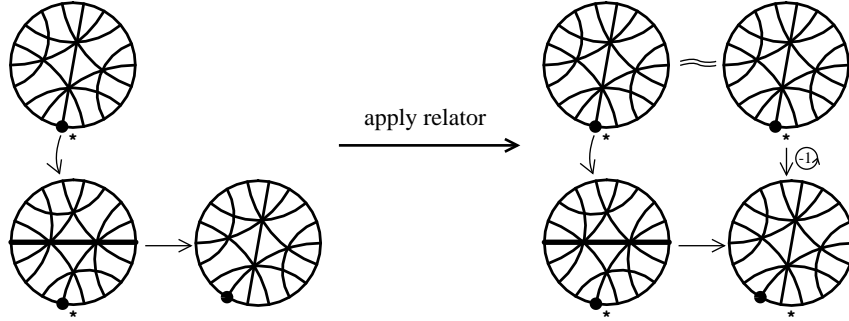


FIGURE 51. Doing an inverse good elementary move

Now we come to the most laborious portion of the algorithm:

Subroutine: Do a bad elementary move. Initialize by computing the state s'_1 : in the chord diagram s_1 , since the chord h has no marked end, and is distinct from h^L , h^R , and h^{OPP} , then we may compute the bad elementary move $s_1 \xrightarrow{h} s'_1$ as described earlier. Now loop through the subroutine *Raising a bad elementary move*.

Subroutine: Raising a bad elementary move. Given a normal form $s_K \rightarrow \cdots \rightarrow s_1$, and a bad elementary move $s_i \rightarrow s'_j$ for some $1 \leq i < K$, apply the case analysis below, with the following effect. There is a unique relator in X having as two of its sides the labelled elementary moves $V_{i+1} \rightarrow V_i \rightarrow V'_j$. Moreover, the vertices on this relator may be marked in a unique way so that one of the following is true:

(Another bad elementary move) For some $(a, b) \in \{(1, 1), (1, 2), (2, 1)\}$, there is a bad elementary move $s_{i+a} \rightarrow s'_{j+b}$ and a path in the automaton $s'_{j+b} \rightarrow \cdots \rightarrow s'_j$.

(Normal forms merging) For some $(a, b) \in \{(2, 2), (1, 2), (2, 1), (1, 3), (3, 1)\}$ there is a path in the automaton $s_{i+a} = s'_{j+b} \rightarrow \cdots \rightarrow s'_j$.

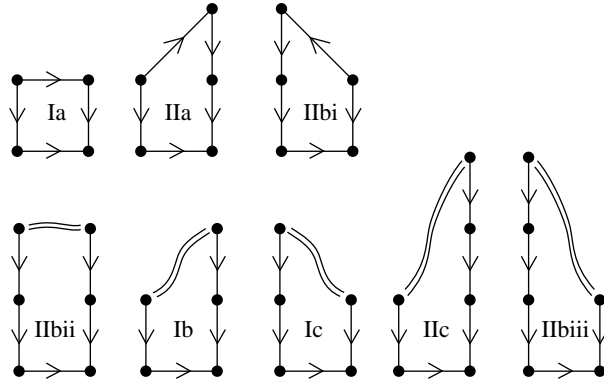


FIGURE 52. Raising a bad elementary move. The figures are labelled according to the case analysis below.

The possible outcomes are illustrated schematically in figure 52.

Before describing the case analysis, it should be clear how the subroutine *Do a bad elementary move* will proceed: as long as the bad elementary move is raised to another bad elementary move using relators of types Ia, IIa, or IIbi in figure 52, we are left with a shorter and shorter initial segment of the original normal form $s_K \rightarrow \dots \rightarrow s_1$. Once the normal forms merge using a relator of type IIbii, Ib, Ic, IIc, or IIbiii, we are done. The normal forms must eventually merge, because there is no bad elementary move leading out of the start state s_K .

Now we describe the case analysis for *Do a bad elementary move*. To simplify the notation, we assume that $i = j = 1$. Suppose the move $s_1 \rightarrow s'_1$ is performed on the chord h_0 of s_1 , and suppose that under the move $s_2 \rightarrow s_1$ the inserted chord is h_1 . If h_0 and h_1 have no adjacent ends in s_1 then a commutator relator applies, otherwise a pentagon relator applies.

Case I: h_0 and h_1 have no adjacent ends in s_1 . The commutator relator in X may be described as

$$V_1 \xrightarrow{h_0} V'_1 \xrightarrow{h_1} U \xrightarrow{h_2} V_2 \xrightarrow{h_3} V_1$$

in one direction, and in the opposite direction as

$$V_1 \xrightarrow{h_1} V_2 \xrightarrow{h_0} U \xrightarrow{h_3} V'_1 \xrightarrow{h_2} V_1$$

as shown in figure 53. We do not yet say in which direction these elementary moves are labelled.

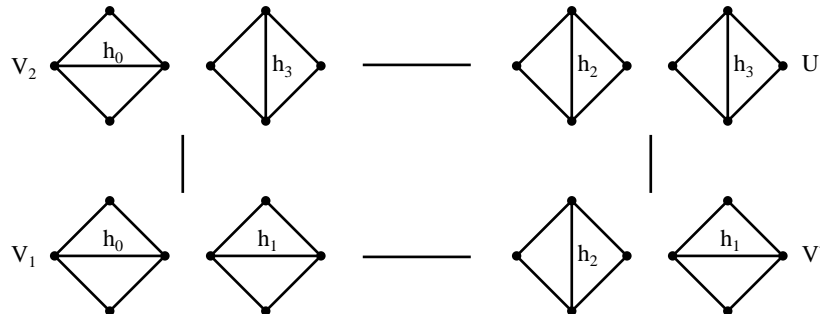


FIGURE 53. A commutator relator

Now compute as follows. Locate h_0 and h_3 in the marked chord diagram s_2 . Decide whether: (a) h_0 has neither a marked end nor an end adjacent to the marked prong of s_2 , nor is h_0 opposite the marked prong of s_2 ; (b) h_0 has a marked end or an end adjacent to the marked prong of s_2 ; or (c) h_0 is opposite the marked prong of s_2 .

Note: if $s_2 \rightarrow s_1$ is a parity arrow then case (a) applies. For the end map induces up a 1-1 correspondence between marked ends of s_2 and of s_1 , and since h_0 is unmarked in s_1 then it is unmarked in s_2 . Also, all prongs outside the support of a parity elementary move are unmarked in both the source and target of the elementary move, and since h_0 is not adjacent to a marked chord then the two triangles adjacent to h_0 are outside the support of $s_2 \rightarrow s_1$, so the prongs opposite h_0 are unmarked.

Case Ia: Neither—nor. Compute the bad elementary move $s_2 \xrightarrow{h_0} s'_2$, so $ps'_2 = U$. Now locate h_3 in s'_2 , and compute the arrow $s'_2 \xrightarrow{h_3} s'_1$. Two examples are given in figure 54, one with parity arrows and another with non-parity arrows.

In this case as in all later cases, the algorithm computes certain arrows, but to be formally correct we must justify that these arrows exist; the reader may want to skip these justifications at first.

The arrow $s'_2 \xrightarrow{h_3} s'_1$ exists because h_3 has the same relationship with the marking in s'_2 as in s_2 , i.e. it either has a marked end or has an end adjacent to the marked prong. Moreover the arrows $s_2 \rightarrow s_1$ and $s'_2 \rightarrow s'_1$ are of the same type: both have the same parity, or both are j -marked for the same j .

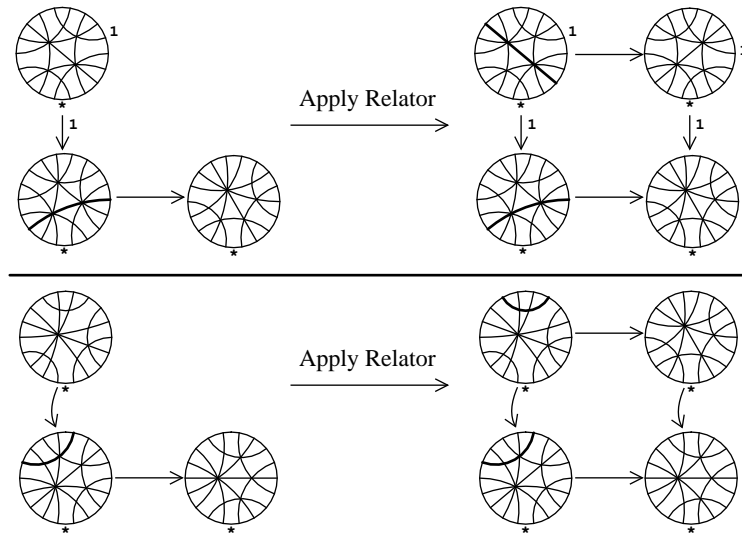


FIGURE 54. Examples of case Ia

Case Ib: h_0 has either a marked end or end adjacent to the marked prong of s_2 . As noted above, this happens only if the arrow $s_2 \rightarrow s_1$ is j -marked for some j , hence h_3 has an end marked j . Compute the arrow $s_2 = s'_3 \xrightarrow{h_0} s'_2$ in the automaton, so $ps'_2 = U$. Now locate h_3 in s'_2 , and compute the arrow $s'_2 \xrightarrow{h_3} s'_1$. Two examples are given in figure 55, one where $s'_3 \rightarrow s'_2$ is a parity arrow and one where it is non-parity.

To justify why the arrows $s'_2 \xrightarrow{h_3} s'_1$ exists, the end map sets up a 1-1 correspondence between ends in s_2 and in s_1 which are marked by some $i < j$. Therefore, since h_0 is unmarked in s_1 , then if h_0 has a marked end in s_2 that marking must be $\geq j$, and it must be $> j$ since h_3 is marked with j ; it follows that after the arrow $s'_3 \xrightarrow{h_0} s'_2$ then h_3 is still marked j in s'_2 . Also, if h_0 is adjacent to the marked prong of s_2 that prong must be marked $> j$, so h_3 is still marked j in s'_2 . Thus, $s'_2 \xrightarrow{h_3} s'_1$ is a j -marked arrow.

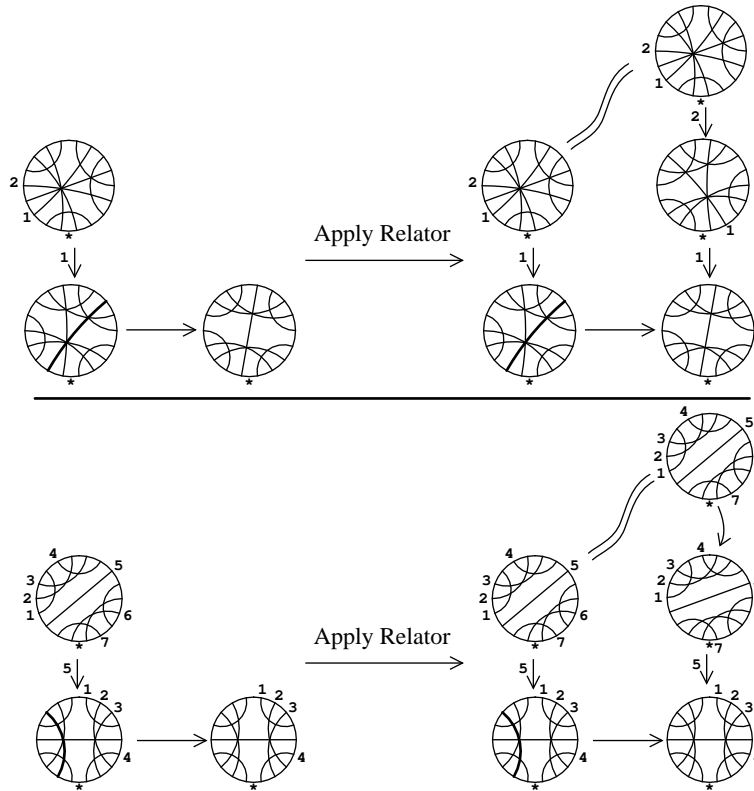


FIGURE 55. Examples of case Ib

Case Ic: h_0 is opposite the marked prong of s_2 . Again, this happens only if the arrow $s_2 \rightarrow s_1$ is j -marked for some j , hence h_3 has an end marked j . Since h_0 is opposite the marked prong of s_2 , then h_0 is the inserted chord under the arrow $s_3 \rightarrow s_2$, and $ps_3 = U$. Now locate h_3 in s_3 , and compute the arrow $(s_3 = s'_2) \xrightarrow{h_3} s'_1$. Examples are given in figure 56. Note that occurrences of case Ib and Ic are “orientation reversals” of each other; c.f. figures 55,56.

The arrow $(s_3 = s'_2) \xrightarrow{h_3} s'_1$ exists because h_3 , being marked by j in s_2 , is also marked by j in s_3 . Thus, the arrow $s'_2 \xrightarrow{h_3} s'_1$ is j -marked.

Case II: h_0 and h_1 have adjacent ends in s_1 . The pentagon relator in X may be described as

$$V_1 \xrightarrow{h_0} V'_1 \xrightarrow{h_1} W \xrightarrow{h_2} U \xrightarrow{h_3} V_2 \xrightarrow{h_4} V_1$$

and in the other direction

$$V_1 \xrightarrow{h_1} V_2 \xrightarrow{h_0} U \xrightarrow{h_4} W \xrightarrow{h_3} V'_1 \xrightarrow{h_2} V_1$$

as shown in figure 57.

Now compute. Locate h_0 and h_4 in the marked chord diagram s_2 . Decide whether: (a) h_0 has no marked end nor end adjacent to the marked prong of s_2 , nor is h_0 opposite the marked prong of s_2 ; (b) h_0 is opposite the marked prong of s_2 ; or (c) h_0 has a marked end or an end adjacent to the marked prong of s_2 .

Case IIa: Neither—nor. Compute the bad elementary move $s_2 \xrightarrow{h_0} s'_3$, whose inserted chord is h_3 , so $ps'_3 = U$. Now locate the chord h_4 in s'_3 and compute the arrow $s'_3 \xrightarrow{h_4} s'_2$, so $ps'_2 = W$. Finally, locate the chord h_3 in s'_2 , and compute the arrow $s'_2 \xrightarrow{h_3} s'_1$. Examples are shown in figure 58.

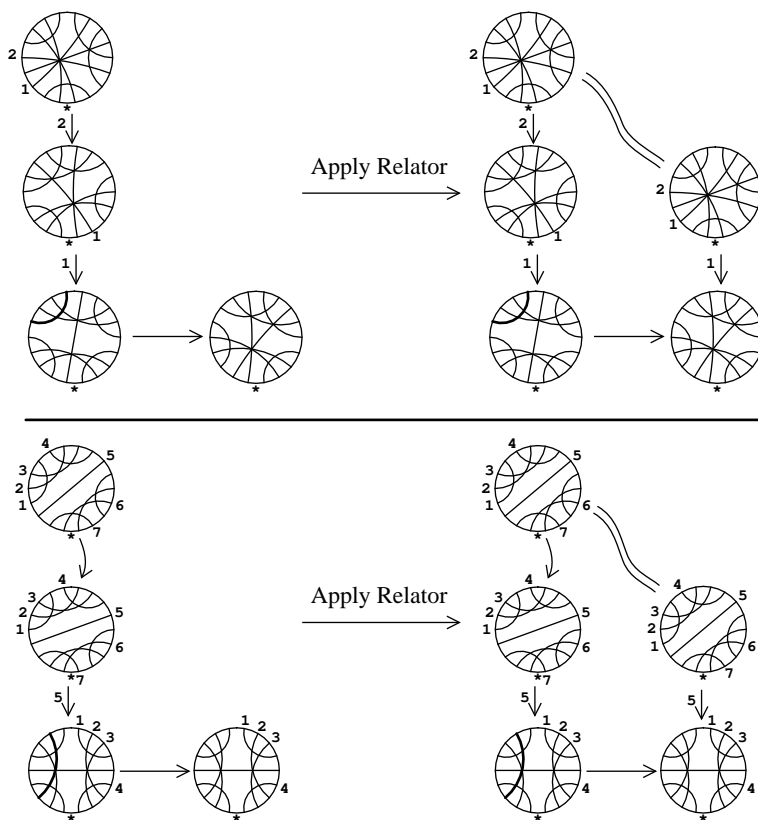


FIGURE 56. Examples of case Ic

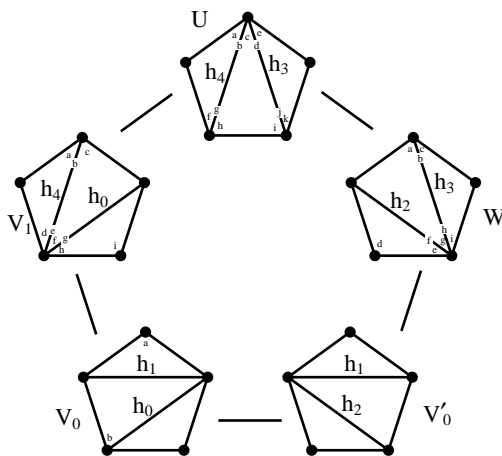


FIGURE 57. A pentagon relator

To see why the arrows $s'_3 \xrightarrow{h_4} s'_2$ and $s'_2 \xrightarrow{h_3} s'_1$ exist, first note that in figure 57, the marking on s_2 must include either a or b in V_2 : the marking must include one of $a-f$, since $s_2 \xrightarrow{h_4} s_1$ is an arrow; but c and f are

excluded because no mark can be on a prong adjacent to or opposite h_0 ; also d and e are excluded because then the marking on s_1 would include b in V_1 , violating the fact that $s_1 \xrightarrow{h_0} s'_1$ is a bad elementary move. It follows that the marking on s'_3 includes a or b in U , showing that $s'_3 \xrightarrow{h_4} s'_2$ is an arrow, of the same type as $s_2 \rightarrow s_1$. Also, it follows that the marking on s'_2 includes a in W , showing that there is an arrow $s'_2 \xrightarrow{h_3} s'_1$; this can be a parity or nonparity arrow, depending on whether h_3 has a marked end.

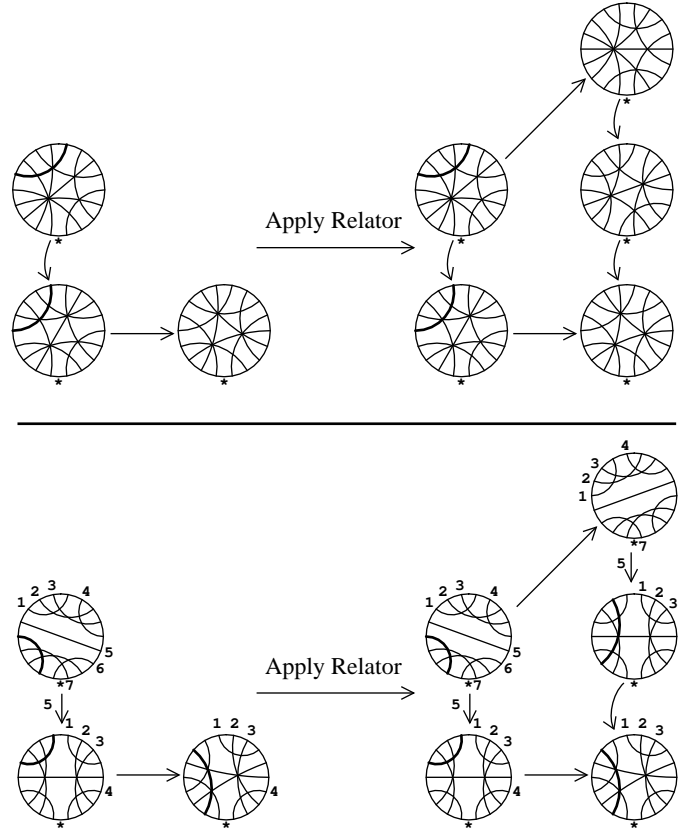


FIGURE 58. Examples of case IIa

Case IIb: h_0 is opposite the marked prong of s_2 . Then the arrow $s_3 \rightarrow s_2$ has inserted chord h_0 , so $ps_3 = U$, and $s_3 \rightarrow s_2$ is performed on h_3 . Locate the chord h_4 in s_3 . Decide whether: (i) h_4 has no marked end, no end adjacent to the marked prong of s_3 , and h_4 is not opposite the marked prong of s_3 ; (ii) h_4 has a marked end or end adjacent to the marked prong of s_3 ; (iii) h_4 is opposite the marked prong of s_3 ; one of these must happen.

Case IIbi. Compute the bad elementary move $s_3 \xrightarrow{h_4} s'_2$, so $ps'_2 = W$. Now locate the chord h_3 in s'_2 , and compute the arrow $s'_2 \xrightarrow{h_3} s'_1$. Examples are given in figure 59. Note that cases of IIa and IIbi are orientation reversals of each other; c.f. figures 58,59.

To see why the arrow $s'_2 \xrightarrow{h_3} s'_1$ exists, note that the marking on s_3 must include one of d, e, j, k in U : since $s_3 \xrightarrow{h_3} s_2$ is an arrow then one of the marks $c-d, i-k$ must be included, but the marks c, i are forbidden because no prong adjacent to or opposite h_4 is marked; it follows that the marking on s'_2 must include one of b, c, h, i in W , so $s'_2 \xrightarrow{h_3} s'_1$ is an arrow.

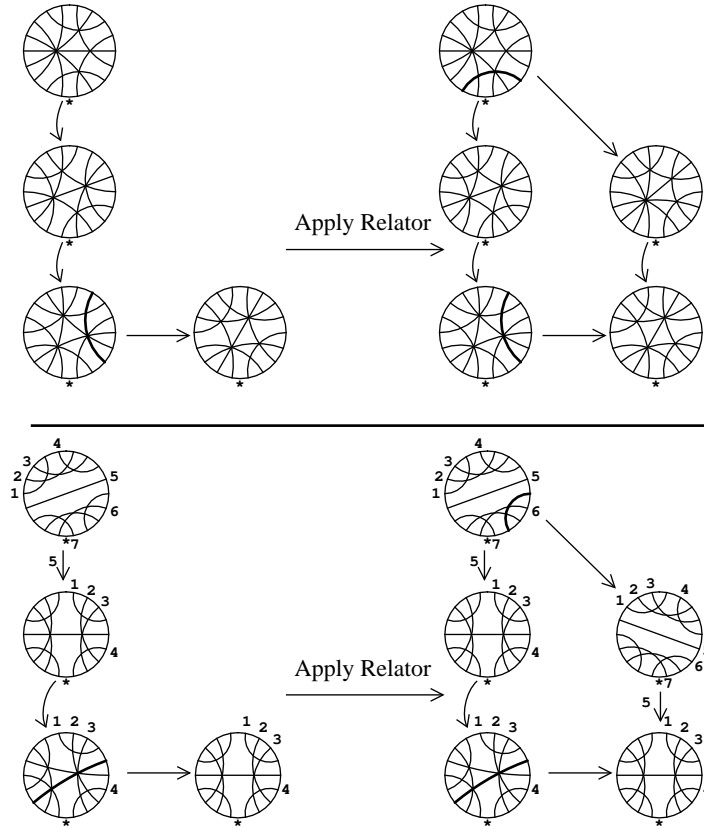


FIGURE 59. Examples of case IIbi

Case IIbii: h_4 has a marked end or end adjacent to the marked prong of s_3 . Compute the arrow $s_3 = s'_3 \xrightarrow{h_4} s'_2$, so $ps'_2 = W$. Now locate the chord h_3 in s'_2 , and compute the arrow $s'_2 \xrightarrow{h_3} s'_1$. Examples are given in figure 60. Note that the orientation reversal of an example of case IIbii is another example of case IIbii; it is instructive to study the orientation reversals of the examples in figure 60.

To see why the arrow $s'_2 \xrightarrow{h_3} s'_1$ exists, note first that the marking on s_3 includes one of $c-e$ or $i-k$ in U , because $s_3 \xrightarrow{h_4} s_2$ is an arrow; we can rule out i because either h_4 has a marked end and no marked prong can be opposite an arc with a marked end (property 5 in the definition of a marking), or the unique marked prong is adjacent to h_4 ; it follows that the marking on s'_2 includes one of $a-c, h, i$ in W , so $s'_2 \xrightarrow{h_3} s'_1$ is an arrow.

Case IIbiii: h_4 is opposite the marked prong of s_3 . Then h_4 is the chord inserted under $s_4 \rightarrow s_3$, so $ps_4 = W$. Locate the chord h_3 in s_4 , and compute the arrow $(s_4 = s'_2) \xrightarrow{h_3} s'_1$. An example is given in figure 61.

To see why the arrow $(s_4 = s'_2) \xrightarrow{h_3} s'_1$ exists, note that the marking on s_3 must include one of $c-e$ or $i-k$ in U , since $s_3 \xrightarrow{h_4} s_2$ is an arrow. However, $c, e,$ and k may be eliminated by the requirement that the unique marked prong is opposite h_4 . Also, i may be eliminated, for if i is included then b and g are not included, so the marking on s_2 includes i but not b and e in V_2 , and by uniqueness of the marked prong $a, c, d,$ and f are also not included, but this violates the requirement that $s_2 \xrightarrow{h_4} s_1$ is an arrow. Thus, the marking on s_3 includes one of d or j in U . It follows that the marking on s_4 includes one of b or h in W , so $(s_4 = s'_2) \xrightarrow{h_3} s'_1$ is an arrow.

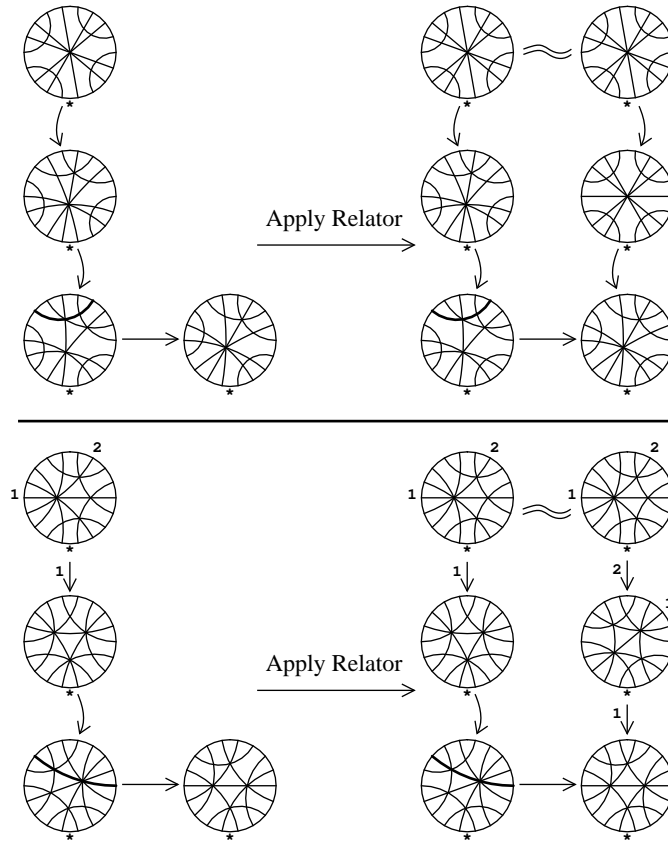


FIGURE 60. Examples of case IIbii

Case IIc: h_0 has a marked end or end adjacent to the marked prong of s_2 . Compute the arrow $(s_2 = s'_4) \xrightarrow{h_0} s'_3$, whose inserted chord is h_3 ; note that $ps'_3 = U$. Now locate the chord h_4 in s'_3 , and compute the arrow $s'_3 \xrightarrow{h_4} s'_2$, so $ps'_2 = W$. Finally, locate the chord h_3 in s'_2 and compute the arrow $s'_2 \xrightarrow{h_3} s'_1$. An example is given in figure 62. Note that occurrences of cases IIbiii and IIc are orientation reversals of each other; c.f. figures 61, 62.

To see why the arrows $s'_3 \xrightarrow{h_4} s'_2$ and $s'_2 \xrightarrow{h_3} s'_1$ exist, first note that the marking on s_1 must include one of a or b in V_1 , because h_1 is inserted under the arrow $s_2 \rightarrow s_1$; however, b is eliminated since $s_1 \xrightarrow{h_0} s'_1$ is a bad elementary move, so a is included. It follows that the marking on s_2 includes one of a , b , or c in V_2 ; let the numerical value of this marking be n . By hypothesis, the marking on s_2 includes some end of h_0 or prong adjacent to h_0 in V_2 ; let the numerical value of this marking be m . Then $m > n$, for after the arrow $s_2 \rightarrow s_1$ there is no marked end of h_0 , nor marked prong adjacent to h_0 , because $s_1 \xrightarrow{h_0} s'_1$ is a bad elementary move. If a or c is marked with n in s_2 we obtain a contradiction, since the prong marking is greater than all end markings. Thus, b is marked with n in s_2 . It follows that after the arrow $(s_2 = s'_4) \xrightarrow{h_0} s'_3$, the marking on s'_3 includes b in U . It then follows that there is an arrow $s'_3 \xrightarrow{h_4} s'_2$, and that the marking on s'_2 includes a in W . Finally, it follows that there is an arrow $s'_2 \xrightarrow{h_3} s'_1$.

This finishes the subroutine *Do a bad elementary move*. A few comments:

Comment 1: Strictly speaking, we have gone around a relator in two ways to obtain markings on $ps'_1 = V'_1$, and we should check that these two markings are identical. It is obvious that the markings are identical outside of the support of the relator, and by checking cases one may see that the markings are identical in

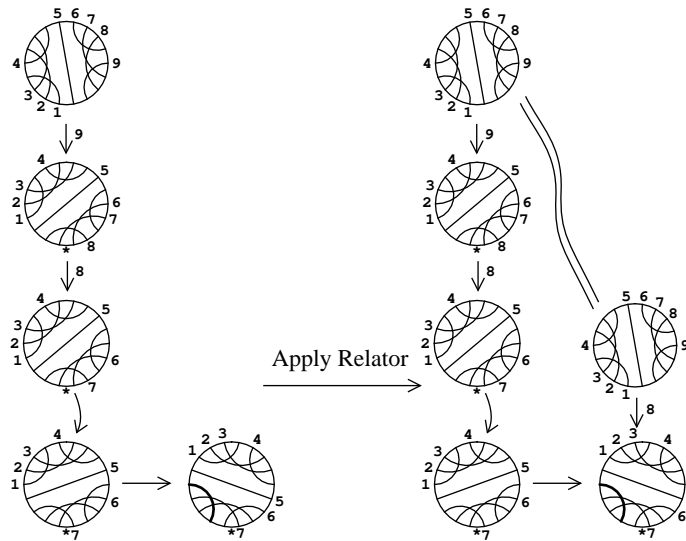


FIGURE 61. Example of case IIbiii

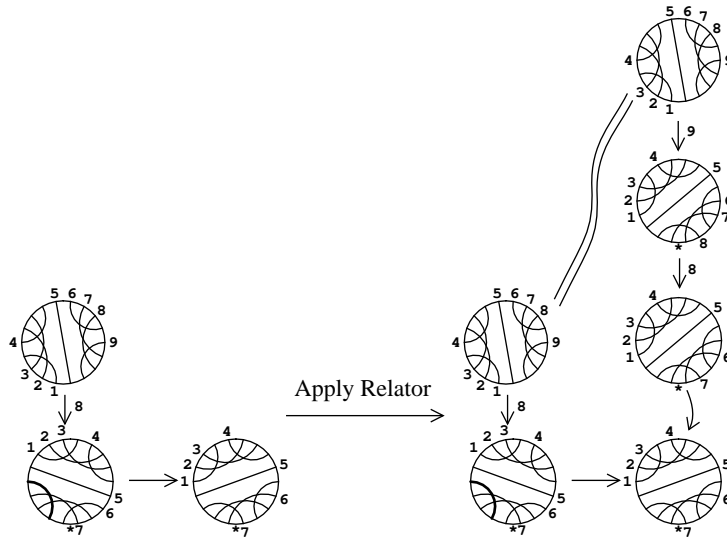


FIGURE 62. Example of case IIc

the support of the relator; alternatively, use the results of [M].

Comment 2: When the arrows on the left side of the relator are all parity arrows, then the relator must be case Ia, IIa, IIbi, or IIbii. Moreover, the arrows on the right side must also be parity arrows. Moreover, in cases I, IIa, and IIbi all of the arrows in the relator have the same parity; in case IIbii, the arrows on the left side have the parities dd' for some choice of $d \neq d' \in \{L, R\}$, and the arrows on the right side have parities $d'd$. The diagrams for each of these cases, figures 54,58,59,60, each show an example where the arrows are all parity arrows. This observation can be used to make some computational shortcuts: once it has been determined that the arrows on the left hand side of the relator are all parity arrows, and once the top chord

diagram on the right hand side of the relator has been computed, then the parities of the arrows on the right hand side are determined, and from this information the arrows may be computed.

This completes the description of the algorithm for computing normal forms.

Finally, observe from the description of the algorithm that \mathcal{L}_0 is an asynchronous automatic structure, because the input and output normal forms under any run of the subroutine *Do one move* are asynchronous fellow travellers.

Examples of doing a bad elementary move.

Figures 63,64 show some examples of applying the subroutine *Do a bad elementary move*. Figure 63 finishes the computation of the normal form for the example word given in figure 41, using two more applications of *Do a bad elementary move*. The left side of the figure shows v^4 as computed in figure 49, and the bottom of the figure shows the last two generators $D_4 \rightarrow D_5 \rightarrow D_6$ from figure 41. Then v^5 is computed from v^4 using an elementary move–relabelling relator, followed by a run of the subroutine *Do a bad elementary move*, using relators of types IIa, IIc; then v^6 is computed using relators of types IIa, IIbi. Some of the relators used in figures 63 and 64 were described in figures 54–62, and the numerals written on these relators refer to the relevant figure.

Figure 64 shows another application of *Do a bad elementary move*. This is a more typical example than figure 63: given the fact that an arbitrary element of \mathcal{L}_0 has at most $\kappa = 12g - 6$ nonparity arrows, if the word is very long the relators do not interact very often with nonparity arrows.

IV. INTERLUDE: THE SUFFIX UNIQUENESS PROPERTY FOR AN AUTOMATIC STRUCTURE

In this section, we describe some properties of \mathcal{L}_0 , as a motivation for our proof in the next section that the computation of normal forms in \mathcal{L}_0 runs in quadratic time.

In [EHLPT] it is proved that an automatic group has a quadratic time algorithm for the word problem. We define a property of automatic structures called *suffix uniqueness*, and using this property we give another description of a quadratic time algorithm for the word problem. Our algorithm is more efficient than the one described in [EHLPT], as can be seen by comparing the proofs. For asynchronous automatic structures, the method of [EHLPT] yields an exponential time algorithm; the property of suffix uniqueness applies equally well to asynchronous automatic structures, and in this case we obtain an exponential time algorithm as well.

Let G be a groupoid with finite generating set \mathcal{A} , and let \mathcal{L} be a synchronous or asynchronous automatic structure over G , with word acceptor \mathcal{M} and fellow traveller constant K . Let B_K be the set of elements in G represented by words of length $\leq K$ in the generating set \mathcal{A} ; elements of B_K do not have to start at the base point of \mathcal{L} . Let ${}_n\mathcal{L}$ be the set of suffixes of \mathcal{L} of length between 1 and n . Assuming that \mathcal{M} has no inaccessible states, then ${}_n\mathcal{L}$ is the set of all nontrivial paths in \mathcal{M} of length at most n ending at an accept state. We say that \mathcal{L} satisfies *suffix uniqueness* if it is prefix closed, no two normal forms represent the same element of G , and there exists an integer $n \geq 1$, a finite subset $\mathcal{S} \subset {}_n\mathcal{L} \times B_K$, and a function $F: \mathcal{S} \rightarrow {}_K\mathcal{L}$, with the following property:

If $w, w' \in \mathcal{L}$ are K -fellow travellers, then setting $g = \bar{w}^{-1}w' \in B_K$, there exists a unique suffix s of w such that $(s, g) \in \mathcal{S}$, and $F(s, g)$ is a suffix of w' . Moreover, writing $w = \hat{w}s$ and $w' = \hat{w}'F(s, g)$, then \hat{w} and \hat{w}' are K -fellow travellers.

For example, from the description of the subroutine *Do one move* it follows that the asynchronous automatic structure \mathcal{L}_0 for the groupoid \mathcal{MCGD} satisfies suffix uniqueness, with fellow traveller constant $K = 1$ and maximal suffix length $n = 3$.

From the suffix uniqueness property, we obtain an algorithm for the word problem as follows. Given an arbitrary word $w = w_1 \cdots w_M$, by induction compute the normal form v^m representing $w(m) = w_1 \cdots w_m$. To do this, suppose $v = v^{m-1}$ is computed. We must compute the normal form $v' = v^m$ representing $w^{m-1}w_m$. We compute v' by induction, producing longer and longer suffixes of v' . Set $a_0 = v$ and $a'_0 = v'$.

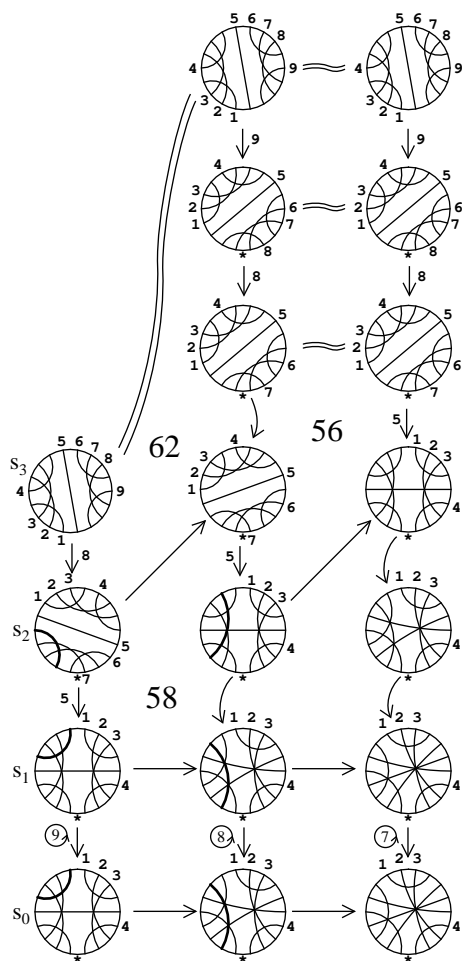


Figure 63

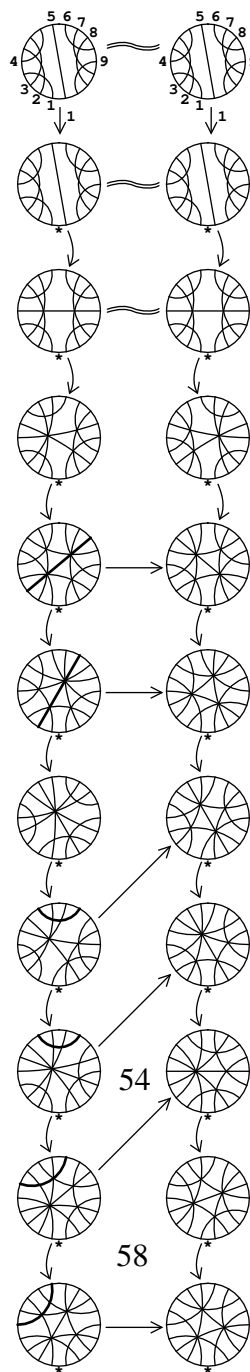


Figure 64

Since a_0 and a'_0 are K -fellow travellers, then we may factor a_0 uniquely as $v = a_1 s_0$ so that $(s_0, w_m) \in \mathcal{S}$, and then set $s'_0 = F(s, w_m)$, so s' is a suffix of v' and $v' = a'_1 s'_0$ for some a'_1 . It follows that a_1 and a'_1 are

K -fellow travellers, so we may continue by induction. Since a_i is decreasing in length, eventually we compute $v' = s'_J \dots s'_1 s'_0$.

Note that this algorithm is exactly the same as the algorithm described in the previous section, for computing normal forms in \mathcal{L}_0 representing elements of \mathcal{MCGD} .

The computation time of this algorithm may be estimated as follows. Since \mathcal{S} is finite, then the number of steps J in the computation of v' is bounded by a linear function of the length of v . If the structure \mathcal{L} is asynchronous, then $\text{Length}(v^m)$ is growing exponentially, and we have an exponential time algorithm for the computation of v^M . If the structure \mathcal{L} is synchronous, then $\text{Length}(v^m)$ is growing linearly, and we have a quadratic time algorithm for computing v^M .

From this argument, the most we can conclude is that the algorithm described in §III runs in exponential time. However, we can perhaps do better using the following ideas.

Let $\mathcal{L}, \mathcal{L}'$ be asynchronous automatic structures on a groupoid G with generating set \mathcal{A} . We say that \mathcal{L}' is a *factorization* of \mathcal{L} if, for each $v \in \mathcal{L}$ and $v' \in \mathcal{L}'$ such that $\bar{v} = \bar{v}'$, there exists a sequence $0 = n_0 < n_1 < \dots < n_J = \text{Length}(v)$ with steps of bounded length such that $\bar{v}(n_j) = \bar{v}'(j)$ for $j = 0, \dots, J$. Suppose moreover that \mathcal{L} and \mathcal{L}' both satisfy suffix uniqueness, and that \mathcal{L}' is an automatic structure. Then the above described algorithm for the word problem, *using the asynchronous structure \mathcal{L}* , runs in quadratic time, improving the a priori fact that the algorithm runs in exponential time. The reason is that lengths of normal forms in \mathcal{L}' grow linearly, and the factors have bounded length, therefore lengths of normal forms in \mathcal{L} grow linearly, hence the algorithm runs in quadratic time.

In the next section we use this technique for showing that normal forms in \mathcal{L}_0 can be computed in quadratic time, by finding an automatic structure \mathcal{L}_1 for \mathcal{MCGD} that is a factorization of \mathcal{L}_0 .

V. DEHN TWISTS, SYNCHRONOUS NORMAL FORMS, AND QUADRATIC COMPUTATION TIME

The key to understanding the synchronous normal forms is to see how Dehn twists arise in the asynchronous normal forms \mathcal{L}_0 . This is described in the *Dehn twist lemma* of [M], which we review here. A word in \mathcal{L}_0 will be factored into subwords which represent either Dehn twists or fractions of Dehn twists; this leads to a language \mathcal{L}_1 which is a factorization of \mathcal{L}_0 as in the last section. The properties of this factorization are used in [M] to prove that \mathcal{L}_1 is an automatic structure for \mathcal{MCGD} . For our present purposes, we use the language \mathcal{L}_1 to prove that the algorithm described above, for computing normal forms in \mathcal{L}_0 , runs in quadratic time:

Theorem: Quadratic computation time. *Given a word v of relabelling moves and labelled elementary moves, with $\text{Length}(v) = K$, the algorithm computes the normal form of v using at most $(12g - 12)K^2$ relators.*

Comment 1: As we shall see, the number $12g - 12$ is the maximum length of a factor in the Dehn twist factorization.

Comment 2: At any stage of the algorithm, the time needed to apply the next relator is bounded by a constant, hence the algorithm computes the normal form of v in quadratic time.

Comment 3: For genus 2 we need at most $12K^2$ relators. In any given run of the algorithm, the author is able to apply the required relator using at most 2 minutes of time, leading to a computation time of at most $25K^2$ minutes (experience shows that this is a very conservative estimate).

Dehn twist blocks.

Consider an ideal triangulation δ and a prong of δ marked with a $*$. Then $(\delta, *)$ is the special case of a marked ideal triangulation, with no end markings; we call this a *prong marked ideal triangulation* or *prmit*. We use Δ to denote $(\delta, *)$. Choose a parity $d \in \{L, R\}$; we use $-d$ to denote the opposite parity. Consider the arc h^{-d} of δ , equipped with a transverse orientation pointing into the marked triangle. The arc h^{-d} forms a simple closed curve in S , whose regular neighborhood N is an annulus, and the transverse orientation points towards one of the boundary components of N , a simple closed curve we denote $\gamma = \gamma(\Delta, d)$. Let

$\tau = \tau(\Delta, d)$ be the Dehn twist of parity d around γ ; see figure 65. Our parity convention for Dehn twists is that a Right Dehn twist is a positive one, i.e. on an oriented annulus $A = \mathbf{R} \times [0, 1]/(x, y) \equiv (x + 1, y)$ forming a regular neighborhood of γ , the Dehn twist is given by the linear map $(x, y) \mapsto (x + y, y)$ which takes a vertical segment to a segment of positive slope, i.e. a segment that slopes up and to the Right.

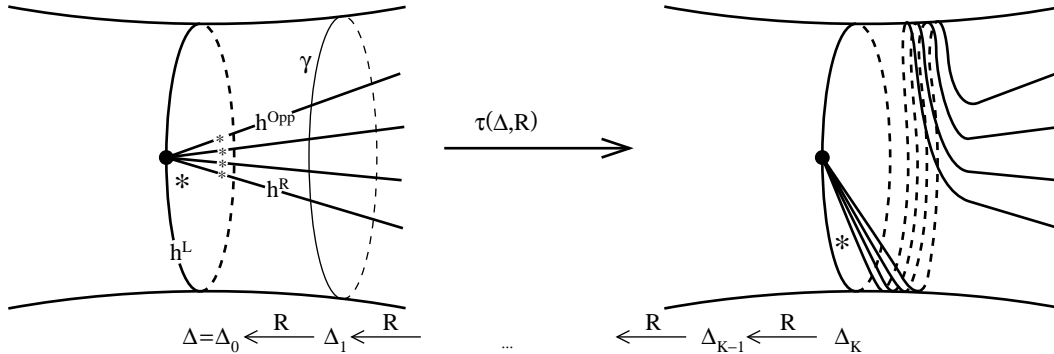


FIGURE 65. The Dehn twist $\tau(\Delta, R)$

The following lemma is basically the first part of the *Dehn twist lemma* of [M]:

Dehn twist lemma (part I). *Let $\cdots \xrightarrow{d} \Delta_2 \xrightarrow{d} \Delta_1 \xrightarrow{d} \Delta_0$ be a (finite or infinite) sequence of d -elementary moves ending with $\Delta = \Delta_0$. Let $\tau = \tau(\Delta, d)$ be the Dehn twist defined above. Then there exists a constant $K = K(\Delta, d)$, depending only on the combinatorial type of Δ , such that $\tau(\Delta_i) = \Delta_{i+K}$ for all $i \geq 0$.*

The proof is sketched below.

The sequence $\Delta_K \xrightarrow{d} \cdots \xrightarrow{d} \Delta_0$ is called a *Dehn twist sequence* of parity d . The number K is called the *Dehn twist length*. Note that after taking combinatorial types, then $\{\Delta_K\} \xrightarrow{d} \cdots \xrightarrow{d} \{\Delta_0\}$ is a closed path in \mathcal{M}_0 , lying entirely in \mathcal{M}_0^1 : the path is closed because Δ_0 and $\Delta_K = \tau(\Delta_0)$ have the same combinatorial type, and it is in level 1 because there are no end markings. We call this a *Dehn twist block* of parity d in \mathcal{M}_0^1 ; later, after putting in end markings, we shall define Dehn twist blocks in higher levels.

Some examples are given in figures 66–69. Figure 66 shows a Left Dehn twist block on a torus, of length 1. All Left Dehn twist blocks in \mathcal{M}_0^1 on a torus are orientation preserving conjugate to this one, and all Right Dehn twist blocks are orientation reversing conjugate.

Figure 67 shows a Right Dehn twist block of length 1, on a surface of genus 2, obtained by putting a marked prong into the second elementary move of figure 5. This example exhibits a characteristic property of Dehn twist sequences of length 1 when the genus is at least 2: the Dehn twist length is 1 if and only if h^{-d} is a boundary arc of a 1-handle piece, and the $*$ is inside the 1-handle piece. Figure 68 shows an example of a Right Dehn twist block of length 2.

In figure 69, note that a single elementary move returns to the original state, completing a simple closed loop w in \mathcal{M}_0 and thereby defining a mapping class Φ , but Φ is not a Dehn twist. The separating closed curve γ is invariant under Φ ; on the left component the restricted mapping class is the identity, and on the right component the restricted class has some finite order k whose value we leave as an exercise. The mapping class Φ^k is a Dehn twist τ , and the non-simple closed loop w^k in \mathcal{M}_0 is a Dehn twist block of length k .

Now we give the formula for Dehn twist lengths $K(\Delta, d)$, and we sketch the proof of the Dehn twist lemma. The curve γ cuts off certain half-arcs of δ , namely those half-arcs in the annulus bounded by γ and h^{-d} . These half-arcs determine a subset of $\mathcal{E}(\delta)$ denoted $\mathcal{E}^* = \mathcal{E}^*(\Delta, d)$. In figure 65 these half-arcs are

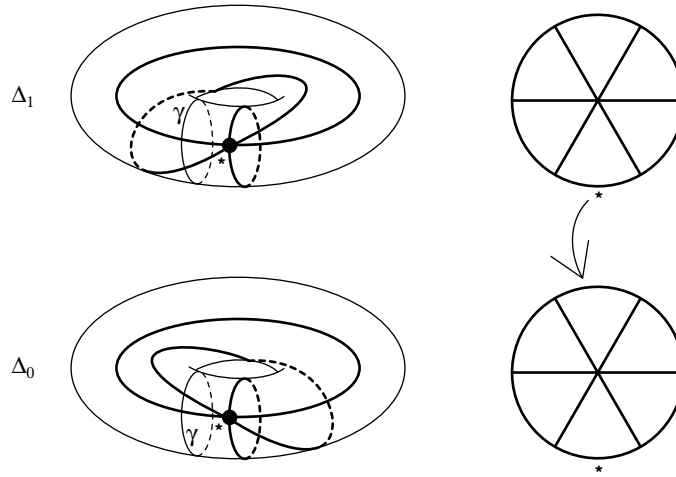


FIGURE 66. A Left Dehn twist block on a torus: Δ_1 is obtained from Δ_0 by a Left Dehn twist about the curve γ .

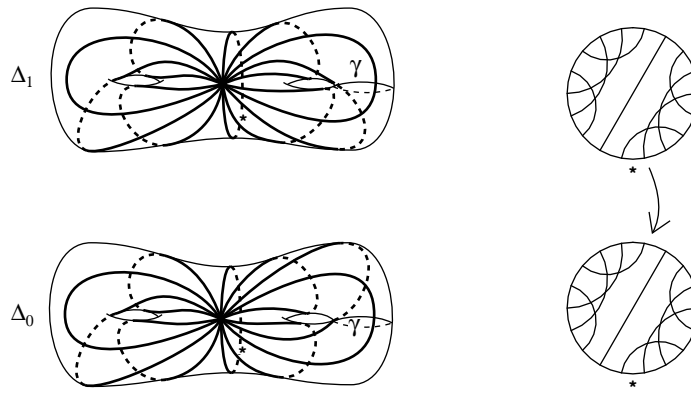


FIGURE 67. A Right Dehn twist block of length 1 on a surface of genus 2

labelled with a *. In figures 66 and 67, $|\mathcal{E}^*| = 2$. In figure 68, $|\mathcal{E}^*| = 3$. And in figure 69, $|\mathcal{E}^*| = 8$. Note that the arc h^{OPP} always has at least one end in \mathcal{E}^* . Define $\hat{\mathcal{E}}^* = \hat{\mathcal{E}}^*(\Delta, d) = \mathcal{E}^* - \mathcal{E}(h^{\text{OPP}})$. Let $K(\Delta, d) = |\hat{\mathcal{E}}^*|$. Thus, $K(\Delta, d) = |\mathcal{E}^*| - 2$ or $|\mathcal{E}^*| - 1$ depending on whether or not h^{OPP} has one or two ends in \mathcal{E}^* . In figures 66, 67, 68 only one end of h^{OPP} is in \mathcal{E}^* , so $K(\Delta, d) = 1, 1, 2$ respectively. In figure 69 both ends of h^{OPP} are in \mathcal{E}^* , so $K(\Delta, d) = 6$.

The number $K(\Delta, d)$ may be computed from the chord diagram of Δ as follows. Recall that the “marked triangle” is the triangle having the marked prong as a corner. Locate the chord corresponding to h^{-d} . The endpoints of this chord separate the remaining chord ends into two subsets; the subset containing e^d corresponds to \mathcal{E}^* . Now count the number of elements in \mathcal{E}^* , subtract 1 if the marked triangle is twisted (because then only one end of h^{OPP} is in \mathcal{E}^*), and subtract 2 if the marked triangle is untwisted (because both ends of h^{OPP} are in \mathcal{E}^*); the result is $K(\Delta, d)$; see figure 70. In figures 66-69, only figure 69 has an untwisted marked triangle, hence only in that case is 2 subtracted to compute $K(\Delta, d)$; in the other cases 1

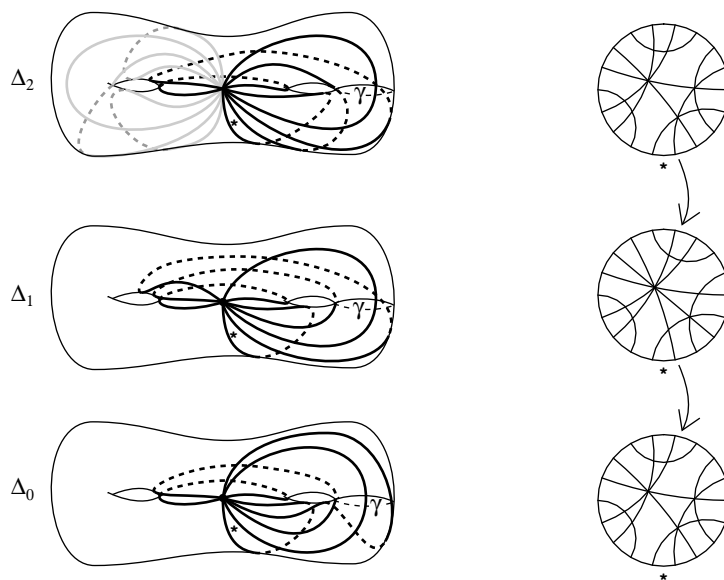


FIGURE 68. A Right Dehn twist block of length 2 on a surface of genus 2. The shaded arcs of Δ_2 should be included in Δ_1 and Δ_0 as well, but are omitted from the diagram for clarity.

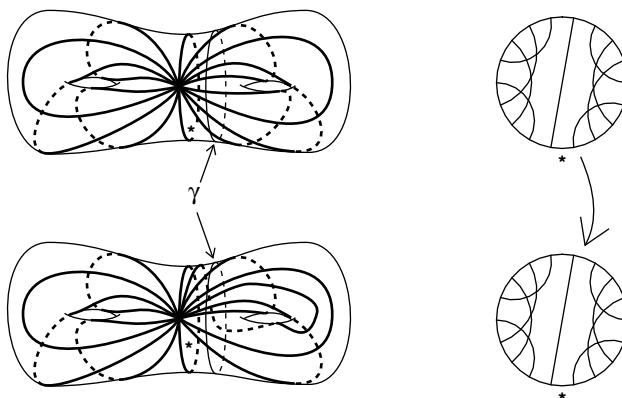


FIGURE 69. What is the Dehn twist length? (Hint: see figure 24c)

is subtracted. Other examples of computing $K(\Delta, d)$ are given in figure 71.

The key observation in proving the Dehn twist lemma is that for any prong marked ideal triangulation Δ and any $d \in \{L, R\}$, the arc h^{OPP} is obtained up to isotopy from h^d by letting the Dehn twist $\tau(\Delta, d)^{-1}$ act on a half-arc representing e^d , where the half-arc is chosen to intersect γ exactly once. This is illustrated in figure 72, which shows separately the cases where the marked triangle is twisted and untwisted. Note in the twisted case that h^d and h^{OPP} each have a unique end in \mathcal{E}^* , and the twist about γ takes h^d to h^{OPP} . But in the untwisted case where h^d and h^{OPP} have both ends in \mathcal{E}^* , the twist *does not* take h^d to h^{OPP} ; by allowing the twist to act *only* on the end e^d of h^d , we thereby obtain h^{OPP} .

This observation is applied as follows. Let $\hat{\Delta}_i$ be obtained from Δ_i by removing h_i^{OPP} . After removing

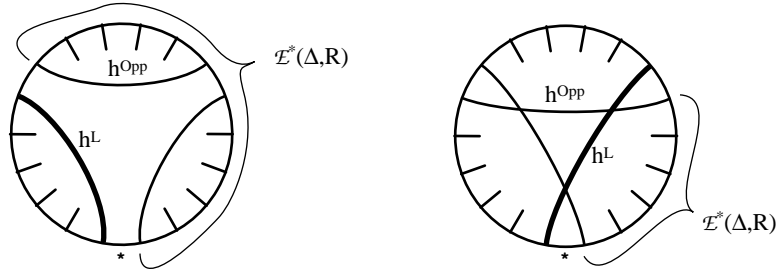


FIGURE 70. If the marked triangle is untwisted then both ends of h^{Opp} are in \mathcal{E}^* ; but if it is twisted only one end of h^{Opp} is in \mathcal{E}^* .

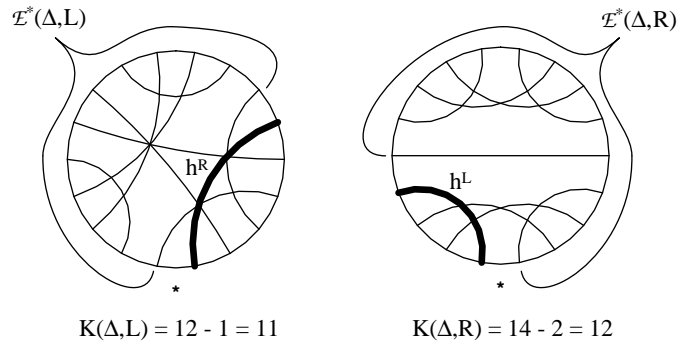


FIGURE 71. Examples of computing $K(\Delta, d)$

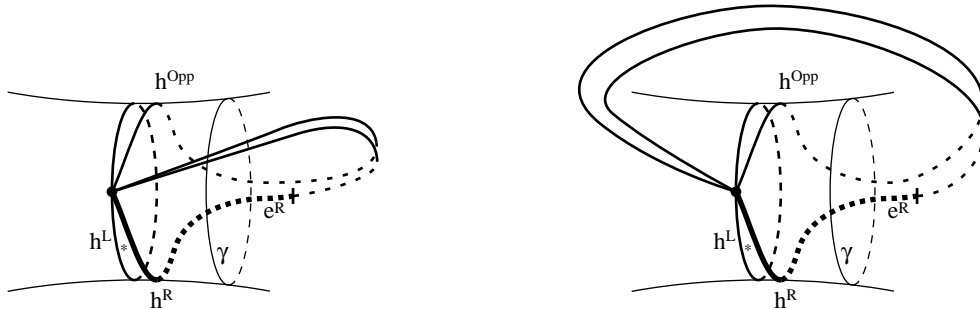


FIGURE 72. Up to isotopy, h^{Opp} is obtained from h^R by letting $\tau(\Delta, R)^{-1}$, the Left Dehn twist about γ , act on the half-arc representing e^R .

h_i^{Opp} , the marked prong is now located in a complementary 4-gon of $\hat{\Delta}_i$. Note that Δ_i may be recovered from $\hat{\Delta}_i$ by triangulating this 4-gon using an arc opposite the marked prong. Consider the good elementary move $\Delta_{i+1} \rightarrow \Delta_i$. Note that $\hat{\Delta}_i$ is obtained from $\hat{\Delta}_{i+1}$ by inserting h_{i+1}^{Opp} and then removing h_{i+1}^d . Using the key observation, it follows that $\hat{\Delta}_i$ is obtained from $\hat{\Delta}_{i+1}$ by letting τ^{-1} act on the half-arc representing e_{i+1}^d . Travelling along the sequence $\hat{\Delta}_K, \dots, \hat{\Delta}_1, \hat{\Delta}_0$, then τ^{-1} acts in turn on a representative half-arc of each end in $\hat{\mathcal{E}}_K^*$. Since these half-arcs represent all the points in $\hat{\Delta}_K \cap \gamma$, it follows that $\tau^{-1}(\hat{\Delta}_K) = \hat{\Delta}_0$.

hence $\tau^{-1}(\Delta_K) = \Delta_0$ so $\tau(\Delta_0) = \Delta_K$. In order to get the full periodicity statement $\tau(\Delta_i) = \Delta_{i+K}$, note that $h_i^{-d} = h_{i+1}^{-d}$ so $\tau(\Delta_i, d) = \tau(\Delta_{i+1}, d)$, and also $K(\Delta_i, d) = |\hat{\mathcal{E}}_i^*| = |\hat{\mathcal{E}}_{i+1}^*| = K(\Delta_{i+1}, d)$. This finishes the proof of the Dehn twist lemma.

We can now determine the range of possible Dehn twist lengths. Obviously $K(\Delta, d) \geq 1$. To determine when equality is achieved, note that $|\mathcal{E}^*(\Delta, d)| \geq 2$ with the minimum achieved if and only if h^{-d} is the boundary of a 1-handle piece and the $*$ is inside the 1-handle piece, in which case the marked triangle is inside the 1-handle piece and therefore twisted; this is the only way the Dehn twist length can be 1, because if $|\mathcal{E}^*(\Delta, d)| = 3$ then the marked triangle is still twisted so the Dehn twist length is 2. To find the maximum Dehn twist length, recall that $\mathcal{E}(\delta) = 12g - 6$. Now h^{-d} cuts off one subset of $\mathcal{E}(\delta)$ of size at least 2, and h^{-d} itself has 2 ends, hence $|\mathcal{E}^*(\Delta, d)| \leq 12g - 6 - 2 - 2 = 12g - 10$. This size is achieved if and only if h^{-d} is on the boundary of a 1-handle piece and the $*$ is outside the 1-handle piece, in which case the marked triangle is untwisted and so the Dehn twist length is $12g - 10 - 2 = 12g - 12$. Also, when $|\mathcal{E}^*(\Delta, d)| = 12g - 11$ then the Dehn twist length is at most $12g - 11 - 1 = 12g - 12$. Therefore we have an optimal upper bound of $12g - 12$ for the Dehn twist length. An example of a maximal length Dehn twist sequence on a surface of genus 2 is given in figure 72. It is an exercise to show that this is the unique maximal length Right Dehn twist block in genus 2.

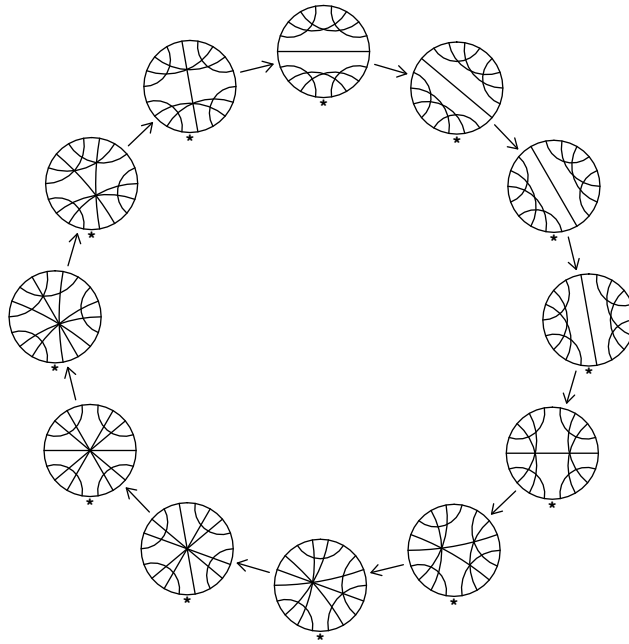


FIGURE 73. A Right Dehn twist block in genus 2, of maximal length 12

An automaton for synchronous normal forms. First we define a new generating set \mathcal{A}_1 for \mathcal{MCGD} , over which the new automaton \mathcal{M}_1 is defined. The set \mathcal{A}_1 is obtained from \mathcal{A}_0 by adding Dehn twist generators and fractions thereof.

In the last section we defined Dehn twist blocks in \mathcal{M}_0^1 . Define a *Dehn twist generator* to be the path in X obtained by projecting a Dehn twist block from \mathcal{M}_0^1 to X . Every Dehn twist generator is a closed curve in X , so it defines a group element in \mathcal{MCG} . Define a *fractional Dehn twist generator* to be any subword of a Dehn twist generator; this may not be a closed curve, and so may not define a group element.

Define a new alphabet \mathcal{A}_1 to be the set of all relabelling generators, Dehn twist generators, and fractional

Dehn twist generators. Note that every labelled elementary move is either a full or fractional Dehn twist generator, so $\mathcal{A}_0 \subset \mathcal{A}_1$. There is a map from \mathcal{A}_1 to \mathcal{MCGD} , taking each generator to its homotopy class.

Consider a full or fractional Dehn twist generator $w = w_1 \cdots w_n$. Let $s_0 \xrightarrow{w_1} s_1 \xrightarrow{w_2} \cdots \xrightarrow{w_n} s_n$ be any path in \mathcal{M} that lifts w and stays among the accept states. This path is called a full or fractional *Dehn twist block* if the subpath $s_1 \rightarrow \cdots \rightarrow s_n$ stays in a single level of \mathcal{M} ; we allow $s_0 \rightarrow s_1$ to drop between levels.

Chord diagrams of Dehn twist blocks in arbitrary levels are understood as follows. Suppose that $s_0 \xrightarrow{d} s_1 \xrightarrow{d} \cdots \xrightarrow{d} s_n$ is a full Dehn twist block in level 1, of parity d . Thus, none of the chord diagrams have labelled ends, and each $s_i \rightarrow s_{i+1}$ is a parity d arrow. Dehn twist blocks in higher levels are obtained by introducing end markings, as follows. Recall the set of chord ends $\mathcal{E}^* = \mathcal{E}^*(s_0, d)$: the two ends of h_0^{-d} divide the remaining chord ends of s_0 into two subsets, one of which contains e^d , that subset being $\mathcal{E}^*(s_0, d)$. If end markings $1, \dots, k-1$ are introduced to form a new state s'_0 , and if none of the labelled ends are in $\mathcal{E}^* \cup \text{Opp}(\mathcal{E}^*)$, then we obtain a Dehn twist block $s'_0 \xrightarrow{d} s'_1 \xrightarrow{d} \cdots \xrightarrow{d} s'_n$ staying entirely in level k ; figure 74 shows an example. Then if additional end markings $k, \dots, l-1$ are inserted so that the end e^d is marked with k , and if a different marked prong is then chosen, we obtain a Dehn twist block $s'_0 \xrightarrow{d} s'_1 \xrightarrow{d} \cdots \xrightarrow{d} s'_n$ where the first move drops from level l to level k and the rest of the block stays in level k . Figure 75 shows an example, adding end markings to the example from figure 74.

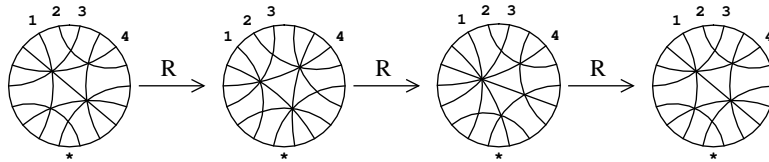


FIGURE 74. A Right Dehn twist block in level 5

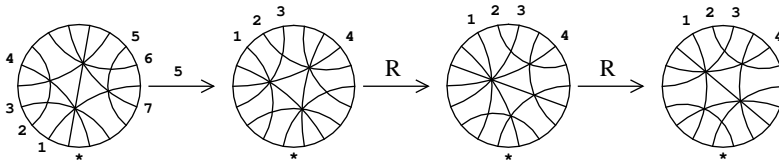


FIGURE 75. A Right Dehn twist block which drops from level 8 to level 5

Chord diagrams of fractional Dehn twist blocks are constructed similarly, except that the restrictions on end markings are somewhat weaker. Suppose $s_0 \rightarrow s_1 \rightarrow \cdots \rightarrow s_n$ is a fractional Dehn twist block in level 1, of parity d . Instead of worrying about all of \mathcal{E}^* , only worry about those ends in \mathcal{E}^* which will eventually become e^d for one of the states s_0, \dots, s_{n-1} , i.e. those ends which lie on a chord that will eventually be removed in performing one of the elementary moves in the block; let that set be denoted $\mathcal{E}^\#$. To get a fractional Dehn twist block that stays in level k , we may mark chord ends of s_0 with $1, \dots, k-1$ as long as the marked ends are not in $\mathcal{E}^\# \cup \text{Opp}(\mathcal{E}^\#)$. To get a fractional Dehn twist block that drops from level l to level k , add more end markings $k, \dots, l-1$ so that e^d is marked with k , and then move the marked prong if desired. An example of a fractional Dehn twist block in level 6 is given in figure 76, adding an end marking to the first two moves in figure 74. This example cannot be extended to any longer full or fractional Dehn twist block, because in the final state of the block the end e^R in the final state is marked with a 5, so the move on h^R drops down to level 5.

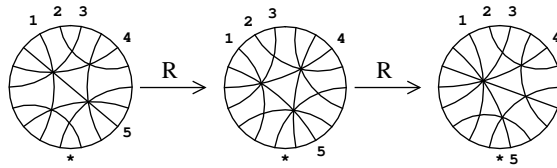


FIGURE 76. A Right fractional Dehn twist block in level 6, which cannot be extended to a longer block

Now we are ready to define the automaton \mathcal{M}_1 . Its state set is (almost) the same as the state set of \mathcal{M}_0 . In addition to the old arrows of \mathcal{M}_0 , we add new arrows representing Dehn twist blocks and fractional Dehn twist blocks, which jump over the corresponding path in \mathcal{M}_0 . In order to preserve uniqueness, we require that fractional Dehn twists can occur only at the very beginning of a parity block, so the states of \mathcal{M}_1 must remember whether a full Dehn twist has just occurred.

To define the states of \mathcal{M}_1 : the failure states, and inconsistent accept states are the same as for \mathcal{M}_0 . For every consistent accept state s of \mathcal{M}_0 , we define three accept states in \mathcal{M}_1 , namely (s, O) , (s, L) , and (s, R) , whose meanings are as follows. In state (s, d) the previous letter was a full Dehn twist of parity d , and in state (s, O) the previous letter was not a full Dehn twist. If s_0 is the start state of \mathcal{M}_0 then (s_0, O) is the start state of \mathcal{M}_1 .

Now we define arrows of \mathcal{M}_1 . The arrows coming out of failure states and inconsistent states all lead to failure states as before. For every relabelling arrow $s \rightarrow s'$ of \mathcal{M}_0 , noting that s is a consistent state and s' is inconsistent, we define three relabelling arrows $(s, O) \rightarrow s'$, $(s, L) \rightarrow s'$, and $(s, R) \rightarrow s'$, all named with the same relabelling generator.

Consider now a consistent accept state s_0 of \mathcal{M}_0 . Consider also a full or fractional Dehn twist block $s_0 \rightarrow s_1 \rightarrow \dots \rightarrow s_n$ of parity d , ending at s_n in level k , and let w be the full or fractional Dehn twist generator to which this block projects. If w is full, construct arrows from the states (s_0, O) , (s_0, R) , (s_0, L) to the state (s_n, d) , all named with w . If w is fractional and s_0 is in level k , construct arrows from the states (s_0, O) , $(s_0, -d)$ to (s_n, O) , both named with w ; the arrow from (s_0, d) named with w leads to the appropriate failure state. If w is fractional and s_0 is not in level k , construct arrows from the states (s_0, O) , (s_0, L) , (s_0, R) to (s_n, O) , all named with w . All other arrows which have not been specifically constructed here should lead to the appropriate failure state.

The effect of this construction is that a fractional Dehn twist block cannot follow a full Dehn twist block of the same parity, unless the fractional block drops down to a lower level.

The language \mathcal{L}_1 accepted by \mathcal{M}_1 is related to the language \mathcal{L}_0 in the following manner. Given any word $w \in \mathcal{L}_0$, recall that w is factored into uncombing blocks, and each uncombing block is in turn factored into parity blocks. Now look at a parity block. Using the Dehn twist lemma, that block can be factored in a unique manner as a fractional Dehn twist block, followed by some number of full Dehn twist blocks. Doing this factorization for each parity block in \mathcal{L}_0 , one obtains a word w' in the generators \mathcal{A}_1 , such that w and w' represent the same element of \mathcal{MCGD} , and $w' \in \mathcal{L}_1$. We say that w' is the *Dehn twist factorization* of w .

Synchronization.

In this section we review the results of [M] that are used to prove that \mathcal{L}_1 satisfies the fellow traveller property. We shall use these results to prove directly that our algorithm for the word problem runs in quadratic time.

Given a word $w := w_1 \dots w_k$, recall the notation for a prefix subword $w(t) := w_1 \dots w_t$. We also use notation for an infix subword $w[i, j] := w_{i+1} \dots w_j$. Note that if $a < b < c$ then $w[a, b]w[b, c] = w[a, c]$ and $w(a)w[a, b] = w(b)$.

Consider two normal forms $v, w \in \mathcal{L}_0$, such that $\alpha = \bar{v}^{-1}\bar{w}$ is an elementary move generator. In applying the subroutine *Do one move* to the word $v\alpha$, the algorithm applies some number of relators to obtain w ,

and we want to estimate that number. The most interesting case is when the algorithm classifies the move α as a bad elementary move, in which case the estimate will arise by studying how Dehn twist boundaries interact with the operations of the algorithm. Understanding this interaction is also the key to proving the synchronous fellow traveller property for \mathcal{L}_1 .

Let $v', w' \in \mathcal{L}_1$ be the Dehn twist factorizations of v, w , with $\text{Length}(v') = M$ and $\text{Length}(w') = N$. Thus, we may write $v = v[s_0, s_1] \circ \cdots \circ v[s_{M-1}, s_M]$ where $v'_m = v[s_{m-1}, s_m]$, and similarly $w'_n = w[t_{n-1}, t_n]$. We think of the parameter values s_0, \dots, s_M and t_0, \dots, t_N as “Dehn twist boundaries”. We regard v'_m and w'_n as individual letters of \mathcal{A}_1 , but they may also be regarded as words in \mathcal{A}_0 and as such we may speak of their subwords.

To start, we study how Dehn twist boundaries interact under the situation where α is a good or inverse good elementary move, or more generally when one of v, w is a prefix subword of the other. Supposing v is a prefix subword of w , then there exists $n \leq N - 1$ such that $t_n \leq s_M < t_{n+1}$, and we say that w' extends v' by $N - n$ Dehn twist units, namely $w[s_M, t_{n+1}], w'_{n+2}, \dots, w'_N$. All but the first of these units are letters of w' ; the first unit is a suffix of w'_{n+1} , possibly the whole word, but either way it forms a letter in the alphabet \mathcal{A}_1 . To compare Dehn twist boundaries in this situation:

Good proposition. *Suppose w' extends v' by K Dehn twist units. Then $w'(N - t)$ extends $v'(M - t)$ by at most K Dehn twist units, for all $t \geq 0$.*

Proof. The boundaries of the Dehn twist factorizations of v and w are identical up until the last parity block in v ; suppose that $v'(A)$ and $w'(A)$ end at the beginning of that parity block. In that parity block, the initial fractional Dehn twist factors of v and w may have different lengths, but for the rest of the parity block the full Dehn twist factors have the same length, hence if $A < B \leq M$ then one of $v'(B)$ or $w'(B)$ extends the other by at most one Dehn twist unit. It follows that if $t_n \leq s_M < t_{n+1}$, then $t_{n-1} \leq s_{M-1} < t_{n+1}$, so $w'(N - 1)$ extends $v'(M - 1)$ by at most K Dehn twist units. Now continue by induction. \diamond

Now suppose that α is a bad elementary move. The algorithm *Do a bad elementary move* applies a sequence of relators, producing a sequence of bad elementary moves connecting shorter and shorter initial subwords of v and w , until reaching identical initial subwords. More precisely, there exists $P \geq 1$ and sequences $0 \leq i_0 < i_1 < \cdots < i_P$, $0 \leq j_0 < j_1 < \cdots < j_P$ with the following properties:

- (1) If $0 < p \leq P$ then $v(i_p)$ and $w(j_p)$ differ by a bad elementary move; we say that $v(i_p)$ and $w(j_p)$ are *matching bem ends* (bem is the acronym for “bad elementary move”).
- (2) If $1 < p \leq P$ then there exists $(a, b) \in \{(1, 1), (1, 2), (2, 1)\}$ such that $i_{p-1} + a = i_p$, and $j_{p-1} + b = j_p$.
- (3) There exists $(a, b) \in \{(1, 1), (1, 2), (2, 1), (2, 2)\}$ such that $i_0 + a = i_1$ and $j_0 + b = j_1$. Furthermore:
 - (3a) If $(a, b) = (2, 2)$ then $v(i_0) = w(j_0)$.
 - (3b) If $(a, b) \in \{(1, 1), (1, 2), (2, 1)\}$ then one of $v(i_0), w(j_0)$ extends the other by a single good elementary move.
- (4) In particular, $|i_0 - j_0| \leq 1$. We refer to the intervals $[i_0, i_1]$ and $[j_0, j_1]$ as the *irregular regions*.

Remark: in [M] we also say, in case (3b), that $v(i_0)$ and $w(j_0)$ are *matching bem ends* (despite the fact that their difference is a good or inverse good elementary move).

The relation between the Dehn twist factorizations of v and w is given in the following, which although not stated explicitly in [M] is proved implicitly:

Bad proposition. *Suppose $\alpha = \bar{v}^{-1}\bar{w}$ is a bad elementary move. Recall the notation s_0, \dots, s_M and t_0, \dots, t_N for the Dehn twist boundaries of v, w , and note that $v(s_M)$ and $w(t_N)$ are matching bem ends. Then there exists a constant $A \geq 0$ such that $v(s_{M-a})$ and $w(t_{N-a})$ are matching bem ends for $0 \leq a < A$. Moreover, one of the following happens:*

- (1) *One of $v(s_{M-A})$ and $w(t_{N-A})$ extends the other by one Dehn twist unit.*

or

- (2) $v(s_{M-A})$ and $w(t_{N-A})$ differ by 2 elementary moves (one bad and one good), and one of $v(s_{M-A-1})$ and $w(t_{N-A-1})$ extends the other by at most two Dehn twist units.

The point of this proposition is that as you move backwards along v and w , moving synchronously one Dehn twist block per step, then the corresponding Dehn twist boundaries will be matching *bem* ends, hence differing by a single generator in \mathcal{A}_0 . This continues until you reach the irregular regions, at which time the difference can become as large as two Dehn twist units.

Sketch of proof. We have defined three progressively finer factorizations of normal forms in \mathcal{L}_0 : the uncombing block factorization, the parity block factorization, and the Dehn twist factorization. Corresponding to each of these is a proposition in [M] which describes the interaction of the factorization with *bem* ends: *bemsrespect combing blocks*, *bemsrespect parity blocks*, and the second part of the *Dehn twist lemma*. We invoke these in the proof.

Now look at the final Dehn twist blocks $v[s_{M-1}, s_M]$ and $w[t_{N-1}, t_N]$, and go case by case through the different possibilities.

If $v[s_{M-1}, s_M]$ is a full uncombing block, then by *bemsrespect combing blocks* it follows that $w[t_{N-1}, t_N]$ is also a full combing block, and $v(s_{M-1}), w(t_{N-1})$ differ by a single elementary move, either good, bad, or inverse good. If it is good or inverse good, then evidently one of v'_{M-1} or w'_{N-1} extends the other by one Dehn twist unit, proving item (1) of the *Bad proposition*. If it is bad, then the proof continues by induction.

If $v[s_{M-1}, s_M]$ is a full Dehn twist block, then by the second part of the *Dehn twist lemma* it follows that $w[t_{N-1}, t_N]$ is also a full Dehn twist block, and $v(s_{M-1}), w(t_{N-1})$ differ by a single bad elementary move. The proof now continues by induction.

The remaining case is where $v[s_{M-1}, s_M], w[t_{N-1}, t_N]$ are fractional Dehn twist blocks which are not full uncombing blocks. In this case, either $v(s_{M-1})$ and $w(t_{N-1})$ differ by a bad elementary move, or both are in the irregular regions; this follows from *bemsrespect parity blocks*. When they differ by a bad elementary move, continue by induction as before.

When both s_{M-1} and t_{N-1} are in the irregular regions, then the proof of synchronization in [M] analyzes carefully where the Dehn twist boundaries may occur. Roughly speaking, since the two sides of the relation in the irregular regions are quite short, they cannot throw off the synchronization by too much. The conclusions of the argument from [M] are as follows, proving item (2) of the *Bad proposition*: the irregular region is of type (2, 2) as in (3a) above; the relation which applies is always of type IIbii; the words $v'(M-1)$ and $w'(N-1)$ differ by two elementary moves (one bad and one good); and one of $v'(M-2), w'(N-2)$ extends the other by at most two Dehn twist units. This argument is summarized in figure 18 of [M], the last figure of section III.2. There are three cases to the argument, and in figure 77 we present examples for each of the three cases, paralleling the schematic pictures in figure 18 of [M]. These cases are distinguished as follows. We assume that all the arrows in the relator IIbii are parity arrows, with parities LR on the left side and RL on the right side. The arrows below the relator on the left and right have the same parity, say L; these arrows are part of the final letters of v'_M and w'_N . The three cases are distinguished by whether the arrow above the relator is no parity, Left parity, or Right parity. If no parity, the example in figure 77a is typical: $v'(M-2)$ extends $w'(M-2)$ by at most two Dehn twist units, each unit being a single elementary move; it could happen that the no parity arrow pictured is an entire Dehn twist block, in which case the Dehn twist boundary t_{N-1} would be one arrow lower in figure 77a, and $v'(M-2)$ would extend $w'(M-2)$ by a single Dehn twist unit. If Left parity, the example in figure 77b is typical: $v'(M-2)$ extends $w'(M-2)$ by one Dehn twist unit, consisting of a single elementary move. If Right parity, the example in figure 77c is typical: $v'(M-2)$ extends $w'(M-2)$ by at most two Dehn twist units, one being a single elementary move and the second being a fractional Dehn twist generator; the example in figure 77c shows the second unit being a single elementary move, but the letter $w'(M-2) = w[t_{N-2}, t_{N-1}]$ can be any full or fractional Dehn twist generator, in which case the second unit can be an arbitrarily long fractional Dehn twist generator. The

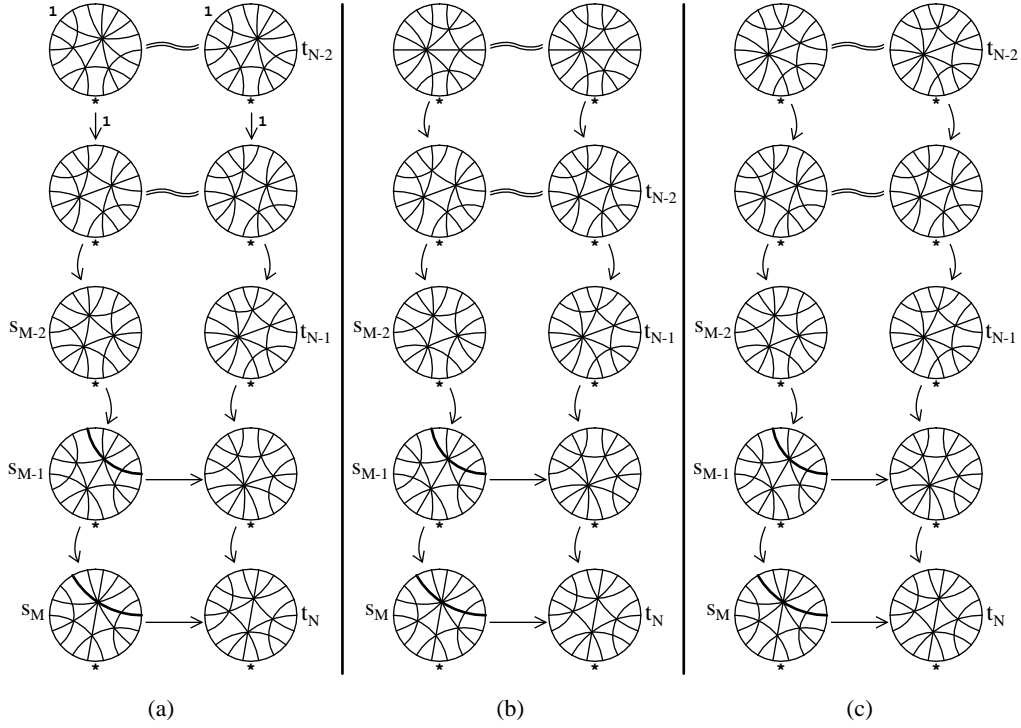


FIGURE 77. Dehn twist boundaries in the irregular regions

general argument given in [M] shows that figures 77a–c are typical: the irregular regions affect the Dehn twist boundaries in one of the three ways exemplified in these figures.

◇

The *Good and Bad propositions* may be used to prove the synchronous fellow traveller property for \mathcal{L}_1 , as follows. Consider $v', w' \in \mathcal{L}_1$, with $M = \text{Length}(v')$ and $N = \text{Length}(w')$. Let d_i denote distance measured with the generating set \mathcal{A}_i . Noting that each letter in \mathcal{A}_1 is a word of length at most $12g - 12$ in the letters of \mathcal{A}_0 , to prove the fellow traveller property it suffices to assume that $d_0(\bar{v}', \bar{w}') = 1$ and prove that $d_1(\bar{v}'(t), \bar{w}'(t)) \leq 4$ for all t . The case where \bar{v}', \bar{w}' differ by a relabelling generator is easy.

Suppose \bar{v}', \bar{w}' differ by an elementary move generator. Applying the *Good and bad propositions* we see that $d_1(\bar{v}'(M - t), \bar{w}'(N - t)) \leq 2$ for all t . This shows that $|M - N| \leq 2$, so $d_1(\bar{v}'(t), \bar{w}'(t)) \leq 4$ for all t .

From this argument we obtain the following important fact which is needed in estimating computation time:

Lemma: Length grows additively. *Given $v, w \in \mathcal{L}_0$ such that $d_0(\bar{v}, \bar{w}) \leq 1$, if $v', w' \in \mathcal{L}_1$ are the Dehn twist factorizations, then $|\text{Length}(v') - \text{Length}(w')| \leq 2$.* ◇

Proof of theorem: Quadratic computation time. Consider $v, w \in \mathcal{L}_0$ with $d_0(\bar{v}, \bar{w}) \leq 1$, and $\alpha = \bar{v}^{-1}\bar{w}$. Let the Dehn twist factorizations be $v', w' \in \mathcal{L}_1$.

We claim that the number of relators used by the subroutine *Do one move* to compute w from $v\alpha$ is at most $(12g - 12) \text{Length}(v')$. If the generator $\alpha = \bar{v}^{-1}\bar{w}$ is a relabelling generator, then only 1 relator is used. If α is a good or inverse good elementary move, then at most 2 relators are used.

Suppose that α is a bad elementary move, and apply the *Bad proposition*. For $1 \leq a < A$, consider the relators that are applied by the algorithm to compute the (possibly fractional) Dehn twist block $w[t_{N-a}, t_{N-a+1}]$

from the Dehn twist block $v[s_{M-a}, s_{M-a+1}]$. These relators are all of types Ia, IIa, or IIbi, each relator touching one of the good elementary moves in $v[s_{M-a}, s_{M-a+1}]$ and no two relators touching the same one, but there are at most $12g - 12$ elementary moves since this is a Dehn twist block or fraction thereof. Thus, at most $12g - 12$ relators are used. Also, the algorithm uses at most $12g - 12$ relators to compute $w[t_{N-A}, t_{N-A+1}]$ from $v[s_{M-A}, s_{M-A+1}]$: if these are full Dehn twist blocks then it follows as before; and if these are fractional Dehn twist blocks then except for the top relator, each relator touches some elementary move in $v[s_{M-A}, s_{M-A+1}]$ and no two relators touch the same one, but there are at most $12g - 13$ elementary moves in a fractional Dehn twist block, and adding one more for the top relator gives $12g - 12$. This proves the claim.

Taking this claim together with the lemma *Length grows additively*, we reach the conclusion that for any word v of length K in the generators \mathcal{A}_0 , the number of relators used by the algorithm to compute the normal form of v is at most $(12g - 12)[1 + 3 + 5 + \cdots + (2K - 1)] = (12g - 12)K^2$.

Remark: The constant $12g - 12$ can be improved slightly, by noticing that in constructing the relators touching a Dehn twist block, if the block has full length $12g - 12$ then there must be at least one relator of type IIbi which touches two moves in the block, so the number of relators adjacent to a Dehn twist block is at most $12g - 13$. Therefore the number of relators needed by the algorithm is at most $(12g - 13)K^2$.

BIBLIOGRAPHY

- [ECHLPT] D. Epstein, J. Cannon, D. Holt, S. Levy, M. Paterson, W. Thurston, *Word processing in groups*, Jones & Bartlett, 1992.
- [Har] J. Harer, *The virtual cohomological dimension of the mapping class group of an oriented surface*, Invent. Math. **84** (1986), 157–176.
- [Hat] A. Hatcher, *On triangulations of surfaces*, Topology Appl. **40** (1991), no. 2, 189–194.
- [M] L. Mosher, *Mapping class groups are automatic*, Preprint (1993).
- [STT] D. D. Sleator, R. E. Tarjan, W. P. Thurston, *Rotation distance, triangulations, and hyperbolic geometry*, J. Amer. Math. Soc. **1** (1988), 647–681.

MATHEMATICAL SCIENCES RESEARCH INSTITUTE, BERKELEY CA 94720
E-mail address: mosher@msri.org